Core Design Optimization and Steady State Criticality Analysis of the Canadian Nuclear Battery™

CORE DESIGN OPTIMIZATION AND STEADY STATE CRITICALITY ANALYSIS OF THE CANADIAN NUCLEAR BATTERY™

By Sameer REODIKAR,

A Thesis Submitted to the School of Graduate Studies in the Partial Fulfillment of the Requirements for the Degree Master of Applied Science

McMaster University, Department of Engineering Physics, August 19, 2021

McMaster University
Master of Applied Science (2021)
Hamilton, Ontario (Department of Engineering Physics)

TITLE: Core Design Optimization and Steady State Criticality Analysis of the Canadian Nuclear Battery™
AUTHOR: Sameer Reodikar (McMaster University)
SUPERVISOR: Dr. Adriaan Buijs & Dr. John Luxat
NUMBER OF PAGES: ix, 91

Abstract

The nuclear microreactor, although not a novel concept, is a fast-emerging technology. Microreactors are small modular reactors that have a thermal power level between 1 and 20 MW. They take the smallness and modularity to a whole new level in the sense that they are entirely factory-built and shipped to the intended location, rather than constructed onsite. One such design is the 2400 kW_{th} Canadian Nuclear Battery™ (CNB) design being developed by Dunedin Energy System Ltd. for use in remote northern territories as a potential alternative to diesel electric power plants. Key technical features of the reactor include a heat pipe cooled core, graphite neutron moderator, high assay low enriched uranium (HALEU), TRISO coated fuel particle and use of burnable poison particles for long term reactivity control. This thesis reports the methodology used for 3D neutronics modeling and core design of the CNB using the Monte Carlo particle transport code SERPENT 2.1. Optimization of the fuel enrichment, amount of burnable poison, lattice pitch, and poison particle size is carried out by performing burnup calculations to achieve a reasonable reactivity swing over 20 years of full power operation without refueling. The worth of the reactivity control system, shutdown margin, fuel and graphite temperature reactivity coefficients, coolant void coefficients, neutron flux , and power distribution over the reactor lifetime are evaluated. Additionally, a preliminary single lattice cell thermal-hydraulic and neutronic coupling is performed along with a viability study of the control drum system as an alternative form of reactivity control.

Acknowledgements

I would like to thank my supervisors Dr. Adriaan Buijs & Dr. John Luxat for their support during my research. I would like to express my deepest gratitude to Dr. Buijs for his motivation, guidance, suggestions, and continuous support throughout my research and academics. I truly appreciate all the faith that he showed in me during my early phase of my studies and allowing me the opportunity to join his research team for my MASc. There is no doubt that this dissertation would not have been possible without him. His knowledge, enthusiasm and patience has been a source of inspiration and motivation to me. Apart from the subject of my research, I learnt a lot from him, which I am sure, will be useful in different stages of my life.

I would also like to thank the members of my research group including Lorena Pilar, Manav Sood , Gizem Bakir and Sam Tcherner for their general support and collaboration.

Finally, this thesis would not have been possible without the confidence, endurance and support of my family. My family has always been an endless source of inspiration and encouragement and I would like to thank them for their affection, understanding and patience.

Contents

List of Figures

List of Tables

Chapter 1

Introduction

1.1 Small Modular Reactors and Microreactors

It has been almost 65 years since Shippingport Atomic Power Station, the first commercial nuclear reactor in North America started operating but today's nuclear power plant projects still deal with the similar concerns that plagued the earliest units viz. reactor safety, the high capital cost of construction and operational costs, length of refueling and unplanned outages, spent fuel management and concerns with weapon-grade nuclear material proliferation. Big strides were made in all the areas mentioned above with the advancement of science and technology but the concerns largely remained. This motivates the development of innovative designs of small and microreactors especially for remote areas off the main power grid where the economics of scale does not work, in-situ construction will not be easy or even possible and availability of skilled manpower for operation, maintenance, and refueling is limited.

The International Atomic Energy Agency (IAEA) classifies any nuclear reactor with a power output of less than 300MWe as a small reactor and a recent development of subcategory of reactor power typically up to 10MWe as microreactors (Subki 2020). Most of the microreactor designs would be able to produce 1–20 MW of thermal energy that could be used directly as heat or converted to electric power (Zohuri 2020).

This thesis discusses the core design optimization of a microreactor commercially named Canadian Nuclear Battery™(CNB). The reactor design is being developed by Dunedin Energy Systems Ltd. with the aim to "bring the many benefits of nuclear energy to markets that have traditionally been thought of as too small or too remote to be served by nuclear energy, particularly in northern and arctic Canada"(Dunedin 2021). The high-level design requirements for the CNB are similar to most of the micro modular reactors, namely,

1. The reactor can be fully assembled in a factory and shipped out to the location. This will eliminate difficulties associated with construction in Canadian Arctic and the high capital costs associated with it.
2. It must be possible to ship the entire reactor by airplane.
3. Self-regulation and passive safety should be inherent design features. This will eliminate the requirement of a large number of specialized operators.
4. A long core life operating up to 15 years without refueling, which precludes the requirement of a skilled refueling crew and containment boundary breach that is necessary for refueling.

1.2 Reactor Physics Fundamentals

1.2.1 Neutron Interactions

The design of all nuclear fission reactors fundamentally depends on the ways in which neutrons interact with matter. It is essential to note that neutrons being electrically neutral never interact with the atoms but only with the nuclei. The interactions of neutrons with nuclei can be in one of the following ways: (Lamarsh 1977)(Scriven 2014)

- **Elastic scattering**: In this process, the neutron strikes a nucleus that is in its ground state, gets scattered, and the nucleus is left in its ground state. Although the neutron loses energy and can get scattered in a different direction in this collision, the momentum of the system is conserved.
- **Inelastic scattering:** This process is similar to the elastic scattering except for the fact that the nucleus is left in its excited state. Hence, this interaction does not occur unless the neutron has enough energy to place the nucleus in its first excited state. This threshold energy is lower for a nucleus having a higher mass number (e.g., the threshold for inelastic scattering is 4.8 MeV for ^{1}2C but only 44 keV for ^{238}U). The excited nucleus then decays back to the ground state by emission of γ-rays.
- **Radiative Capture:** In this interaction, the colliding neutron is absorbed by the nucleus, and one or more γ-rays are emitted, leading to a loss of neutrons from the system. This interaction falls under the category of absorption reactions.

- **Fission Reaction:** This neutron interaction is the principal source of nuclear energy for practical application. It is based on the fact that heavier nuclei (above the mass number of 50) have lower binding energy[1] per nucleon than lighter nuclei, and a more stable configuration can be obtained by splitting the heavy nucleus into two lighter nuclei, releasing a significant amount of energy ($\tilde{2}00$ MeV per fission) and a few neutrons. Although spontaneous fission can occur, it is rare, and it cannot be relied upon for practical application. The rapid fission of heavy nuclei can be made possible by supplying the energy to the nucleus in the form of a neutron interaction. For fissile nuclei, like ^{235}U, absorption of a zero-energy neutron is sufficient to fission, while fissionable but non-fissile materials like ^{238}U need to be struck by an energetic neutron (>0.6 MeV) for fission to occur. This interaction also falls under the category of absorption interaction but is not parasitic and is the major source of neutron multiplication in the reactor.

- **Charged Particle Reactions:** In this interaction, the nucleus absorbs the neutron and releases a charged particle like a proton or an alpha particle. One of the important reactions of this type is the ^{10}B(n,α)^{7}Li reaction. The probability of this reaction occurring is very large for low energy neutrons in the Boron medium and thus ^{10}B is often used to absorb low energy neutrons in control rods.

Neutron interactions are stochastic in nature and the probability of a particular interaction occurring is given in terms of quantities known as microscopic cross-sections. These can be quantified physically in terms of a "characteristic area" where a larger area means a larger probability of interaction. The standard unit for measuring a nuclear cross-section (denoted as σ) is the barn, which is equal to 10^{-28} m^2. Another useful quantity derived from microscopic cross-section is the macroscopic cross-section and is simply defined as the multiplication of microscopic cross-section and number density N of the medium and is shown in equation 1.1.

$$\Sigma = N\sigma. \tag{1.1}$$

Thus the microscopic cross-section is an intrinsic property of the nuclei while the macroscopic cross-section is applicable for a lump of matter. The microscopic and macroscopic cross-sections are additive algebraically. Thus the total cross-section, microscopic or macroscopic, is the sum of absorption and scattering cross-sections as shown in equation

---

[1] Binding energy of a nucleus is the energy needed to be supplied to break the nucleus into individual nucleon

1.2,

$$\Sigma_t = \Sigma_a + \Sigma_s \qquad \sigma_t = \sigma_a + \sigma_s. \tag{1.2}$$

This is further applicable to a group of different materials. The total macroscopic cross-section over materials, say X and Y can be given as shown in equation 1.3,

$$\Sigma_t = N_X \sigma_t^X + N_Y \sigma_t^Y, \tag{1.3}$$

This total cross-section is a function of variables like incident neutron energy, the temperature of the nucleus and shows both spatial and time dependence. The data of nuclear cross-sections for each interaction for all the materials is stored in a database called the nuclear data libraries. The cross-section values are the results of experiments and may incorporate some analytical processing. This gives near-continuous point-wise data for reaction cross-sections as a function of neutron energy and the temperature of the material.

1.2.2 Neutron Transport and Diffusion Equation

The neutron transport equation is the governing equation of the reactor physics and is an exact deterministic equation for continuity or conservation of neutrons in space. The solution of the neutron transport equation simulates the lifetime and motion of neutrons in a reactor. Before discussing the neutron transport problem it is prudent to define the nuetron flux since the reactor power is a direct function of the neutron flux in the reactor. A neutron in space can be defined by its position ($\overrightarrow{r}$), energy (E), direction of travel (Ω) and time (t). The neutron density is defined as $N(\overrightarrow{r}, E, \Omega, t)$ such that $N(\overrightarrow{r}, E, \Omega, t) dV dE d\Omega$ is the expected number of neutrons in volume dV about $\overrightarrow{r}$ travelling in a cone of dΩ about Ω in energies between E and $E + dE$ at a particular time t. From this the angular flux (having the units n/cm^2-s) can be defined as,

$$\psi_t(\overrightarrow{r}, E, \Omega, t) = vN(\overrightarrow{r}, E, \Omega, t), \tag{1.4}$$

where v is the neutron velocity.

The scalar flux is defined as the integral of ψ over all directions as given by eq. 1.5

$$\phi_t(\overrightarrow{r}, E, t) = \int_{4\pi} d\Omega \psi_t(\overrightarrow{r}, E, \Omega, t). \tag{1.5}$$

The neutron flux physically translates to the number of neutrons traveling through a unit area per unit time and is an important parameter to describe the spatial and temporal behavior of neutrons in the reactor. The integral form of neutron transport is given by equation 1.6.

$$
\begin{aligned}
&\overbrace{\frac{1}{v}\frac{d\psi}{dt}}^{①} + \overbrace{\Omega \cdot \nabla\psi(x,\Omega,E,t)}^{②} + \overbrace{\Sigma_t(x,E,t)\psi}^{③} = \\
&\qquad \overbrace{\int_0^\infty \int_{4\pi} \Sigma_s(x,\Omega^{'} \rightarrow \Omega, E^{'} \rightarrow E,t)\psi(x,\Omega^{'},E^{'},t)de\Omega^{'}dE^{'}}^{④} \\
&\qquad \overbrace{+\frac{\chi(E)}{4\pi}\int_0^\infty \int_{4\pi} \nu\Sigma_f(x,E^{'},t)\psi(x,\Omega^{'},E^{'}t)d\Omega dE^{'}}^{⑤} + \overbrace{S(x,\Omega,E,t)}^{⑥} \qquad (1.6)
\end{aligned}
$$

The individual terms in equation 1.6 are given as (Duderstat and Hamilton 1976)

1. Rate of change of neutron population in a given volume
2. Leakage term, neutrons leaving the volume
3. Loss term, neutrons scattering to different energy or volume and neutrons getting absorbed
4. Inscattering term, neutrons scattered into direction and energy of interest E
5. Fission term, neutron creation in the volume due to fission where ν is the average number of neutrons of energy E produced in fission and $\chi(E)$ is the probability density function for all neutrons (prompt and delayed[2]) of energy E produced in the fission
6. External neutron source

The solution of the neutron transport equation is the main subject of most of the stochastic and deterministic nuclear computational solvers.

1.2.3 Monte-Carlo Methods

The Monte Carlo method is different than other numerical analysis techniques in the fact that it uses random (or pseudo-random) sampling to construct a solution to a physical problem. A stochastic model is set up, and by sampling from the appropriate probability distribution functions, statistical methods are used to estimate a numerical

---

[2] The delayed neutrons in steady state will have a constant contribution and are included in the source term

answer (Carter and Cashwell 1975). The advantage in the use of randomness to solve the neutron transport problem lies in the fact that the neutron interactions are stochastic in nature and a possible method to solve the problem lies in numerical simulation of the stochastic behavior. Additionally, the evaluation of linear integral equations in many dimensions through the use of the Monte-Carlo method is computationally efficient (Kalos et al. 1968).

The fundamental drawback of the Monte Carlo method is that all the evaluations are statistical and as such have an inherent uncertainty associated with them. The magnitude of the relative statistical error is roughly inversely proportional to the square root of the number of the simulated neutrons in the space where the results are tallied. For the problems of neutron transport in reactors, the Monte Carlo method requires the use of sophisticated mathematical tools like importance sampling, splitting & Russian roulette, antithetic variates, bias sampling, stratification, correlate sampling, eigenvalue solution, etc. to make the process rigorously justifiable (Carter and Cashwell 1975)(Kalos et al. 1968).

A rudimentary explanation of the Monte-Carlo methodology as applied to the neutron transport problem is given below:

- Monte-Carlo codes are based on the number of neutron cycles and each cycle consists of a fixed number of neutrons that are tracked one at a time. Since neutrons don't interact with each other calculation can be done one neutron at a time and in parallel.
- Each neutron starts at a particular location and random numbers are assigned to it, one to determine the direction and another to determine the path length.
- Once the neutron interacts with the nucleus, more random numbers are sampled based on the probability density functions or cumulative distribution functions to estimate which interaction it will undergo.
- This process continues until the neutron disappears (leaks or gets absorbed).
- Each path of the neutron from its creation to disappearance is called neutron history and each cycle is made of a fixed number of neutron histories
- Once a cycle ends, the next cycle starts with the neutrons in the positions created by the previous cycle.

- Tallies can be scored between each cycle and these can be used in the end to get some physical results(for eg. thermal neutron flux, fission heat deposition, fast neutron flux etc.).

A multi-purpose three-dimensional continuous-energy Monte Carlo particle transport and burnup code, developed at VTT Technical Research Centre of Finland, Ltd (Leppänen et al. 2014) is used in this thesis for core design and optimization of the Canadian Nuclear Battery™.

1.2.4 Multiplication Factor, Reactivity

The principal measure of the sustainability of a fission chain reaction is the multiplication factor (k). The multiplication factor is defined as the ratio of the rate of neutron production to the rate of neutron loss(Duderstat and Hamilton 1976). It naturally follows that

k < 1 → The loss of neutrons dominates the production of neutrons and the fission chain reaction dies out over time

k = 1 → The production and loss rates of neutrons are equal and the fission reaction is self-sustaining. This state is referred to as critical.

k > 1 → The production rate of neutrons is higher than its loss rate and the fission rate and the number of neutrons will go on increasing exponentially.

Two types of multiplication factors are generally used: k_∞ which is valid only for infinite systems with no leakage, and k_{eff} for practical application that takes leakage of neutrons into account.

A rather useful term in reactor physics to represent how much the system is removed from criticality is the reactivity of the system given by equation-1.7

$$\rho = \frac{k_{\mathrm{eff}} - 1}{k_{\mathrm{eff}}}, \tag{1.7}$$

Consequently a negative reactivity implies that the system is subcritical ($k_{\mathrm{eff}} < 1$), a positive reactivity ($k_{\mathrm{eff}} > 1$) implies the system is supercritical and the reactivity is 0 ($k_{\mathrm{eff}} = 1$) for critical systems.

1.2.5 Temperature Coefficients of Reactivity and Doppler Broadening

Many parameters that determine the k_{eff} of a system depend on temperature. Thus a change in temperature of materials in the system alters the reactivity of the system. The extent to which the reactivity is affected by changes in temperature is given in terms of the temperature coefficient of reactivity (Lamarsh 1977), denoted as α_T and is defined by the relation given in equation-1.8,

$$\alpha_T = \frac{d\rho}{dT} \tag{1.8}$$

Using the definition of ρ from equation 1.7 and differentiating, α_T can also be given as shown in equation-1.9

$$\alpha_T = \frac{1}{k^2}\frac{dk}{dT} \tag{1.9}$$

The algebraic sign of α_T has a huge impact on the response of the reactor. If α_T is positive, an increase in reactor temperature leads to an increase in reactivity which in turn leads to an increase in reactor power and a further increase in temperature. Thus, in the absence of external intervention, a positive α_T causes the temperature to go on increasing at a rate determined by the magnitude of α_T until the reactor melts. On the contrary, a negative α_T reduces the reactor power on temperature increase making the reactor inherently stable. The magnitude and sign of temperature coefficient of reactivity thus have a significant bearing on the safety of a reactor.

The fuel temperature feedback is negative for most of the reactors because of the phenomenon called as nuclear Doppler effect (Lamarsh 1977). As shown in Figure-1.1, at intermediate energies between thermal and fast regions, the absorption cross-section (sum of fission and capture cross-section) shows large resonances in nuclides like ^{238}U and ^{239}Pu. This resonances are described assuming that the nuclei are at rest condition with zero energy. When the temperature of nuclei increases, the atoms gain thermal motion owing to increase in their thermal energy. Thus even a mono-energetic beam of neutrons appears to the nuclei to have a continuous energy spectrum leading to the resonance peaks becoming shorter and wider as the temperature increases. This change in shape of the resonance is called as Doppler broadening. Although the shape changes, the total area under the resonance curve remains the same and the number of neutrons absorbed in the resonance is then proportional to the average neutron flux in the resonance. Now, as the temperature increases, the magnitude of absorption cross-section decreases due to the Doppler effect and this in turn causes the average flux to increases. This implies that as temperature increases, flux increases and consequently resonance absorption increases.

Although the resonance absorption increases both the fission and capture cross section, given the large amount of non-fissile ^{238}U in the fuel, the capture phenomenon tends to be more dominating. This decreases the multiplication factor and thus accounts for the negative fuel temperature coefficient of reactivity. ^{239}Pu has a resonance peak at 0.3 eV and it is fissile, resulting in a gradual decrease in the k_{eff} with burnup in reactors where production of ^{239}Pu is significant as compared to the amount of ^{235}U (eg. CANDUs) but since the CNB uses HALEU fuel, the impact of ^{239}Pu is expected to be negligible since the production of ^{239}Pu will be small as compared to the amount of ^{235}U in the reactor at any point of time.

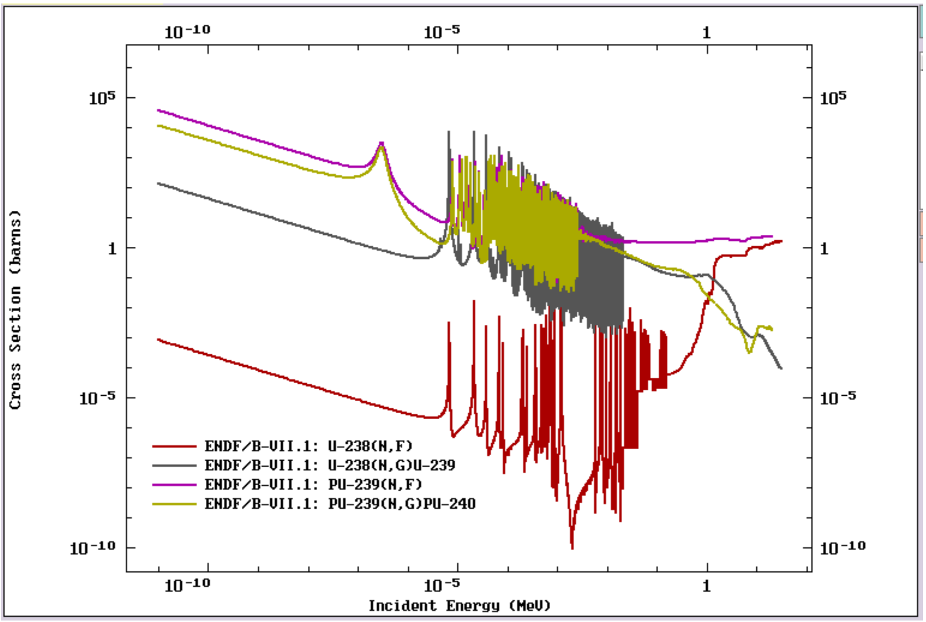

Figure 1.1: Neutron fission and capture cross section for ^{238}U and ^{239}Pu(Zerkin 2021).

1.2.6 Neutronic and Thermal-hydraulic Coupling

Neutronic and Thermal-hydraulic coupling is one of the most important design and operational aspect of nuclear reactors. A coupled system is defined as two or more distinct sub-systems where each sub-system is governed by its own set of differential equations but some of the variables are shared so that the sub-systems cannot be solved separately (Lewis et al. 1984). The neutronic and thermal-hydraulic coupling is characterized mainly by the fact that the neutron interaction cross-sections are a function of material temperatures which impacts the reactivity coefficients. As a result, the spatial power distribution in the reactor is significantly impacted by changes in the core material temperatures. Since coolant density is a direct function of temperature for most of the fluids, the spatial density variations also affect the reactor neutronic behavior, especially if the coolant is a strong neutron absorber and/or moderator. The steady-state neutronic & thermal-hydraulic coupling is an iterative process and is better explained with the flowchart shown in Figure-1.2 The basic steps followed for neutronic and thermal-hydraulic coupling are:

1. The first run of the neutronic solver to obtain the power distribution in the reactor is done with nominal temperature and density values
2. The power distribution so obtained serves as an input for the first run of the TH solver which calculates the spatial variation of temperature and density of the coolant
3. The temperature and density distribution is fed back to neutronic solver which takes into account the reactivity feedback from the variation of the temperature and densities
4. A new power distribution is calculated and checked for convergence with the values from the previous iteration
5. If the convergence is not reached, the next iteration of the TH solver run is carried out with the updated power distribution profile and the loop continues until convergence is obtained.

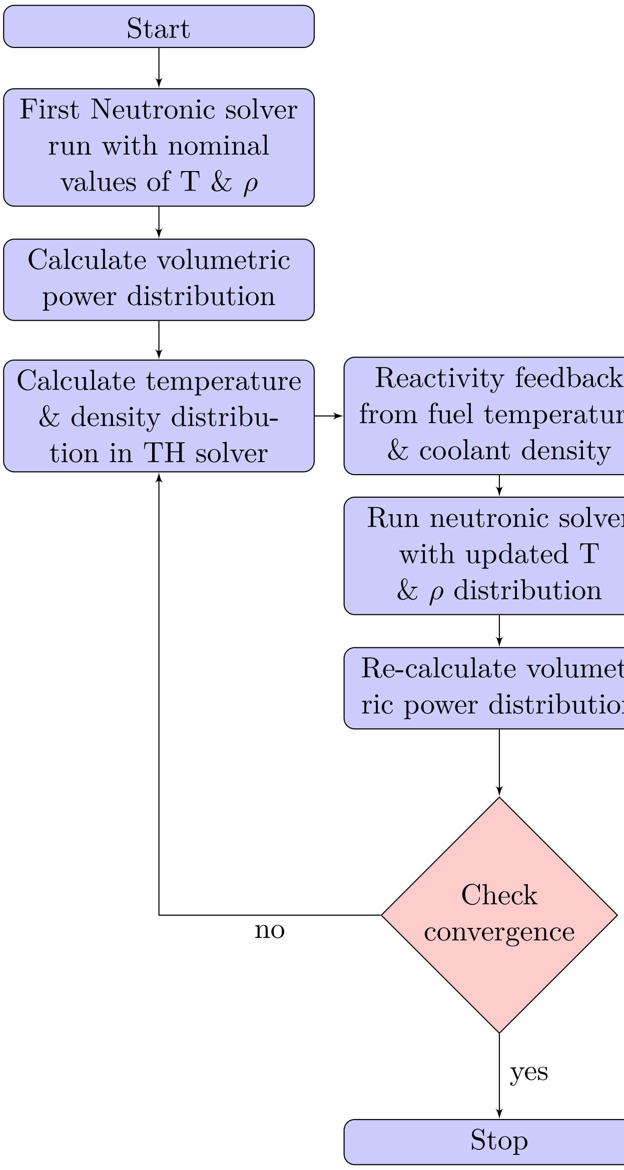

FIGURE 1.2: Flow chart for neutronics and thermal-hydraulic coupling.

Chapter 2

Reactor Core Design Description

2.1 CNB Design Overview

The Nuclear Battery program originated in Canada in 1984 at Atomic Energy of Canada Limited (AECL) in collaboration with the Los Alamos National Laboratory (LANL) to develop a 20 kWe nuclear power supply but was later canceled. (Kozier and Rosinger 1988) The name 'Nuclear Battery' highlights the passive and solid-state feature of the core, where the graphite core block acts as a thermal energy storage cell.

The current design of CNB can produce 2.4 $\mathrm{MW_{th}}$ for a fuel lifetime of 20 effective full power years(EFPYs). The fuel in the CNB is based on TRISO (triply-isotropic) coated fuel particles. The fuel kernel is spherical, about 0.5 mm in diameter, and consists of high assay low enriched Uranium (HALEU, $< 20\%$ ^{235}U). Each fuel particle is protected by coating it in successive layers of low-density buffer graphite, high-density pyrolitic carbon, silicon carbide ceramic, and an outer layer of pyrolitic carbon resulting in TRISO particles of less than 1 mm in diameter. The TRISO particles are mixed in graphite binder to form cylindrical fuel rods around 2.5 cm in diameter. There are around 500 fuel rods in the core arranged in a hexagonal lattice with a solid graphite moderator surrounding them. The core graphite moderator is further surrounded by graphite radial reflector as well as graphite top and bottom reflectors to achieve a good neutron economy. The reactor dimensions are approximately 4 m in diameter and 2.5 m height.

The core operates at a nominal temperature of 773 K. Heat is transferred from fuel compacts via conduction through solid graphite moderator to the alkali metal heat pipes regularly dispersed in the core lattice. The heat pipes are sealed metal tubes around 5 cm in diameter and 3 m high. The heat pipes are thin-walled and constructed of niobium alloy since it has good resistance to creep at high temperatures. A wick structure lines the inside of the heat pipe to provide uniform distribution and return path for liquid working fluid without interfering with the fast-moving central vapor core. Each heat pipe consists of a few hundred grams of alkali liquid metal like sodium or potassium which act as the heat transfer working fluid. The heat pipe passively transfers large amounts of heat in a near isothermal manner since the heat transfer is predominantly by latent heat through a phase change. The active cooling pumps are conspicuous by their absence and the core cooling is completely passive while also increasing overall thermal efficiency by eliminating pumping losses. The heat is transferred to the organic secondary coolant circulating through tubes coiled around the condenser portion of heat pipes outside the core which is referred to as vaporizer. Each heat pipe has its individual vaporizer which is connected to common inlet and outlet headers. The heated supercritical vapor then goes through an organic Rankine cycle and electricity is produced with a Carnot efficiency of approximately 54% (Kozier and Rosinger 1988).

Reactivity control is provided by solid neutron absorber control and shutdown rods, while long-term reactivity control is provided by burnable absorber particles mixed in the fuel compacts. This helps in bringing the reactivity swing for 20 years of full power operation within the limits of the reactivity control system as well as flattens the core radial flux profile. The high-level features of the CNB reactor core module are shown in Figure-2.1.

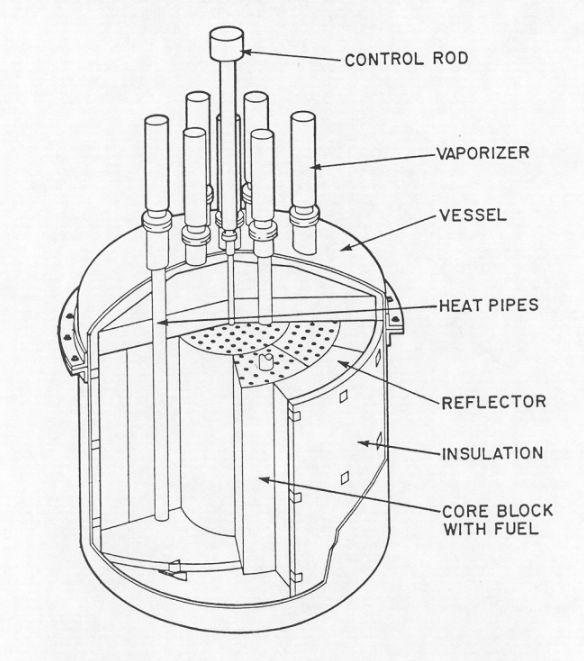

FIGURE 2.1: Design features of the CNB reactor core module(Kozier and Rosinger 1988).

2.2 Reactor Core Design

The current study discusses the analysis of two core designs (Core-A and Core-B), with Core-A design being closer to the original design by AECL for 15 full power years of operation (FPOY) and the Core-B design being an optimized one for an operational life of 20 FPOY. The analyses carried out to arrive at the final design parameters (materials and dimensions) for Core-B are discussed in Chapter-4. The common design features shared by both the cores are:

1. The core layout resembles a regular hexagon consisting of $\approx$ 500 fuel rods, $\approx$150 heat pipes, and solid boron carbide reactivity control & shutoff rods.
2. The inter-space between the fuel rods, control rods, and the heat pipes is filled with graphite moderator.
3. The core is surrounded by a cylindrical radial reflector, top and bottom graphite reflector around 60 cm thick(Penner and Donnelly 1987).
4. The control rods and heat pipes penetrate the top reflector to pass into the core while the bottom reflector is completely solid.

2.3 Use of burnable poison and core zoning

A fundamental feature of the CNB design is lifetime refueling, resulting in a large excess reactivity at the Beginning of Life (BOL) which needs to be accounted for. If active reactivity devices like movable control rods are used to control the excess reactivity over the entire operational life of the reactor they could introduce significant concerns with respect to reactor safety and would require the use of extremely fast-acting engineered safety systems. One of the best ways to passively reduce the excess reactivity in the core at BOL is the use of burnable poisons. Burnable poison remains in the core and does not need to be actively controlled thus eliminating any safety concerns with respect to their accidental removal.

2.3.1 Selection of Burnable Poison Nuclide

Burnable poisons are nuclides (e.g. ^{167}Er, ^{157}Gd) that have a high neutron absorption cross-section, but on the absorption of neutrons get converted into materials of relatively low absorption cross-section. As a result, at the BOL, they provide very high negative reactivity but as the reactor operates, the poison material burns up and the negative reactivity of the burnable poison decreases over the life of the reactor. Ideally, the poison should decrease its negative reactivity worth at the same rate that the fuel's excess positive reactivity is depleted[1]. The depletion of poison and fuel is a function of their neutron absorption cross-section. Hence, the burnable poison selected was ^{167}Er in the form of natural erbium oxide (Er_2O_3) since it has a similar cross-section as ^{235}U as shown in the Figure-2.2(Zerkin 2021).

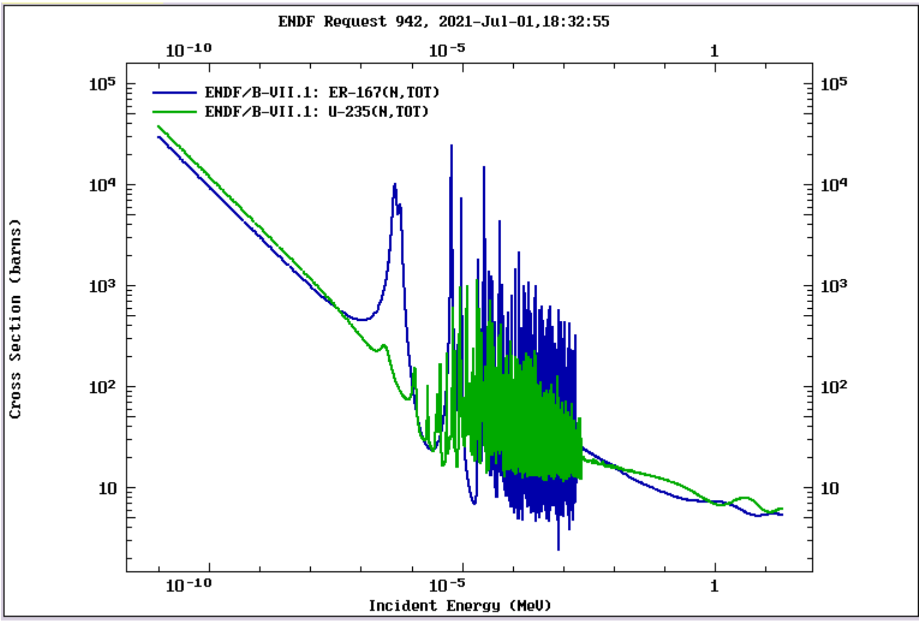

FIGURE 2.2: Comparison of ^{235}U and ^{167}Er cross-sections(Zerkin 2021).

The natural isotopic abundance of various isotopes of erbium used in this study is shown in Table-2.1(De Biévre et al. 1984).

2.3.2 2-Zone Core

Burnable poison in the form of spherical particles is used in this study. The use of spherical burnable particles offers some degree of freedom in design that can be used to 'tailor' the excess reactivity as a function of core burn up (Dam 2000). For distributing burnable poison particles in the core, it is divided into two zones with poison located in the central area of the core and no poison in the outer area of the core. At BOL the poison in the central part of the core shifts the thermal flux outwards resulting in a higher neutron leakage and lower k_{eff}. Additionally, over the reactor life the burnup in

---

[1] Theoretically, the poison should deplete at a slightly higher rate so that it burns out completely by the end of life resulting in lowest fuel penalty

Table 2.1: Natural abundance of erbium isotopes.

Isotope	Abundance (%)
Er-162	0.137
Er-164	1.609
Er-166	33.61
Er-167	22.93
Er-168	26.79
Er-170	14.93

the central poisoned portion of the core is less than that what it would have been in the absence of poison which results in a higher k_{eff} at End of Life (EOL)

In this case, there are two types of fuel that are used: one with poison particles mixed uniformly with fuel TRISO particles in the fuel compact and the other with no poison particles. The packing fraction for both the fuel types is 55%. Spherical natural Erbium Oxide particles are dispersed with the fuel TRISO particles in the inner zone, while the fuel rods in the outer zone consist of only fuel particles. The inner zone extends from the reactor center-line radially out to around 11 pitch lengths and consists of 300 fuel rods; the outer zone contains the remaining 222 fuel rods. The core zoning is illustrated for quarter core in Figure-2.3. The optimum size of the Er_2O_3 particles is found to be 150μm which is just adequate for providing the required reactivity worth at the BOL as well as for the self-shielding needed to spread the worth of poison over the entire life of the reactor.

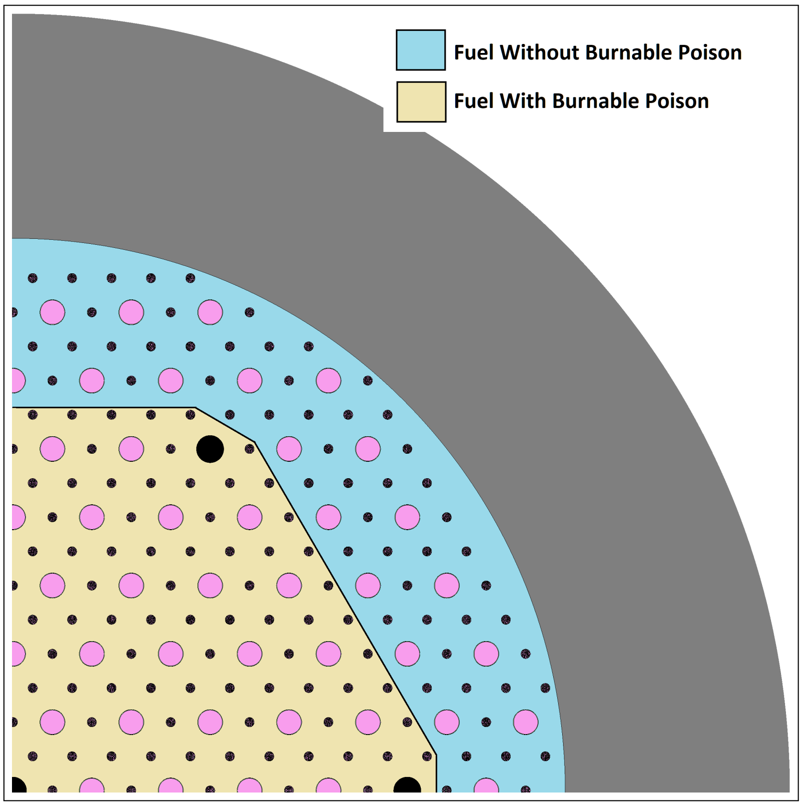

Figure 2.3: Two-zone core design for the CNB.

Chapter 3

Simulation Methodology

Serpent is a multi-purpose three-dimensional continuous-energy Monte Carlo particle transport code, developed at VTT Technical Research Centre of Finland, Ltd. The development started in 2004, and the code has been publicly distributed by the OECD/NEA Data Bank and RSICC since 2009. Serpent started as a simplified reactor physics code for the generation of homogenized group constants but the capabilities have extended well beyond traditional reactor physics modeling for the current development version, Serpent 2. Serpent can be run in parallel in multi-core workstations using thread-based OpenMP. In addition to the transport simulation, parallelization is also available for the burnup calculations. The applicability of Serpent can be roughly divided into three categories (Leppänen et al. 2014):

1. Traditional reactor physics applications, including spatial homogenization, criticality calculations, fuel cycle studies, research reactor modeling, validation of deterministic transport codes, etc.

2. Multi-physics simulations i.e. coupled calculations with thermal-hydraulics, CFD, and fuel performance codes

3. Neutron and photon transport simulations for radiation dose rate calculations, shielding, fusion research, and medical physics

3.1 Salient Features of Serpent

3.1.1 Geometry and particle tracking

The geometry description in Serpent is based on a universe-based constructive solid geometry (CSG) model similar to MCNP. This allows us to define practically any two- or three-dimensional core configuration. The CSG geometry is composed of material cells which are defined by elementary and derived surfaces that can be combined using Boolean operators such as intersection and unions. Serpent has conventional square and hexagonal lattices and provides special geometry types for randomly-dispersed particle fuel which has been extensively used in this thesis to model and disperse the TRISO particles in the graphite binder fuel compacts.

The geometry model in Serpent reads the coordinates of fuel and poison particles from a separate input file and generates the geometry as it is defined, without any approximations. The model works on several levels (particles inside a pebble and pebbles inside the core) and it has been tested in realistic double-heterogeneous reactor configurations consisting of over 60 million randomly positioned units (Suikkanen et al. 2010)(Rintala et al. 2015).

The particle transport in Serpent is based on the combination of conventional surface-tracking and the Woodcock delta-tracking method (Woodcock et al. 1965). This tracking method is proven to be efficient for cases where the particle mean free path is long as compared to the dimensions. This is typical of the neutronic calculations involving TRISO particles fuel. The traditional delta-tracking method is subject to certain efficiency problems related to localized heavy absorbers, which in Serpent are avoided by switching to surface-tracking when necessary (Leppänen 2010). The main drawback of delta-tracking is that the track-length estimate of particle flux is not available, and reaction rates have to be calculated using the potentially less-efficient collision estimator. This is usually not a big issue unless reaction rates are calculated in volumes where the collision density is low.

3.1.2 Neutron Interaction Data Libraries

Serpent uses continuous-energy cross-sections data in the form of ACE format data libraries. The neutron interaction cross sections are based on collision kinematics, ENDF reaction laws, and probability table sampling in the unresolved resonance region. Cross-section libraries that are provided in Serpent installation are JEFF-2.2, JEFF-3.1, JEFF-3.1.1, ENDF/B-VI.8, and ENDF/B-VII evaluated nuclear data files. The data is available for 432 nuclides and spans temperatures between 300 and 1800K in steps of 300K. (Leppänen et al. 2014) Temperature-dependent neutron scattering data is also available for light and heavy water and graphite. Since the data format is shared with MCNP, any continuous-energy ACE format data library generated for MCNP can be used with Serpent as well. As a consequence, the results from Serpent calculations can be expected to agree with MCNP to within the bounds of statistical uncertainty. For the analysis in this thesis, cross-section data from ENDF/B-VII is used.

During the simulation run the continuous energy cross-section data available from the libraries is stored in the form of a unionized energy grid, used for all reaction modes (Leppänen 2009). This results in a significant improvement in computational performance in terms of processing power as the macroscopic cross-sections for each material are pre-generated before the transport simulation, instead of calculating the cross-sections by summing over the constituent nuclides during tracking. The drawback is that more computer memory is required for storing redundant data points. This becomes quite significant in burnup calculations as it may include hundreds of actinides and fission products. To overcome this issue, Serpent 2 provides different optimization modes for small and large burnup calculation problems, in which the unionized energy grid approach is used selectively (Leppänen and Isotalo 2012).

3.1.3 Doppler-broadening of Cross Sections

Since the neutron interaction data libraries are available only in temperature steps of 300 K, an interpolation routine is required to get accurate cross sections at intermediate temperature points. For this purpose, Serpent has a built-in Doppler-broadening preprocessor routine which allows adjusting the temperatures of ACE format cross-sections. The method has been validated with good results and the routine works efficiently without significant computational overhead (Viitanen et al. 2009).

Another option for adjusting the material temperatures, which is specially developed for multiphysics calculation and used in the neutronic and thermal-hydraulic coupling in this thesis is the target motion sampling (TMS) on-the-fly temperature treatment routine since it can model a wide variety of material temperatures or even continuous temperature distributions. Instead of averaging the cross-sections over the Maxwellian distribution (actual Doppler-broadening), the TMS method accounts for thermal motion explicitly, by making a coordinate transformation in the target-at-rest frame before handling the collision physics. (Viitanen et al. 2015).

3.1.4 Burnup Calculation Methodology

The burnup solver is built into Serpent and does not require coupling to any external code. Burnable materials can be sub-divided into depletion zones automatically using the divisor routine available in Serpent. The irradiation history can be defined in units of time or the actual burnup. Either the total power, power density, flux, or fission rate can be used for normalization of the reaction rates and the irradiation history can be subdivided into several separate depletion intervals (uniform or non-uniform). Standard ENDF format data libraries are available for reading radioactive decay data and fission yield data used in the burnup calculations. The concentrations of all included nuclides that have decay data are tracked during the burnup calculation. Flux averaged transmutation cross-sections can be calculated by Serpent either during the transport simulation or by calculating cross-section using the fine-group flux spectrum tallied for each material once the transport calculation finishes.

The method used in this thesis for solving the Bateman equations is the built-in Transmutation Trajectory Analysis (TTA) method (Cetnar 2006), based on the analytical solution of linearized depletion chains. The second option available in Serpent is the Chebyshev Rational Approximation Method (CRAM), an advanced matrix exponential solution developed for Serpent at VTT(Pusa and Leppänen 2012), the potential of which to improve computational performance for the current study can be explored in the future. In any case, the two methods have been shown to yield consistent results, when used with Serpent (Leppänen and Pusa 2009).

Burnup Algorithms

The solution to Bateman equations assumes that the transmutation cross-sections remain constant in time. This is not the case in reality, since nuclide compositions change over time changing the transmutation cross-section. This necessitates the division of burnup interval into multiple timesteps in between which the transmutation cross-sections remain constant. Thus finding the optimal step length becomes very significant to the accuracy of the solution. To reduce the dependence of the solution accuracy on the division of the burnup interval certain algorithms can be developed which represent the average composition of nuclides in between the time steps better than the values at the beginning of the step. These methods are known as the predictor-corrector method (PCC). Serpent 2 provides many high-order predictor-corrector methods (Isotalo and Aarnio 2011), however, the one that was used in the current study is the Linear Extrapolation(LE) method. Linear Extrapolation is a new method introduced in Serpent 2 and shows good results despite its simplicity with a negligible increase in computational time. The basic steps that are followed in the LE method are given below:

1. Run the transport calculation and evaluate the flux and the transmutation cross-sections

2. Use Constant Extrapolation if this is the first burnup step to calculate the flux and cross-sections
3. If it is not the first burnup step, run a linear extrapolation using the flux and cross-sections values from previous and current burnup step and recalculate the flux and cross-sections
4. Form the burnup matrix and solve the Bateman equations to arrive at the nuclide composition at the end of the current step
5. Run a transport calculation using the nuclide composition calculated above and obtain the flux and cross-sections
6. The flux and cross-sections calculated at this step will be stored and used as the previous step values in the next burnup step's predictor calculations
7. Proceed with the next burnup step

3.2 Serpent Input and Output Files

The Serpent code has no interactive user interface. All communication between the code and the user is handled through one or several input files and various output files. The part of Serpent simulation that requires the most rigor is setting up the input files. The input files provide serpent with the information about the geometry of the core model, the material composition of the components constituting the core, calculation specific inputs like the criticality source description (number of neutron histories, number of active and inactive cycles, etc.), burnup algorithms, nuclear data libraries to be used for transport, decay and fission yield, method of solving Bateman equation, a method for Doppler broadening, output specific tallies like flux tally, heat deposition tallies, etc. to name a few.

The output files that serpent creates after the simulation is completed, provide detailed information about the calculation criticality eigenvalues viz. the effective multiplication factor (analog and implicit) and the infinite multiplication factor, normalized reaction rates like fission rate, capture rate, etc., values of the six-factor formula, delayed neutron parameters, burnup information of the nuclide composition at the end of irradiation steps, and outputs of the tallies set up before the simulation, etc. Serpent also provides a graphical plotter that can plot the projection of a 3D serpent geometry in all the 3 planes showing errors with overlaps and voids, if any, and also boundaries between the materials.

For better code modularity to run various simulation cases and also to increase the code coherence, the input files of Serpent were divided into multiple parts each dealing with a particular aspect of input. Additional input files are recursively read from the main file using the include-command:

include <filename>,

where <filename> is the file path for the input file by serpent (Leppänen et al. 2014).

This approach aids in the running of various cases which share partial data, by eliminating the need to create input files with redundant information for each case. Only the portion pertinent to the case can be changed in a file and this file can be included while others can be reused[1].

3.2.1 Geometry Input File

The Serpent code uses a universe-based geometry meaning geometry is divided into separate universes, which are all constructed independently and then can be nested inside the other. This allows building a complex geometry like the entire reactor core by dividing it into smaller parts which are much easier to design. This also ensures that regular structures like square and hexagonal lattices which are very common to reactor cores can be easily modeled. For example, for the CNB reactor core model, the highest level consists of a fuel compact in which the TRISO fuel particles are dispersed in a graphite binding matrix. Each compact is defined independently in its universe.

The next level is the hexagonal cell in which the fuel compact is surrounded by the graphite moderator. Similarly, universes are created for control rods and heat pipes hexagonal cells too. The next level is the main core in which the fuel, control rod, and heat pipe universes are arranged in a near hexagonal lattice. Finally, in the last level, this core lattice is surrounded by radial and axial reflectors. The basic building block of each universe is the cell, which is a region in space bounded by predefined surfaces. Each cell can be filled either with homogeneous material composition, void, or another universe.

---

[1] For eg. in lattice pitch optimization study only the file describing the geometry needed to be modified while others were reused as is.

TRISO particle modeling and dispersal routine

Serpent allows creation of randomly dispersed particles to account for the heterogenity effects and even provides an automated dispersal routine, which prompts the user with several questions and produces a particle distribution file containing the cartesian coordinates of dispersed particles in a predefined bounded space. Input option "-disperse" launches the automated particle disperser routine. A screenshot of the routine as used in the current study to disperse TRISO particles in a 15cm high and 1.2cm radius cylindrical fuel compact is shown in 3.1

As inputs, the disperser routine requires the user to select from a predefined list of the geometry shape in which the particles need to be dispersed (cylindrical fuel compact in this case), the radius of the fuel compact, the radius of the particles (TRISO fuel particles in this case) and the packing fraction. Serpent also provides a grow and shake algorithm to improve the computational performance of the routine for packing factors greater than 0.3. The algorithm consists of an initial sampling of random points within the geometry, with acceptance criteria based solely on the points existing within the geometry and populating them with zero-sized particles the number of which for the specified particle size would provide the desired packing fraction. The routine then starts iterating by randomly shifting the particles and slowly allowing them to grow. In each iteration, each particle grows by a user-specified growth factor and shifts in a random direction and a maximum distance as specified by the shake factor. Should the growth cause particle overlap with others, cross the boundary, or exceed the specified size, then the particle is left at its current size until the next iteration. Similarly, should the particle shift cause it to overlap with other particles or cross the target boundary then the particle is left in its original location until the next iteration. This gradual growing and shifting of particles are continued until all particles have met the target particle size(Cole 2015). The growth and shake factors are specified as fractions of particle radius and were found by trial and error to be 0.05 and 0.1 to achieve a packing fraction of 0.55.

The output from the routine is in the form of a file containing the columns giving the x, y and z coordinates of the particle dispersed as well as the radius of the particle and the universe it belongs to. The fuel geometry can be created from this file.

The *'particle'* keyword creates a particle universe consisting of nested spherical shells. The boundaries are defined by sphere surfaces which form all the layers of the TRISO particles. The line 'cell p1c p1 graphF -p1s' defines the graphite binder background

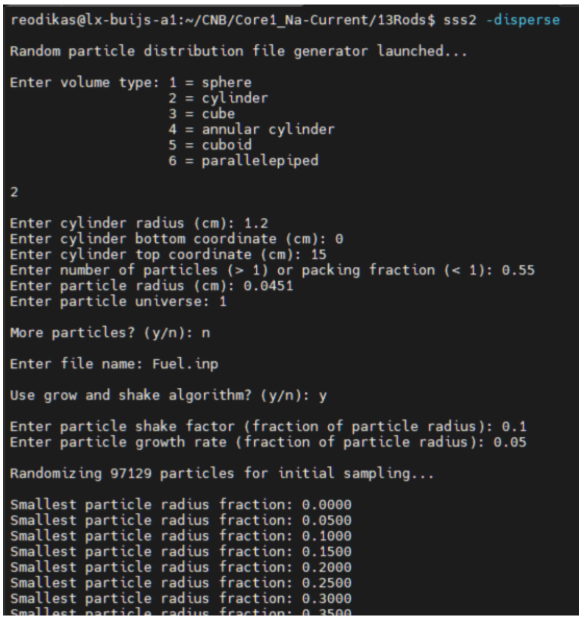

```
reodikas@lx-buijs-a1:~/CNB/Core1_Na-Current/13Rods$ sss2 -disperse

Random particle distribution file generator launched...

Enter volume type: 1 = sphere
                   2 = cylinder
                   3 = cube
                   4 = annular cylinder
                   5 = cuboid
                   6 = parallelepiped

2

Enter cylinder radius (cm): 1.2
Enter cylinder bottom coordinate (cm): 0
Enter cylinder top coordinate (cm): 15
Enter number of particles (> 1) or packing fraction (< 1): 0.55
Enter particle radius (cm): 0.0451
Enter particle universe: 1

More particles? (y/n): n

Enter file name: Fuel.inp

Use grow and shake algorithm? (y/n): y

Enter particle shake factor (fraction of particle radius): 0.1
Enter particle growth rate (fraction of particle radius): 0.05

Randomizing 97129 particles for initial sampling...

Smallest particle radius fraction: 0.0000
Smallest particle radius fraction: 0.0500
Smallest particle radius fraction: 0.1000
Smallest particle radius fraction: 0.1500
Smallest particle radius fraction: 0.2000
Smallest particle radius fraction: 0.2500
Smallest particle radius fraction: 0.3000
Smallest particle radius fraction: 0.3500
```

(A) Input

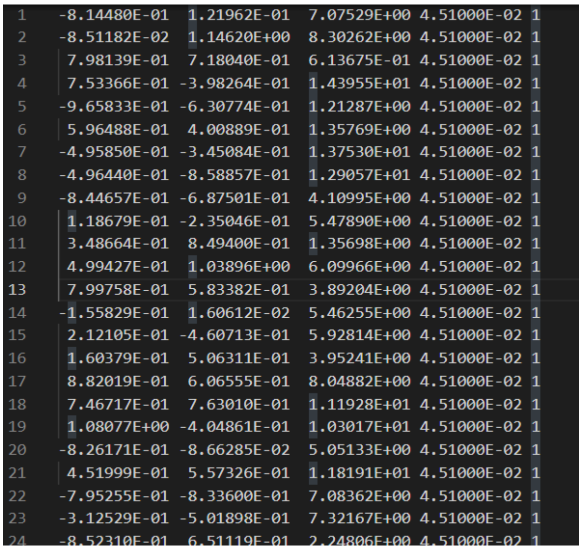

```
-8.14480E-01  1.21962E-01  7.07529E+00 4.51000E-02 1
-8.51182E-02  1.14620E+00  8.30262E+00 4.51000E-02 1
 7.98139E-01  7.18040E-01  6.13675E-01 4.51000E-02 1
 7.53366E-01 -3.98264E-01  1.43955E+01 4.51000E-02 1
-9.65833E-01 -6.30774E-01  1.21287E+00 4.51000E-02 1
 5.96488E-01  4.00889E-01  1.35769E+00 4.51000E-02 1
-4.95850E-01 -3.45084E-01  1.37530E+01 4.51000E-02 1
-4.96440E-01 -8.58857E-01  1.29057E+01 4.51000E-02 1
-8.44657E-01 -6.87501E-01  4.10995E+00 4.51000E-02 1
 1.18679E-01 -2.35046E-01  5.47890E+00 4.51000E-02 1
 3.48664E-01  8.49400E-01  1.35698E+00 4.51000E-02 1
 4.99427E-01  1.03896E+00  6.09966E+00 4.51000E-02 1
 7.99758E-01  5.83382E-01  3.89204E+00 4.51000E-02 1
-1.55829E-01  1.60612E-02  5.46255E+00 4.51000E-02 1
 2.12105E-01 -4.60713E-01  5.92814E+00 4.51000E-02 1
 1.60379E-01  5.06311E-01  3.95241E+00 4.51000E-02 1
 8.82019E-01  6.06555E-01  8.04882E+00 4.51000E-02 1
 7.46717E-01  7.63010E-01  1.11928E+01 4.51000E-02 1
 1.08077E+00 -4.04861E-01  1.03017E+01 4.51000E-02 1
-8.26171E-01 -8.66285E-02  5.05133E+00 4.51000E-02 1
 4.51999E-01  5.57326E-01  1.18191E+01 4.51000E-02 1
-7.95255E-01 -8.33600E-01  7.08362E+00 4.51000E-02 1
-3.12529E-01 -5.01898E-01  7.32167E+00 4.51000E-02 1
-8.52310E-01  6.51119E-01  2.24806E+00 4.51000E-02 1
```

(B) Output

Figure 3.1: Disperser routine to obtain randomly dispersed TRISO particles in fuel compact.

universe in which the particles are to be dispersed. The *'pbed'* keyword fills the graphite binder background with the particles defined by the *'particle'* keyword at coordinates defined in the file generated by the disperser routine. The fuel compacts can now be stacked on top of each other to create one complete fuel rod and this is done by using the *'lat'* keyword. The geometry of the fuels containing both the TRISO and burnable poison particles can be created similarly. The geometry plot showing the distribution of TRISO particles in the fuel is shown in figure-3.2

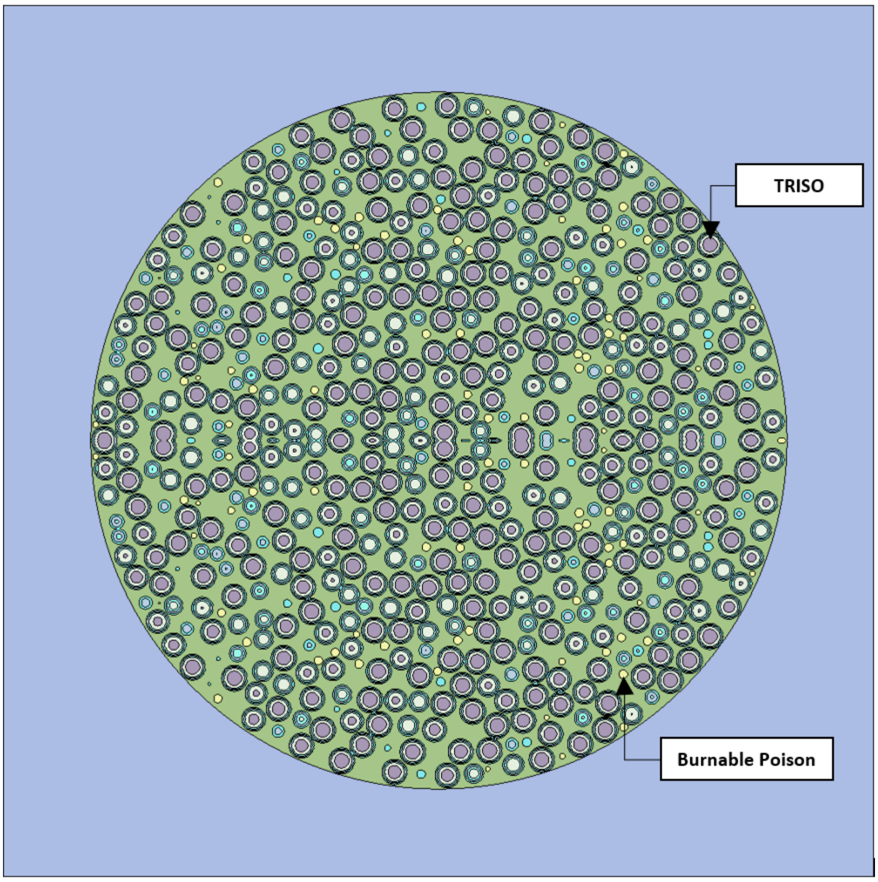

FIGURE 3.2: Serpent Geometry plot showing TRISO and burnable poison particles.

Core Assembly and the Reactor Geometry Model

Individual universes are created for the heat pipe and control rods/shutoff rods (CR/SRs) by using surf and cell commands as discussed above. Each of the 3 CR/SRs universes are exactly similar but defined separately so that they can be simulated to move in and out of the core independently.

The heat pipe, control rod and the fuel rod universe can now be nested and arranged to create the core lattice universe as shown in figure-**??**. The *'lat'* card is used for defining a finite two-dimensional lattice in xy-plane with square or X- or Y-type hexagonal elements. The lattice is infinite in z-direction. Beside the *'lat'* keyword appear options specifying:

UNI : universe name of the lattice

TYPE : lattice type (2 = x-type hexagonal)

X0: x-coordinate of the lattice origin

Y0: y-coordinate of the lattice origin

NX: number of lattice elements in x-direction

NY: number of lattice elements in y-direction

PITCH: lattice pitch

This is followed by a list of $NX \times NY$ universes. Universe 'F1' is the universe of fuel not containing burnable poison, 'F2' is that of the fuel containing burnable poison, 'c1, c2, and c3' specify the reactivity control rod universes, 'hp' specifies the heat pipe universe while '`--`' is the moderator graphite universe that surrounds the space not containing any of the above.

Universe symmetries (*'usym'* card) can be used to simplify construction of complex geometries and also to reduce the number of burnable material zones and thus save computational time. This is used to convert the defined $1/6^{th}$ geometry to whole core geometry. The input values for *'usym'* card are:

UNI: universe name

AX: symmetry axis (3 = z)

BC: boundary condition (2 = reflective)

X0: x-coordinate of the origin

Y0: y-coordinate of the origin

θ_0: azimuthal position where the symmetry segment starts (300°)

θ_w: width of the segment (60°)

The infinite core assembly is then bound by radial, top and bottom reflector to create a finite 3D geometry. The top and front-view of the geometry output plot produced by Serpent is labeled to highlight the different regions and is shown in figure-3.3

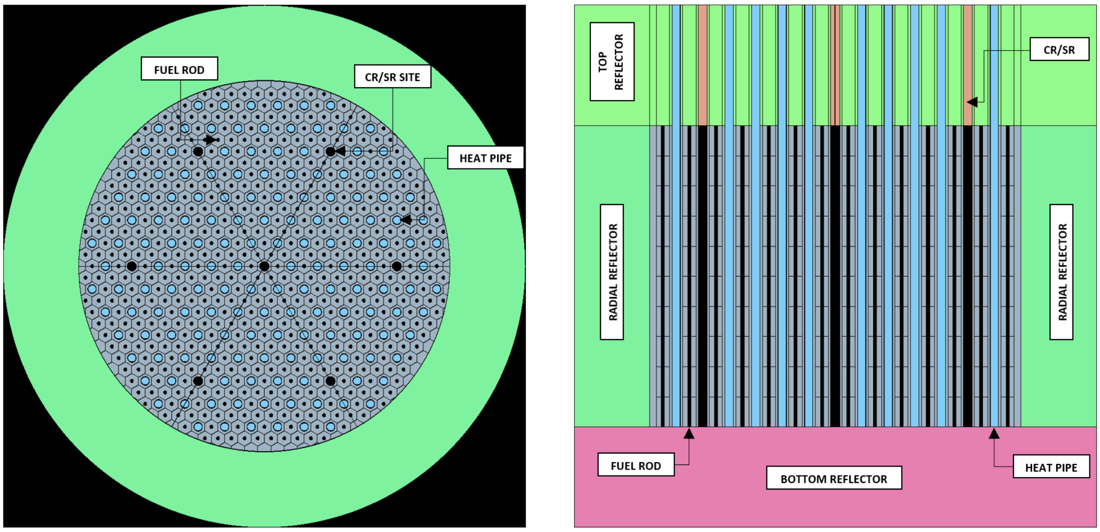

(A) Top View (B) Front View

FIGURE 3.3: Serpent output for reactor geometry.

3.2.2 Material Definition Input

The material definition input is provided using the *'mat'* card in Serpent. For the current study, the material input is provided in a separate file and is included in the main file during Serpent input run. Each material consists of a list of nuclides and each nuclide is associated with a pre-defined cross-section library. The pre-defined library files contain all necessary reaction cross-sections, along with the energy and angular distributions, fission yields, and delayed neutron parameters. Cross-section libraries generated at the correct temperatures are used to correctly model the Doppler-broadening of resonance peaks. It is even more important to use the appropriate thermal scattering libraries for moderator nuclides. Thermal scattering cross-sections are used to replace the low-energy free-gas elastic scattering reactions for some important bound moderator nuclides, such as carbon in graphite. Thermal systems cannot be modeled using free-atom cross-sections without introducing significant errors in the spectrum and the results (Leppänen et al. 2014).

The general format of providing the material composition using *'mat'* card is,
mat <name> <density> [<options>]

<Z> <A>.<id> <fraction>

where,

<Z>	is the element Z
<A>	is the isotopic mass number
<id>	is the library id (for eg. 06c means data generation at 600K)
<fraction>	is the corresponding atomic fractions (+ve values, units $10^{24}/\text{cm}^3$) or mass fraction (-ve values, units g/cm^3)

The name is a string that identifies the material when it is referred to elsewhere in the input file[2], the density of the material can either be given in atomic density (if a positive value is specified) or mass density (if a negative value is specified). The options that are used in the material specifications are,

<moder>	specifies that thermal scattering cross-sections are to be used followed by the thermal scattering data library <thname> and ZA of the scatterer
<burn>	specifies that material is to be depleted in burnup calculation
<tmp>	initiates the doppler broadening preprocessor to calculate the cross section at a temperature above the temperature of the original cross-section library

The thermal scattering cross-section library is specified using,

therm <thname> <lib>

where,

<thname>	is the name of the data library
<lib>	is the library identifier of the library file (for eg. gre7.18t specifies the use of ENDF/B-VII library for graphite at 800K)

The material composition for all other materials in the reactor core is defined similarly.

3.2.3 Solver Options

Solver options are some of the essential options required to be specified for running the static-criticality and burnup simulation in Serpent. Figure-3.4 shows the input file for these options.

Criticality Source Specification

One of the important options is the one specifying the simulated neutron population in criticality source mode. This has a significant impact both on the use of computational resources and solver precision. The population is set using a *'set pop'* card. The numbers following the *'set pop'* keyword specify the neutron population in each cycle (5000 in

---

[2] For eg. to fill a cell in the geometry input

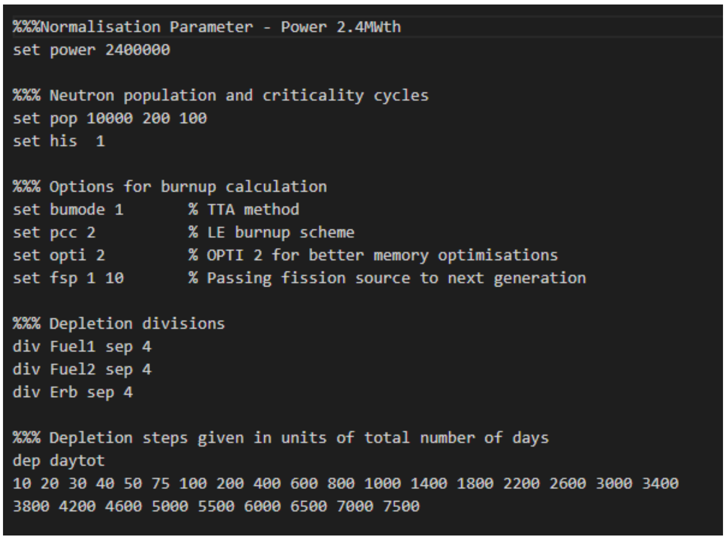

```
%%%Normalisation Parameter - Power 2.4MWth
set power 2400000

%%% Neutron population and criticality cycles
set pop 10000 200 100
set his  1

%%% Options for burnup calculation
set bumode 1       % TTA method
set pcc 2          % LE burnup scheme
set opti 2         % OPTI 2 for better memory optimisations
set fsp 1 10       % Passing fission source to next generation

%%% Depletion divisions
div Fuel1 sep 4
div Fuel2 sep 4
div Erb sep 4

%%% Depletion steps given in units of total number of days
dep daytot
10 20 30 40 50 75 100 200 400 600 800 1000 1400 1800 2200 2600 3000 3400
3800 4200 4600 5000 5500 6000 6500 7000 7500
```

FIGURE 3.4: Solver options for criticality and burnup solver.

this case), the number of active cycles (200 in this case), and the number of inactive cycles (100 in this case) respectively. The simulation is first executed for a fixed number of inactive generations to allow the fission source to converge. This is followed by several active generations, during which the results are collected.

The fission source convergence can be ensured by checking the slope of the Shannon entropy of fission distribution. It has been found that the Shannon entropy converges to a single steady-state value as the source distribution approaches stationarity (Brown 2006). In Serpent, the total Shannon entropy can be obtained by use of the 'set his' card and the number of inactive cycles can be determined by checking the convergence of Shannon entropy. Further, the number of active cycles can be determined by checking the k_{eff} convergence. A simulation was done for 100 inactive and 2000 active cycles to find the optimum number of active and inactive cycles to be run. The total Shannon entropy plotted over the number of inactive cycles and the k_{eff} plotted over the total number of cycles is shown in figure-3.5. It is clear that the fission source converges in around 40 cycles and the value of 100 selected in this study for inactive cycles is more than sufficient for the fission source to converge. This is not surprising since the overall dimension of the reactor core is small. The k_{eff} also seems to converge sufficiently till the 300 cycles and thus 200 active cycles were selected for the simulations.

To determine the optimum neutron population per cycle, cases were run using 1000, 2000, 5000, 10,000, 20,000 and 50,000 neutrons per generation. The variation of k_{eff} with the different number of neutron population is shown in figure-3.6. It can be seen that for

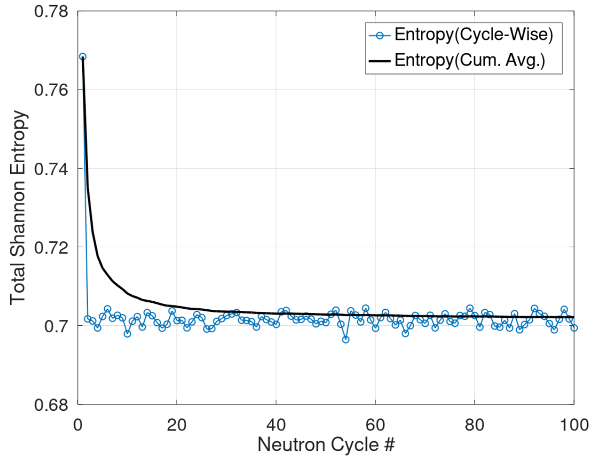

(A) Shannon entropy in inactive cycles

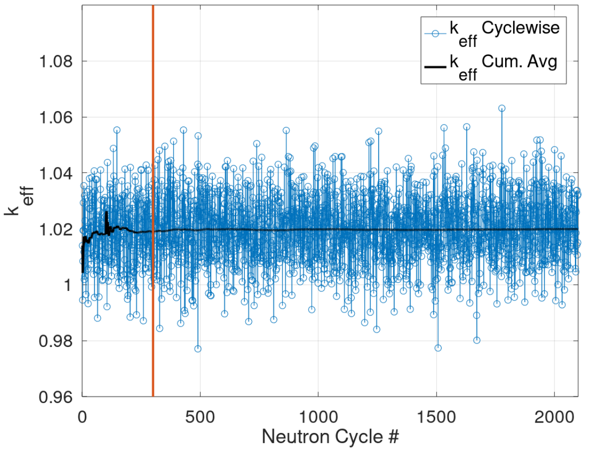

(B) Implicit k_{eff} at each neutron cycle

FIGURE 3.5: Shannon entropy and k_{eff} convergence.

neutron population above 10,000 the k_{eff} value remains almost constant and a decrease in statistical uncertainty with an increase in neutron population. Thus, considering the practical limits on computational time and resources, the use of a neutron population of 10,000 per cycle was considered optimum for the current study.

Burnup & Normalization Parameters

Normalization is needed as the integral reaction rate estimates given by a Monte Carlo simulation are more or less arbitrarily normalized, unless fixed by a pre-defined constant.

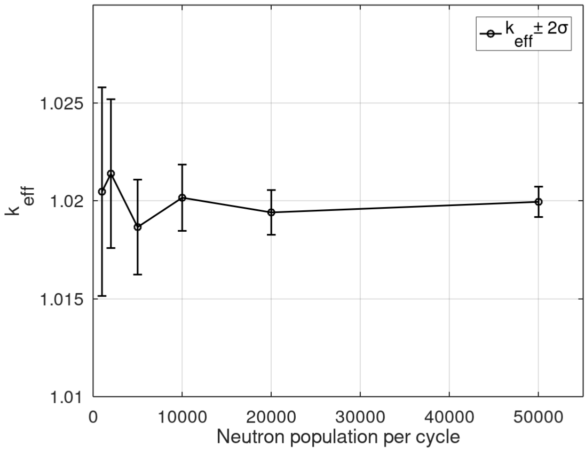

FIGURE 3.6: Variation of k_{eff} with change in neutron population.

Serpent provides a variety of options that can be used for normalization (viz. power density, total flux, fission rate, absorption rate, loss rate, etc.) In the current study, the total fission power in watts is used for normalization using the *'set power'* card.

For burnup calculations, *'set bumode'* option is specified as '1' for using Transmutation Trajectory Analysis for burnup calculation and *'set pcc'* option is set to 2 to use linear extrapolation burnup scheme as explained in section-3.1. The *'set fsp'* option is used to pass the converged fission source to each subsequent burnup cycle eliminating the need to run 100 inactive cycles for fission source convergence at each burnup step.

In burnup calculations, it is essential to subdivide the materials into multiple depletion zones. This is because even though at the beginning of life the material composition in all fuel rod locations is the same, the spatial variation in the neutron flux produces different compositions of depleted fuel at different locations. Significant errors may be introduced to the results if materials are not correctly divided into separate depletion zones. In a complex geometry like the CNB, containing millions of TRISO fuel particles and burnable poison particles, it is not practical nor necessary to use each particle as a separate depletion zone, although that would have the highest fidelity. As a result, a division is done based on fuel compacts using an automated depletion zone divisor routine provided by Serpent. The *'div <MAT> sep <LVL>'* specifies that depletion division is to be done such that each fuel compact is considered as an individual depletion zone. The parameter *LVL* following the *sep* entry determines the number of levels counted backwards from the last one ($LVL = 1$ being the outermost universe). Considering the symmetry of the core, only $1/6^{th}$ of the geometry was defined as mentioned in section

3.2.1. The 1/6th geometry consists of 55 fuel locations with burnable poison and 39 fuel locations without burnable poison. Each fuel location is axially divided into 10 subdivisions thus making a total of 940 depletion zones for fuel and 390 depletion zones for burnable poison. The fuel and burnable poison in the symmetric location in the entire core is then depleted by the same amount as its representative fuel compact in the 1/6th geometry.

With the use of the automated disperser routine, it is important to manually specify the volume of depleted material (fuel or poison) at each depletion location. To facilitate this, Serpent provides a Monte-Carlo based routine for calculating the volumes in each depletion zone. The volumes are calculated by sampling a large number of random points in the geometry, and the estimate represents the exact volumes seen by the particles during the transport simulation. This routine is invoked by command line option *'-checkvolumes'*, followed by the number of random points and the name of the input file. After the execution the routine prints out an output file *'*.mvol'* containing volumes individually for each depletion sub-zone. The contents of the mvol file are seen in figure-3.7. The relative statistical error in the volume calculation in the current study is less than 2%. This file is created before the main Serpent simulation run and the path

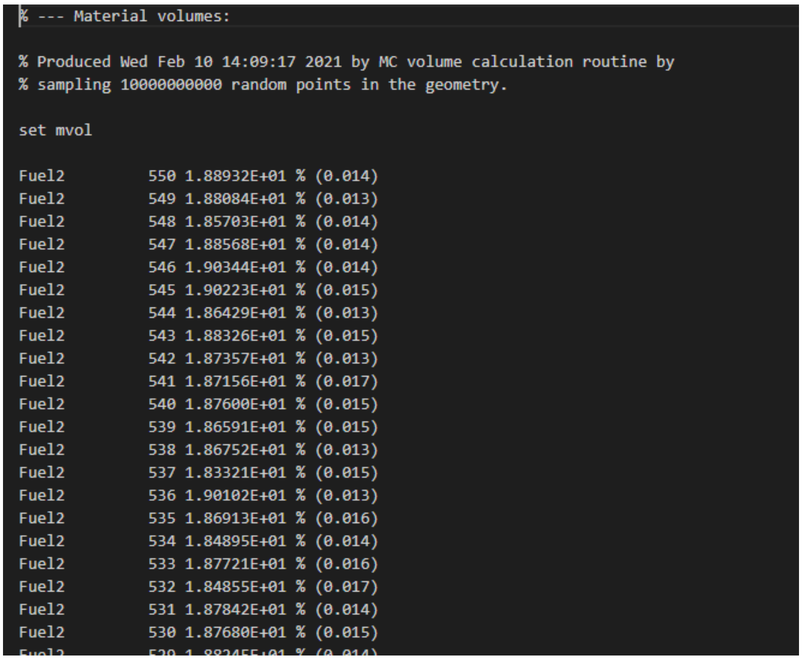

```
% --- Material volumes:

% Produced Wed Feb 10 14:09:17 2021 by MC volume calculation routine by
% sampling 10000000000 random points in the geometry.

set mvol

Fuel2         550 1.88932E+01 % (0.014)
Fuel2         549 1.88084E+01 % (0.013)
Fuel2         548 1.85703E+01 % (0.014)
Fuel2         547 1.88568E+01 % (0.014)
Fuel2         546 1.90344E+01 % (0.014)
Fuel2         545 1.90223E+01 % (0.015)
Fuel2         544 1.86429E+01 % (0.013)
Fuel2         543 1.88326E+01 % (0.015)
Fuel2         542 1.87357E+01 % (0.013)
Fuel2         541 1.87156E+01 % (0.017)
Fuel2         540 1.87600E+01 % (0.015)
Fuel2         539 1.86591E+01 % (0.015)
Fuel2         538 1.86752E+01 % (0.013)
Fuel2         537 1.83321E+01 % (0.015)
Fuel2         536 1.90102E+01 % (0.013)
Fuel2         535 1.86913E+01 % (0.016)
Fuel2         534 1.84895E+01 % (0.014)
Fuel2         533 1.87721E+01 % (0.016)
Fuel2         532 1.84855E+01 % (0.017)
Fuel2         531 1.87842E+01 % (0.014)
Fuel2         530 1.87680E+01 % (0.015)
```

FIGURE 3.7: Volume input file produced by Serpent volume checker routine.

to this file is then included in the main input file to provide volume values for depletion calculations.

The activation of the burnup calculation and the definition of burnup history in terms of number of days is done using the *'dep daytot'* keywords. The time-step sizes for burnup calculations are given in Table-3.1

Table 3.1: Timestep sizes for burnup calculation.

Time Period (Days)	Step Size(Days)
0-50	10
50-100	25
100-200	100
200-1000	200
1000-5000	400
5000-7500	500

3.2.4 Coupled Multi-physics Calculation Interface

Serpent has many built-in multi-physics interfaces to couple external thermal-hydraulic and CFD solvers with the standard serpent input. This allows bringing in temperature and density distributions on a fine grid into the serpent geometry and calculation of neutron interaction cross-sections based on these. The methodology relies heavily on Serpent's capability to carry out on-the-fly temperature treatment as discussed previously.

The multi-physics analysis in the current study is carried out on a single lattice cell and not on the whole core because of mesh limitations with the use of Ansys®Academic Research Mechanical, Release 2020 R1. The coupling routine is semi-automated by writing a python wrapper script to convert the volumetric power distribution output obtained from Serpent simulation to an Ansys readable file format (.xml) and then to read the temperature distribution obtained after the thermal-hydraulic calculation and write them in Serpent readable interface file (.ifc), one for each material.

Since the geometry is comprised of only a single lattice cell the only way of mapping the radial and axial temperature distribution with high fidelity is the point-average interface. The point-average interface brings in the temperatures and densities for a single material in a number of discrete points in the geometry. During neutron transport Serpent calculates the temperature and density at the interaction point as an average of the values of nearby interface points. Approximately 45,000 fuel temperature points and 190,000 moderator temperature points were obtained from the Ansys simulation results. The interface file for the fuel and moderator is illustrated in Figure-3.8

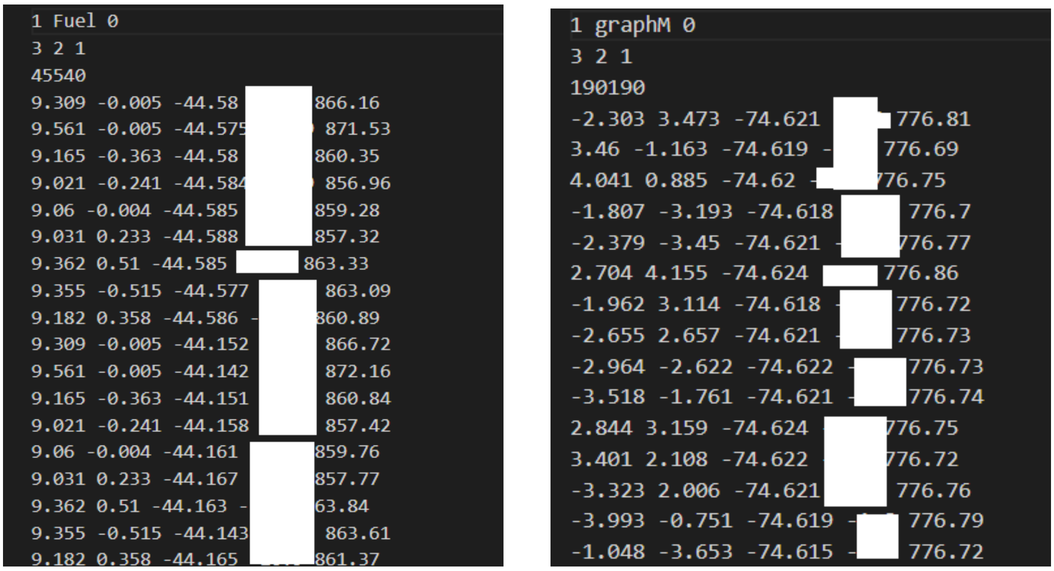

```
1 Fuel 0
3 2 1
45540
9.309 -0.005 -44.58 [redacted] 866.16
9.561 -0.005 -44.575 [redacted] 871.53
9.165 -0.363 -44.58 [redacted] 860.35
9.021 -0.241 -44.584 [redacted] 856.96
9.06 -0.004 -44.585 [redacted] 859.28
9.031 0.233 -44.588 [redacted] 857.32
9.362 0.51 -44.585 [redacted] 863.33
9.355 -0.515 -44.577 [redacted] 863.09
9.182 0.358 -44.586 - [redacted] 860.89
9.309 -0.005 -44.152 [redacted] 866.72
9.561 -0.005 -44.142 [redacted] 872.16
9.165 -0.363 -44.151 [redacted] 860.84
9.021 -0.241 -44.158 [redacted] 857.42
9.06 -0.004 -44.161 [redacted] 859.76
9.031 0.233 -44.167 [redacted] 857.77
9.362 0.51 -44.163 - [redacted] 63.84
9.355 -0.515 -44.143 [redacted] 863.61
9.182 0.358 -44.165 [redacted] 861.37
```

(A) Fuel

```
1 graphM 0
3 2 1
190190
-2.303 3.473 -74.621 [redacted] 776.81
3.46 -1.163 -74.619 - [redacted] 776.69
4.041 0.885 -74.62 - [redacted] 76.75
-1.807 -3.193 -74.618 [redacted] 776.7
-2.379 -3.45 -74.621 - [redacted] 76.77
2.704 4.155 -74.624 [redacted] 776.86
-1.962 3.114 -74.618 - [redacted] 776.72
-2.655 2.657 -74.621 - [redacted] 776.73
-2.964 -2.622 -74.622 - [redacted] 776.73
-3.518 -1.761 -74.621 - [redacted] 776.74
2.844 3.159 -74.624 [redacted] 76.75
3.401 2.108 -74.622 [redacted] 76.72
-3.323 2.006 -74.621 [redacted] 776.76
-3.993 -0.751 -74.619 - [redacted] 776.79
-1.048 -3.653 -74.615 - [redacted] 776.72
```

(B) Moderator

FIGURE 3.8: Interface files for fuel and moderator.

The input syntax of the point average interface type file starts with the specification of three parameters(Leppänen et al. 2014):

TYPE:	The interface type (1 for point-average interface)
MAT:	The name of the material that the data is given for (eg. Fuel,graphM etc.)
OUT:	The output flag, specifying whether an output in 'pin type fuel' is to be generated. Since we do not use 'pin type fuel' this is set to 0

The next line contains:

DIM:	The dimension of the distribution (3 = x-, y- and z-dependence).
RAD:	The exclusion radius, beyond which the points are not included in the average.
EXP:	The exponent for the averaging process. Setting the exponent EXP to 1 means that the average is based on distance, EXP = 2 means square distance, and so on.

Next, the number of points (eg. 45,540 for fuel) to be given is specified and the remaining lines give the data in each of the points, starting with the X, Y, and Z coordinate of the point, the material density at the point (negative value means mass density) and the temperature at that point (in kelvin).

3.2.5 Output Files

After the execution of all transport and burnup cycles Serpent outputs multiple different files. All numerical output is written in Matlab m-format files. The results are post-processed by writing and executing scripts to read and plot this data using GNU-Octave (Eaton et al. 2020) and/or Matlab (*MATLAB version 9.10.0.1684407 (R2021a) Update 3* 2021). The main output file (*_res.m) contains all results calculated by default during the transport cycle (such as run statistics, reaction mode counters, criticality eigenvalues, point kinetic parameters, delayed neutron fraction, six-factor formula, etc.). User-defined detectors to obtain neutron energy spectrum, fission power distribution, neutron flux distribution, etc. produce a separate output file(*_det.m). Similarly, output for a burnup calculation consisting of isotopic compositions for burnable materials, activities, decay heat, etc. are written in a different file (*_dep.m). Additionally, the cycle-wise results for checking the fission source and k_{eff} convergence as discussed in section-3.2.3 is printed in a separate file (*_his.m). The statistical uncertainty which is inherently present in any Monte-Carlo calculation output is reported for each output parameter in terms of relative error in all the above-mentioned files.

Chapter 4

Results

4.1 Optimisation to Minimize Reactivity Swing

Reactivity swing is defined as the difference in the inherent maximum and minimum reactivity in the core during the operational lifetime without taking into account any external reactivity excursions. For a homogeneously fuelled core not containing burnable poison, the maximum reactivity will be at the BOL and the minimum reactivity will be at EOL. The reactivity swing value (mk) is calculated as given in equation-4.1,

$$\begin{aligned}\text{Reactivity Swing} &= \rho_{max} - \rho_{min} \\ &= \left(\frac{1}{k_{\text{eff}}}\right)_{max} - \left(\frac{1}{k_{\text{eff}}}\right)_{min}. \end{aligned} \tag{4.1}$$

It is apparent that to maintain the reactor critical over the operational life of the reactor, the reactivity control system should be designed to account for the reactivity swing.

4.1.1 Initial Estimate of ^{235}U Enrichment

Burnup analysis was carried out for Core-A design by varying ^{235}U enrichments (wt-%) between 11% and 15% to obtain a k_{eff} of 1 at the end of life (EOL). It was determined that 15 wt-% ^{235}U enrichment provided enough reactivity for operating the reactor uninterrupted for 5500 days. The total amount of ^{235}U in the fresh fuel is calculated as 32.85 kg. The results for the k_{eff} variation and reactivity swing are shown in Table 4.1. As observed from the results for 15wt-% enrichment, the excess reactivity at BOL and the reactivity swing over the entire period of reactor operation is so high that it may introduce safety concerns on the reactivity control system designed to suppress it. As explained in Chapter-2, a burnable poison that will remain within the reactor core for its entire lifetime is selected as the means to reduce the initial excess reactivity and

TABLE 4.1: Determination of initial enrichment for 15 years of full power operation.

Enrichment (wt-%)	^{235}U mass (kg)	k_{eff} BOL	k_{eff} EOL	Reactivity Swing (mk)
11	24.079	1.175	0.850	325
13	28.4629	1.214	0.941	239
15	32.85	1.246	1.011	187

to bring the reactivity swing within the limits of a practically feasible reactivity control system design. This was achieved by using natural erbium oxide in the form of uniformly distributed spherical particles in the fuel rods contained in the inner region of the core.

4.1.2 Optimisation of Amount and Size of the Burnable Poison Particles

When using uniformly distributed burnable poison particles, two parameters of the poison particles affect the depletion behavior of burnable poison: the particle radius and the particle number (Tran et al. 2008). To find the optimum poison particle size, a burnup calculation is carried out in Serpent for Core-A design with different sizes of poison particles (viz. particle radii of 450 μm, 300 μm, 250 μm, 200 μm, 150 μm and 100 μm). The fuel enrichment required for 15 FPOYs with burnable poison will be higher than that required without the use of burnable poison since some poison will remain in the core at the end of life. Hence there will be some fuel inventory penalty if burnable poisons are used. The fuel enrichment taken for this study is taken as 19.75% which is just below the limiting value of 20% fuel enrichment for HALEU fuel. The total amount of ^{235}U in the fresh fuel is calculated as 42.73 kg, implying a 9.88 kg fuel penalty due to the use of burnable poison. Poison particles are distributed in the 300 fuel rods in the inner region of the core along with fuel TRISO particles by using the particle disperser routine provided by Serpent and explained in Section-3.2. The particle number for each size will determine the amount of burnable poison in the reactor. This amount of poison is kept fixed such that the k_{eff} is approximately 1 at the EOL. Consequently, the packing fraction of the poison particles in the fuel rods is maintained constant at 0.012 for all particle sizes ensuring that the amount of poison is constant for all cases. The fuel TRISO particle packing fraction in the inner region is 0.538 (= 0.55−poison packing fraction), while that in the outer region is 0.55.

The results obtained after simulating the cases are compared for the reactivity swing value. The variation of the multiplication factor (k_{eff}) as a function of depletion history is shown in Figure-4.1. The values of the reactivity swing as a function of poison particles size is summarised in Table-4.2. From the values of the reactivity swing, we can conclude

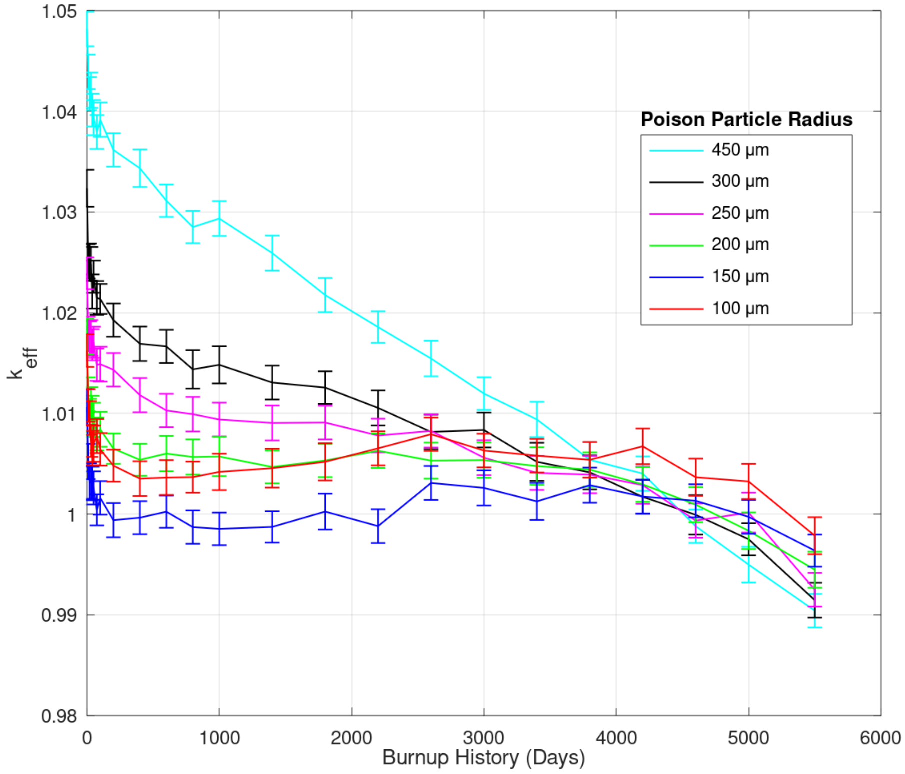

Figure 4.1: Variation of k_{eff} over the depletion history as a function of poison particle size.

Table 4.2: Determination of optimum poison particle size.

Case #	Particle Radius (μm)	Reactivity Swing (mk)
PP-1	450	55.6
PP-2	300	39.9
PP-3	250	30.9
PP-4	200	22.9
PP-5	150	14.1
PP-6	100	18.1

that the poison particle radius of 150 μm gives the lowest reactivity swing. As discussed in Chapter-2, Section-2.3, the central burnable poison pushes the flux outwards at the BOL and reduces the burnup of the inner zone over the reactor life which helps in sustaining the core criticality at EOL.

Figure-4.1 shows the center-line[1] radial thermal flux at BOL, MOL and EOL demonstrating this behavior.

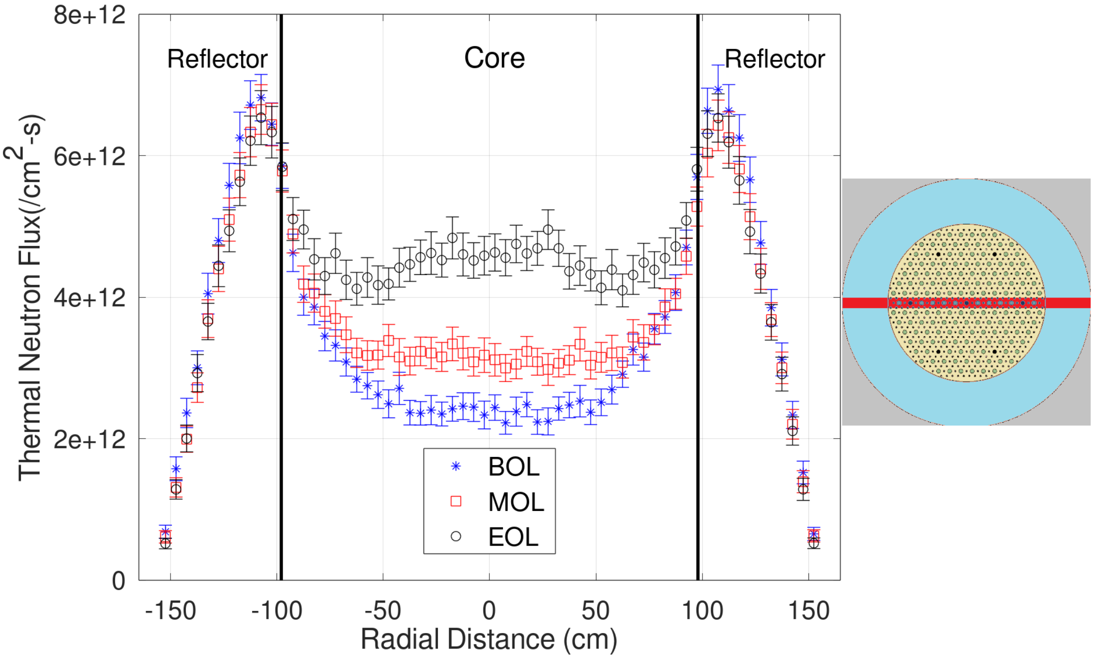

(A) Radial flux

---

[1] Center-line fluxes are tallied in a strip of y = -5 to 5 cm and z = -5 to 5 cm for radial thermal flux and y = -5 to 5 cm and x = -5 to 5 cm for axial thermal flux

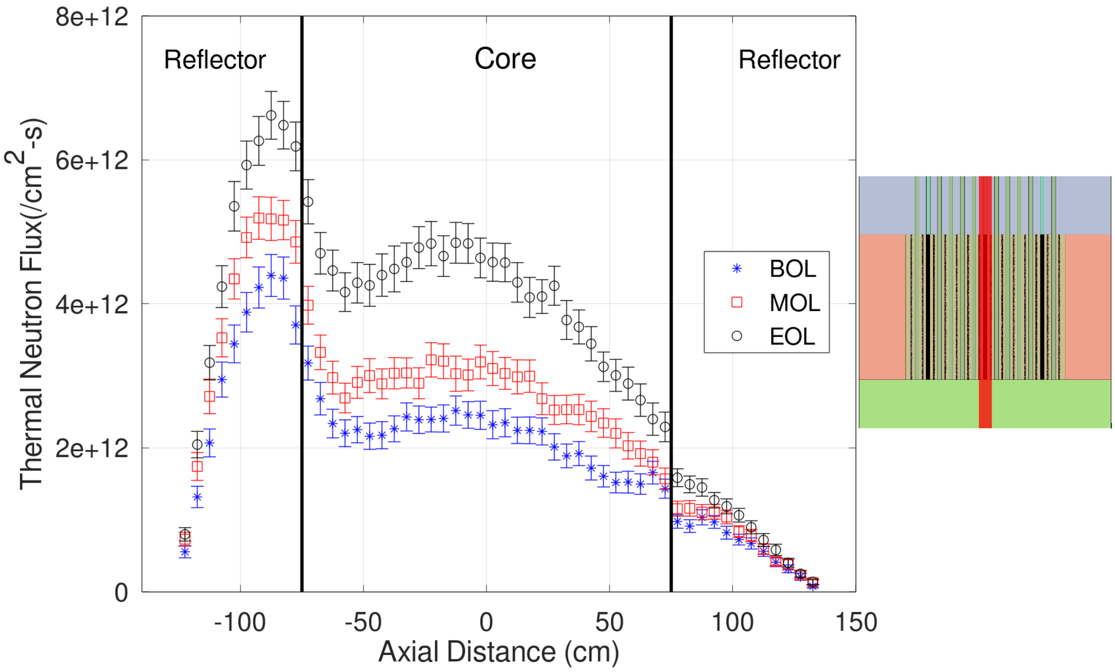

(B) Axial Flux

FIGURE 4.1: Center-line radial and axial flux for case PP-5 (150 μm radius poison particles.)

4.2 Optimisation of Fuel Lattice Pitch

The use of burnable poison in Core-A design brought the value of required fuel enrichment for 15 FPOYs up to 19.75%. To increase the operational life of the reactor to 20 FPOYs would mean increasing the enrichment beyond the limits for HALEU fuels. This being not a very desirable option, analyses were carried out to optimize the fuel lattice pitch and improve the fuel economy. Increasing the lattice pitch also meant an increase in the core diameter and thus there are two ways that the increase in lattice pitch can be affected:

1. Increase the lattice pitch maintaining the reactor diameter constant. This would imply that the reflector thickness be decreased as lattice pitch increases and the amount of graphite in the core remains constant.
2. Increase the lattice pitch maintaining the reflector thickness constant. This would imply that reactor diameter and the weight of graphite will increase as lattice pitch increases.

Both of these approaches were analysed by carrying out static criticality simulations for fresh fuel at BOL to determine the variation in k_{eff} as a function of varying the lattice pitch from 7 cm (original) to 12 cm in increments of 1 cm. The simulation case matrix and the results of the analyses are shown in Table-4.3

Table 4.3: Fuel lattice pitch optimisation case matrix and results.

Case #	Lattice Pitch (cm)	Core Radius (cm)	Radial Reflector Thickness (cm)	Reactor Radius (cm)	k_{eff}
Base	7	98	57	155	1.011
No Change in Reactor Radius					
A-1	8	112	43	155	1.034
A-2	9	126	29	155	1.031
No Change in Reflector Thickness					
B-1	8	112	57	169	1.056
B-2	9	126	57	183	1.085
B-3	10	140	57	197	1.104
B-4	11	154	57	211	1.111
B-5	12	168	57	225	1.113
B-6	13	182	57	239	1.107
B-7	14	196	57	253	1.100

Case A-1 shows that even with a 1 cm increase in lattice pitch length, there is a significant increase in BOL k_{eff} without increasing the total amount of graphite and the overall size of the reactor. Case A-2, however, shows that this advantage seems to plateau when lattice pitch is increased to 9 cm and this is due to the dominating effect of increased neutron leakage from the significantly thinner reflector. Thus Case A-1 seems to be a near-optimum design for the approach in which the overall reactor dimensions and amount of graphite are constrained to remain constant.

The variation of k_{eff} for Case-B is plotted in Figure-4.2. From the plot, it becomes apparent that the k_{eff} increases as the lattice pitch is increased, reaches a maximum value at 12 cm lattice pitch length, and then starts decreasing. This is a classic moderator/fuel ratio vs. multiplication factor curve showing that as the moderator to fuel ratio increases, the k_{eff} rises first due to increased moderation (increasing resonance escape probability and thermal non-leakage probability) but then decreases once absorption by graphite starts dominating (resulting in a decrease in thermal utilization factor). Thus the optimum lattice pitch considering only the k_{eff} behavior seems to be 12 cm. However, as seen from Figure-4.2 the increase in k_{eff} with an increase in lattice pitch length from 10 cm to 12 cm is not very significant. However, there is an increase of almost 20% in reactor radial dimensions at 12 cm lattice pitch length as compared to 10 cm pitch. Hence, a 10 cm lattice pitch is selected for Core-B design to maintain the reactor radius to just under 2 m. With the increase in lattice pitch, the heat pipe OD is also revised to 2.5 inches instead of 2 inches.

The comparison of the flux energy spectrum for 7 cm lattice pitch and 10 cm lattice pitch is shown in Figure-4.3. The effect of the increased lattice pitch is visible in the higher flux peak in the thermal spectrum for 10 cm pitch as compared to a 7 cm pitch (i.e more neutrons are in the thermal region as compared to the fast region for 10 cm pitch).

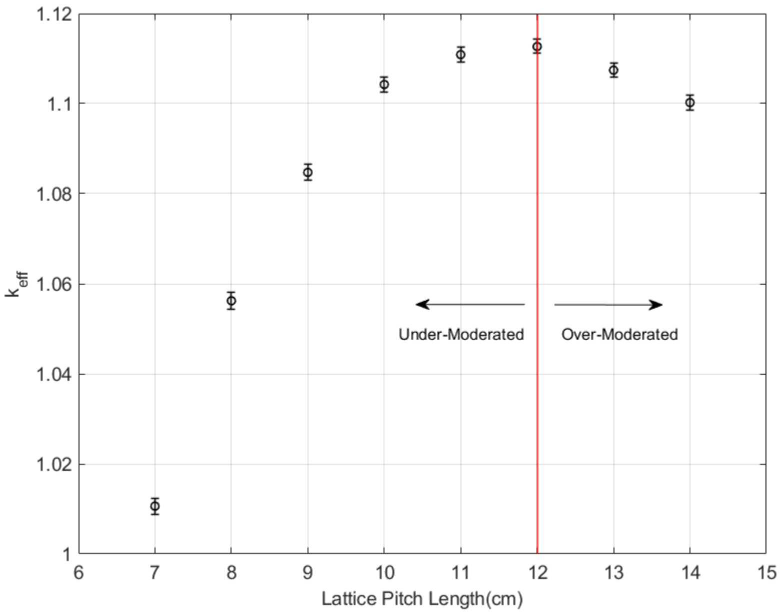

FIGURE 4.2: Variation of k_{eff} with lattice pitch.

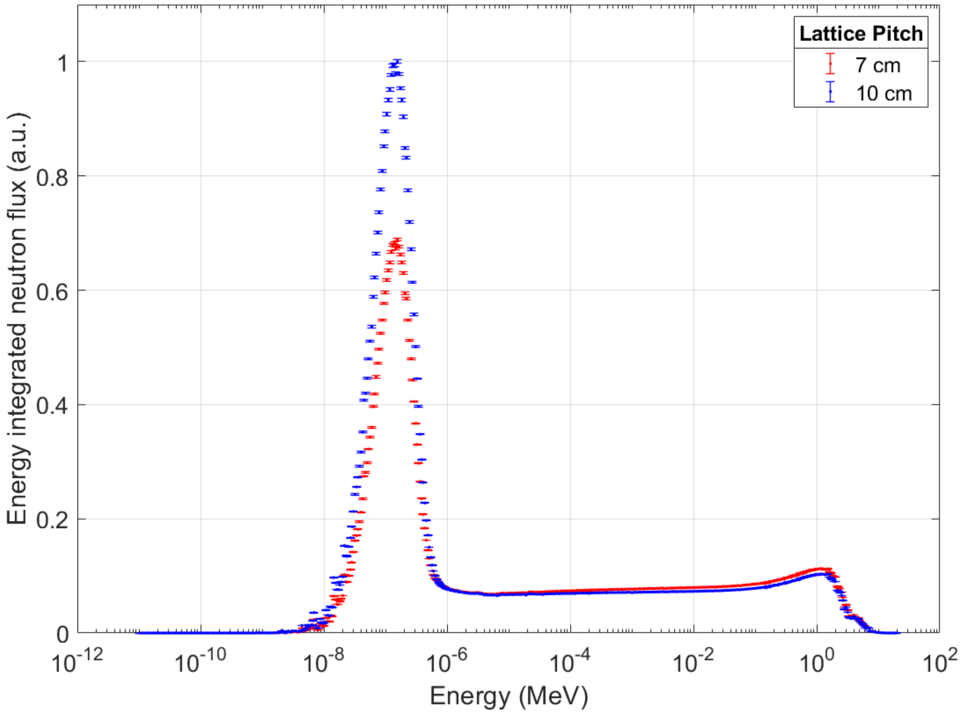

FIGURE 4.3: Energy integrated neutron flux spectrum.

4.3 Coolant Void Reactivity and Change of Coolant to Sodium

The coolant used in the original design is potassium vapor. Natural isotopic abundance of potassium is ^{39}K = 93.26%, ^{40}K = 0.01% and ^{41}K = 6.73% (De Biévre et al. 1984). The comparison of the neutron absorption (n,γ) for potassium with sodium (^{23}Na) is given in Figure-4.4. The neutron absorption cross-section is significantly higher for potassium as compared to sodium. ^{40}K has an especially high absorption cross-section. This implies that as ^{39}K transmutes to ^{40}K with the reactor operation, the absorption cross-section of the coolant would go on increasing as the reactor operates. This introduces concerns about coolant void reactivity. Since the coolant in CNB plays no role in neutron moderation but only in neutron absorption, loss of coolant would directly translate into more neutrons being available for fission implying that the coolant void reactivity would be significantly more positive with potassium as coolant.

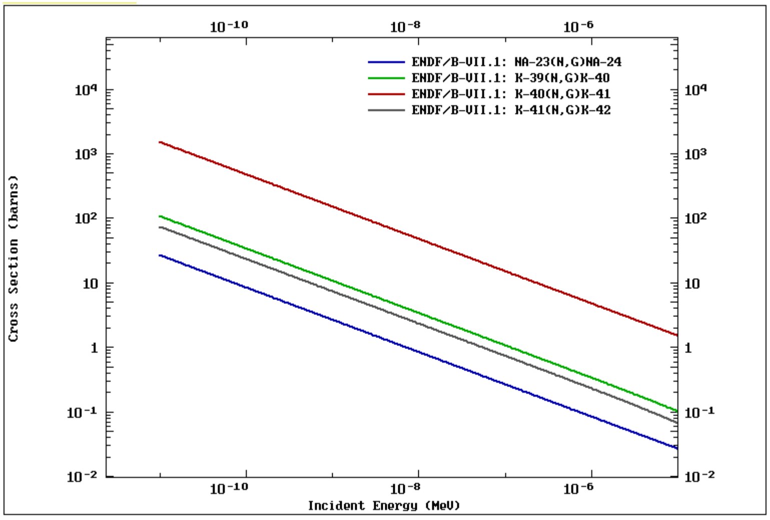

Figure 4.4: Comparison of neutron absorption (n,γ) cross-section for sodium and potassium.(Zerkin 2021)

To analyse the coolant void reactivity, static criticality simulation cases were run by using 'void' as the condition inside all the heat pipes in the reactor, as a worst case scenario, to study its effect on the multiplication factor. The void reactivity was then calculated as,

$$\begin{aligned}\text{Void Reactivity} &= \rho_{void} - \rho_{nom} \\ &= \left(\frac{1}{k_{\text{eff}}}\right)_{void} - \left(\frac{1}{k_{\text{eff}}}\right)_{nom}.\end{aligned} \tag{4.2}$$

where,

ρ_{void} is the reactivity in coolant voided condition at BOL or EOL

ρ_{nom} is the nominal reactivity at BOL or EOL

The void reactivity[2] for K and Na coolant is shown in Table-4.4. They show that the void reactivity for Na coolant is positive and significantly lower than that for potassium. As a result, sodium is chosen as the coolant in the Core-B design.

TABLE 4.4: Void Reactivity(mk)$\pm 2\sigma$ for Na and K coolant.

Time	K Coolant	Na Coolant
BOL	11.22 ± 2.32	3.96 ± 2.28
EOL	14.39 ± 2.41	7.03 ± 2.42

4.4 Increase in Reactor Operational Life to 20 FPOY

The increase in lattice pitch from 7 to 10 cm makes it possible to increase the reactor operational life from the initial value of 15 FPOYs to 20 FPOYs. To achieve this, the fuel rod radius is also increased to 1.2 cm from 1 cm. The combined effect of the increase of lattice pitch and increase in fuel rod radius means that the ^{235}U enrichment in the fuel could be reduced to a value comfortably below 19.75 wt-%. Burnup calculations are carried out to determine the fuel enrichment as well as the amount of burnable poison required to maintain the reactivity swing within reasonable values for 20 years of fuel burnup. Spherical burnable poison particles of a radius 150 μm are used in this study. The case runs and the results with corresponding uncertainties[3] are given in Table-4.5

Although the reactivity swing is lowest for case C-2, as seen from the reactivity swing plots shown in Figure-4.5, the k_{eff} goes below 1 much earlier than the required 20 FPOYs.

---

[2] It should be noted that these void reactivity values are for the case when all 156 heat pipes are voided instantly and simultaneously, a very unlikely scenario.

[3] Uncertainty analysis and error propagation is discussed in Appendix-A

TABLE 4.5: Fuel Enrichment and burnable poison requirement for 20 FPOYs. (p.f. is packing fraction).

Case #	^{235}U (wt-%)	Er_2O_3 p.f.	BOL $k_{\text{eff}} \pm 2\sigma$	EOL $k_{\text{eff}} \pm 2\sigma$	Rx. Swing $\rho \pm 2\sigma$ (mk)
C-1	13%	0.009	1.045 ± 0.0017	0.984 ± 0.0016	59.1 ± 2.4
C-2	15%	0.013	1.018 ± 0.0016	0.991 ± 0.0017	27.1 ± 2.4
C-3	15% (inner) 13% (outer)	0.011	1.024 ± 0.0016	0.994 ± 0.0017	29.5 ± 2.3

To increase the reactor life to 20 years, either the enrichment can be increased or the poison particle packing fraction (and hence the amount of poison) can be reduced. Both of the approaches will increase BOL excess reactivity and the value of reactivity swing. However, as seen from the results in Section-4.1.2, the unpoisoned fuel in the outer zone dominates the contribution to k_{eff} at BOL. Thus the enrichment in the outer zone is reduced along with a reduction in poison packing fraction from 0.013 to 0.011. This result is shown in Case C-3. The reactivity swing value is similar (within uncertainty bounds) to Case C-2 and the reactor does not seem to go below a k_{eff} value of 1 for at least 20 years (7300 days). Thus, for Core-B design a differential enrichment approach (15 wt-% enrichment in inner zone and 13 wt-% enrichment in outer zone) is taken.

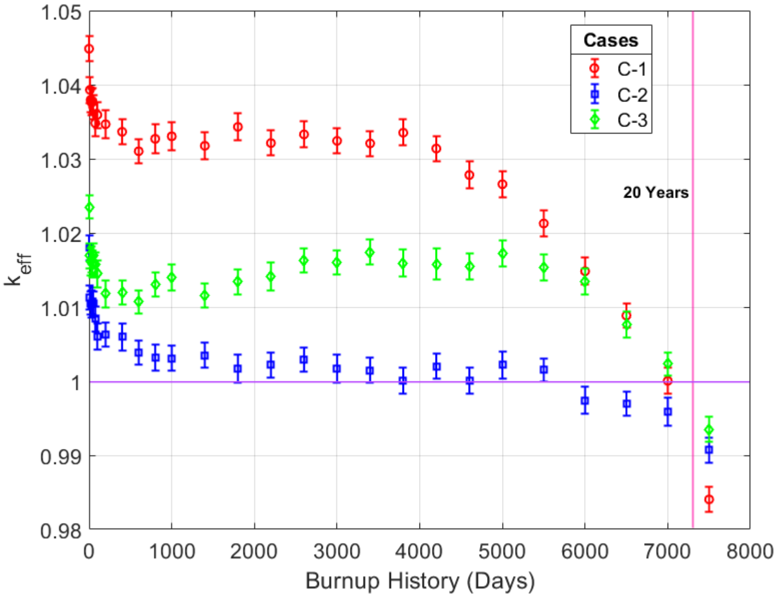

FIGURE 4.5: Reactivity swing for 20 FPOYs.

The change of ^{235}U and ^{167}Er inventory in the reactor as a function of burnup are shown in Figure-4.6. It can be observed that the rate of burnup of fuel and poison is almost the same, resulting in the release of the excess reactivity in the reactor at the same rate as the fissile material burns up which helps in achieving a reasonable reactivity swing.

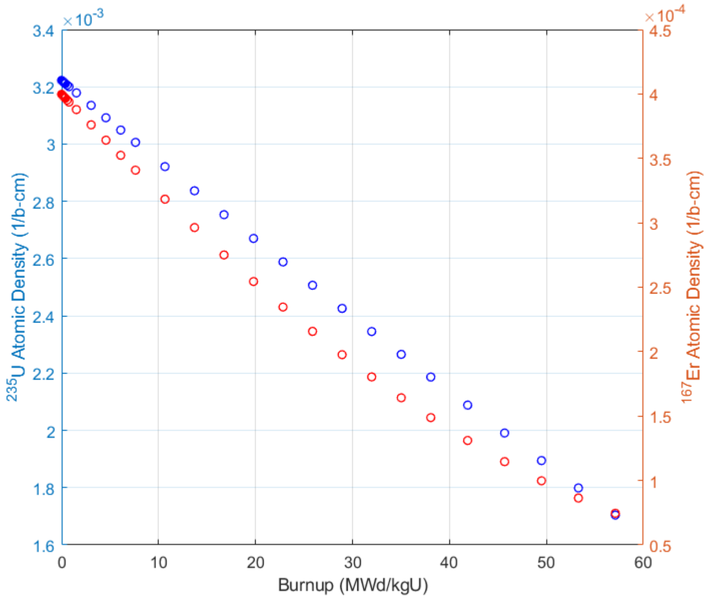

FIGURE 4.6: Depletion of ^{235}U and ^{167}Er inventory with fuel burnup.

4.5 Thermal Flux and Fission Power Distribution

4.5.1 Thermal Flux Distribution & Flux Peaking Factors

The thermal neutron flux distribution for Core-B design is calculated by integrating the neutron flux across neutron energy ranging from 10^{-5} eV to 0.625 eV. The spatial discretization for the radial and axial thermal neutron flux over the operational life of the reactor is given in Table-4.6.

The radial center-line thermal flux is obtained by taking a $z = \pm 5$ cm and $y = \pm 5$ cm slice from the center of reactor and discretizing the x dimensions into 79 divisions (of approximately 5 cm each). Similarly, the axial center-line thermal flux is obtained by taking a $x = \pm 5$ and $y = \pm 5$ cm slice at the center of the reactor and discretizing the

Table 4.6: Spatial discretization for radial & axial thermal neutron flux.

Thermal Flux	Radial discretization		Axial Discretization	
	Range (cm)	No. of Div.	Range (cm)	No.of Div.
Center-line Radial	$x = -197$ to 197 $y = -5$ to 5	79 1	$z = -5$ to 5	1
Center-line Axial	$x = -5$ to 5 $y = -5$ to 5	1 1	$z = -125$ to 135	52
Contour Plots	685 hex cells, 10 cm pitch		$z = -75$ to 75	10

z dimension into 52 divisions of 5 cm interval. The center-line radial and axial thermal flux are shown in Figure-4.7.

The centerline radial thermal neutron flux shows a significant dip in the central part of the core at the BOL due to the high concentration of burnable poison in the inner core. As the poison burns with the continued operation the flux shifts inward, becomes more uniform at MOL, and goes on to peak at the center at EOL. The center-line axial thermal neutron flux, on the other hand, is peaked at the bottom due to the absence of control rods in the bottom reflector region. The flux in the core steadily rises as the poison burns out with the continued operation of the reactor.

Surface plots help visualize the radial and axial flux in the reactor and are obtained by tallying the thermal neutron flux by integrating it over each of the hexagonal lattice cells radially with 10 axial subdivisions. The surface plots of the radial thermal flux at the central slice of the reactor at BOL, MOL, and EOL are given in Figure-4.8 while those for axial thermal flux are given in Figure-4.9. The traveling wave of thermal neutron flux from reactor periphery to center is visible in the surface plots. This results in a steady increase in the average thermal neutron flux in the central slice of the reactor.

The thermal flux peaking factors are defined as the ratio of the maximum thermal neutron flux to the average thermal neutron flux value. The peaking factors are calculated at BOL, MOL and EOL and are given in Table-4.7.

Table 4.7: Thermal Flux peaking factors at BOL, MOL and EOL.

Flux Peaking Factor	BOL	MOL	EOL
Radial	1.58	1.09	1.22
Axial	1.21	1.17	1.26

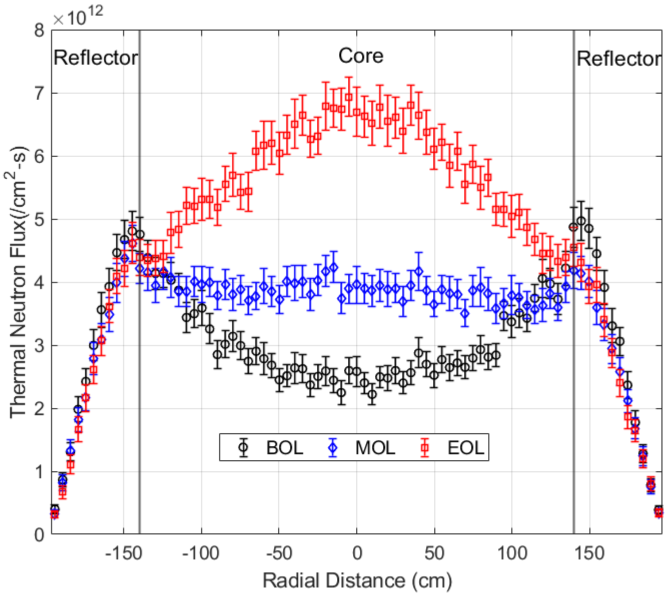

(A) Radial Flux±2σ (n/cm^2-s)

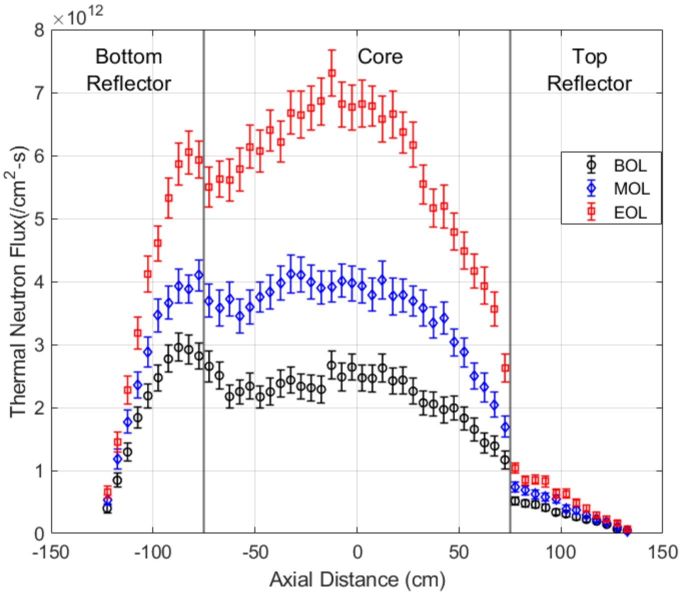

(B) Axial Flux±2σ (n/cm^2-s)

FIGURE 4.7: Center-line thermal neutron flux for Core-B design.

4.5.2 Distribution of Fission Heat Deposition

The thermal power of the CNB is 2400 kW. However, the calculation of the spatial distribution of heat deposition in a nuclear reactor is a complicated process. Neutrons

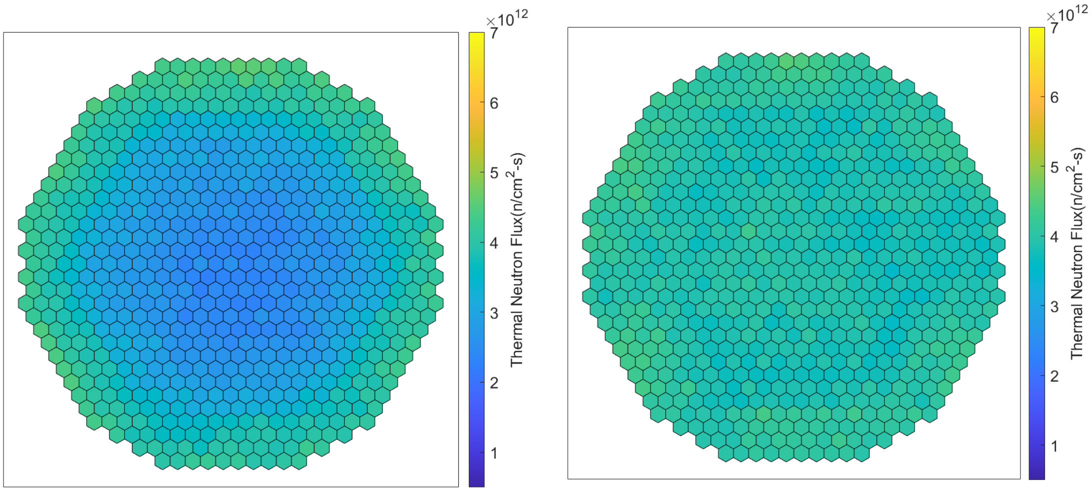

(a) BOL

(b) MOL

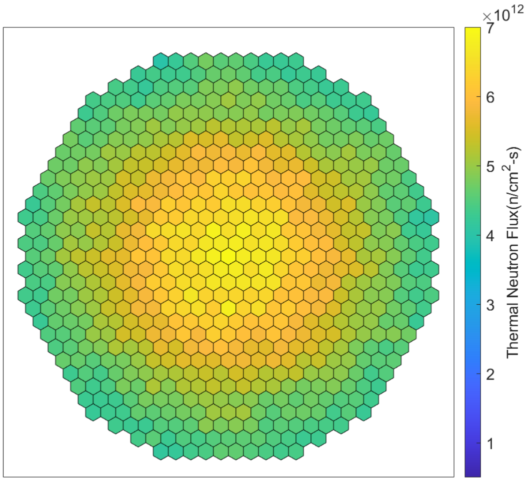

(c) EOL

Figure 4.8: Plots for radial thermal neutron flux distribution for Core-B design.

can deposit their energy in the material in many reactions and some reactions such as fission and radiative capture release additional energy. Additionally, these reactions can produce secondary particles (neutrons or gammas) which transport energy away from the reaction site and deposit it elsewhere. However, Serpent by default does not simulate the transport of photons and their energy is instead deposited locally at the fission sites (Tuominen et al. 2019). Thus the tallies for getting the fission heat deposition are

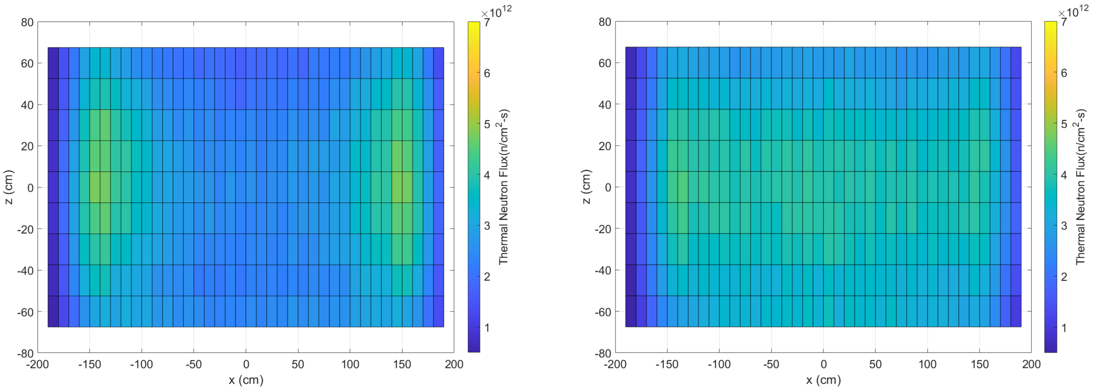

(A) BOL (B) MOL

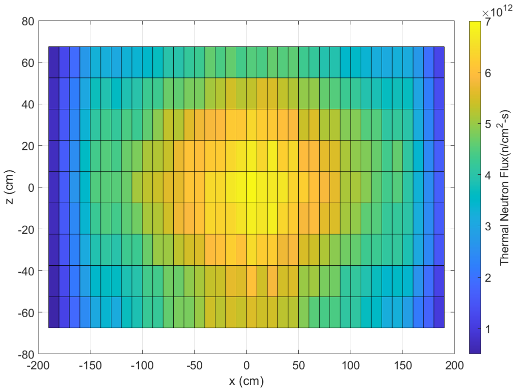

(C) EOL

FIGURE 4.9: Plots for axial thermal neutron flux distribution for Core-B design.

set up such that the power distribution is obtained separately at each of the 522 fuel rod sites. The radial distribution of power in the core at BOL, MOL, and EOL for Core-B design is shown in Figure-4.8.

The power peaking factor is defined as the ratio of maximum fuel rod power to the average fuel rod power and the values for the power peaking factors at BOL, MOL and EOL are given in Table-4.8

TABLE 4.8: Power peaking factors over the operational life of the CNB.

Time	Power Peaking Factor
BOL	1.28
MOL	1.11
EOL	1.34

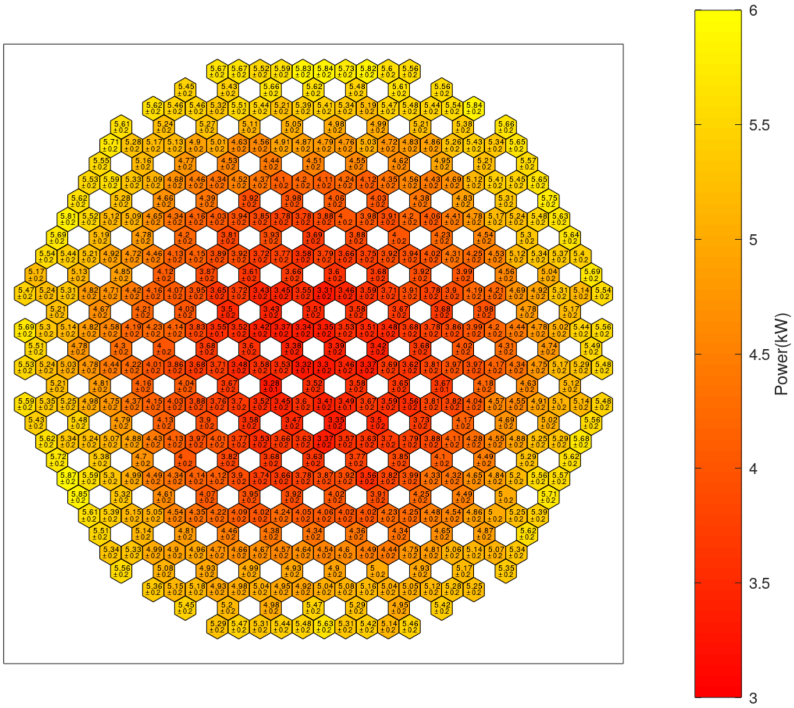

(A) BOL

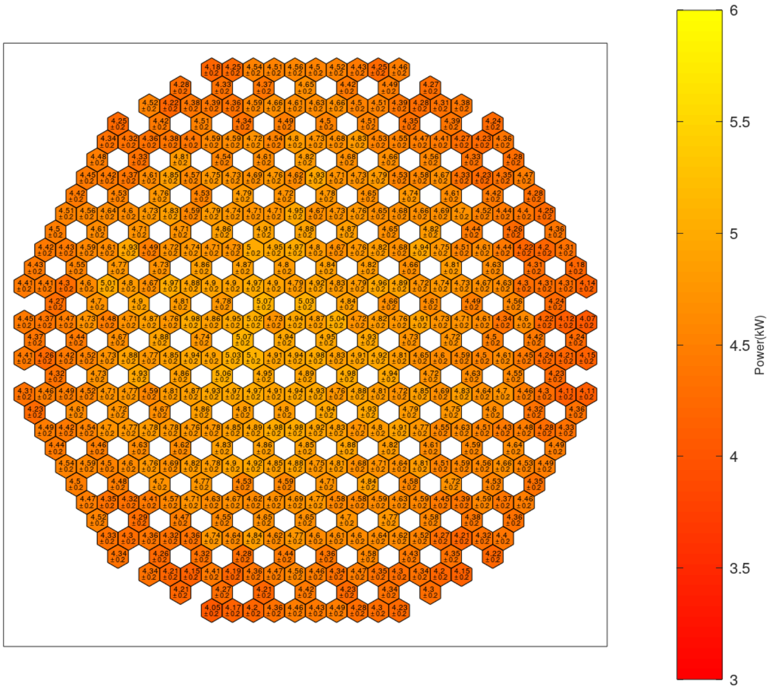

(B) MOL

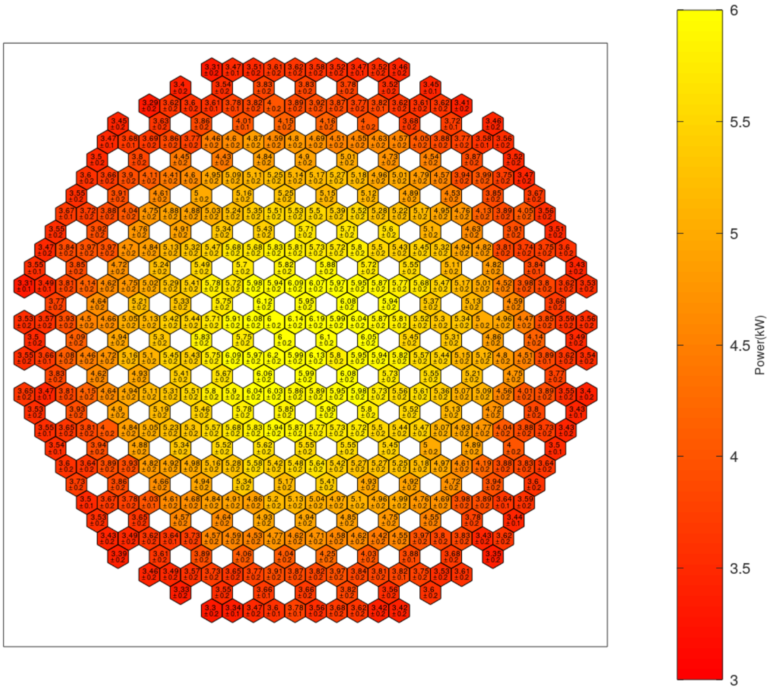

(C) EOL

FIGURE 4.8: Fission energy deposition in fuel elements in CNB.

4.6 Temperature Coefficient of Reactivity

The most important intrinsic safety feature of the reactor design is its negative temperature feedback. As explained in Section-1.2.5 this ensures that in the case of a power excursion the transient self-terminates. Negative temperature feedback exists for both the fuel (through Doppler broadening of absorption resonances) and the graphite moderator (by hardening of neutron spectrum).In CNB, since the moderator is solid, a change in moderator temperature will only affect the thermal spectrum and not the absorption rate in the resonance energy range, hence each temperature coefficient can be analyzed separately.

4.6.1 Fuel Temperature Coefficient of Reactivity

The fuel temperature coefficient of reactivity is the most important feedback that affects the reactor neutronic behavior in case of a reactivity excursion because it is almost instantaneous. A negative fuel temperature coefficient of reactivity (FTC) makes a nuclear reactor design inherently safer by providing immediate negative feedback to a reactivity excursion transient. Additionally, the magnitude of the fuel temperature coefficient value determines the rate of reactivity excursion transient. To estimate the values of the FTC at BOL, MOL, and EOL of CNB operation, static criticality analysis is carried out at fuel kernel temperatures of 300, 600, 900, 1200, 1500 K[4] and the nominal operating temperature of 773K. The temperature of the remaining materials in the model was maintained constant at the nominal temperature of 773K.

The results of the k_{eff} at the various fuel temperatures are used to calculate the fuel temperature reactivity as,

$$\rho_f = \rho_f^{hot} - \rho_f^{cold} = \frac{1}{k_{\text{eff}}^{cold}} - \frac{1}{k_{\text{eff}}^{hot}}. \tag{4.3}$$

The fuel temperature coefficient of reactivity can then be calculated by dividing the value of the fuel reactivity by the difference in temperatures as given by,

$$\alpha_{fT} = \frac{\rho_f}{T_{hot} - T_{cold}}. \tag{4.4}$$

The fuel temperature reactivity (with the baseline k_{eff} at 300 K) and the FTC at the BOL, MOL and EOL are given in Table-4.9, Table-4.10, and Table-4.11 respectively. A

---

[4] These are the temperatures at which the interaction cross-section data is available in the ENDF B-VII.I library without the requirement of explicit Doppler broadening correction algorithms.

least-squares fit (weighted with uncertainties) is carried out and the regression equations are obtained as,

$$\rho_{BOL} = -0.0114 \times T + 2.515 \qquad [p(\chi^2 > observed) = 98.5\%]^{5} \tag{4.5}$$
$$\rho_{MOL} = -0.0123 \times T + 3.438 \qquad [p(\chi^2 > observed) = 99.4\%] \tag{4.6}$$
$$\rho_{EOL} = -0.0149 \times T + 3.366 \qquad [p(\chi^2 > observed) = 87.1\%] \tag{4.7}$$

The reactivity values at BOL, MOL and EOL as a function of temperature and the linear fit along with uncertainty band of $\pm 2\sigma$ are shown in Figure-4.8. The fuel temperature coefficients (along with the fit uncertainty) as given by above equations over the temperature range of 300K to 1500K, are given as,

$$\text{BOL} \rightarrow \alpha_{fT} = -1.14 \pm 0.08\ pcm/K$$
$$\text{MOL} \rightarrow \alpha_{fT} = -1.23 \pm 0.07\ pcm/K$$
$$\text{EOL} \rightarrow \alpha_{fT} = -1.49 \pm 0.11\ pcm/K$$

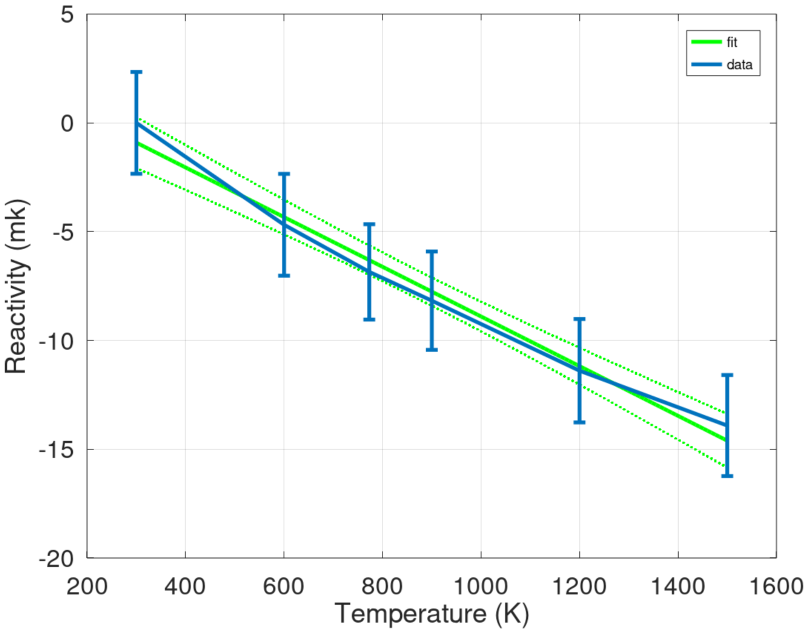

(A) BOL

---

[5] The χ^2 test is used to determine the goodness of the fit and establish a quantitative criteria to reject a polynomial fit. Here, p is the probability of seeing a χ^2 value higher than that which was observed assuming the data are normally distributed around the fit. If $p < 0.01$, the fit can be rejected at 1% level.

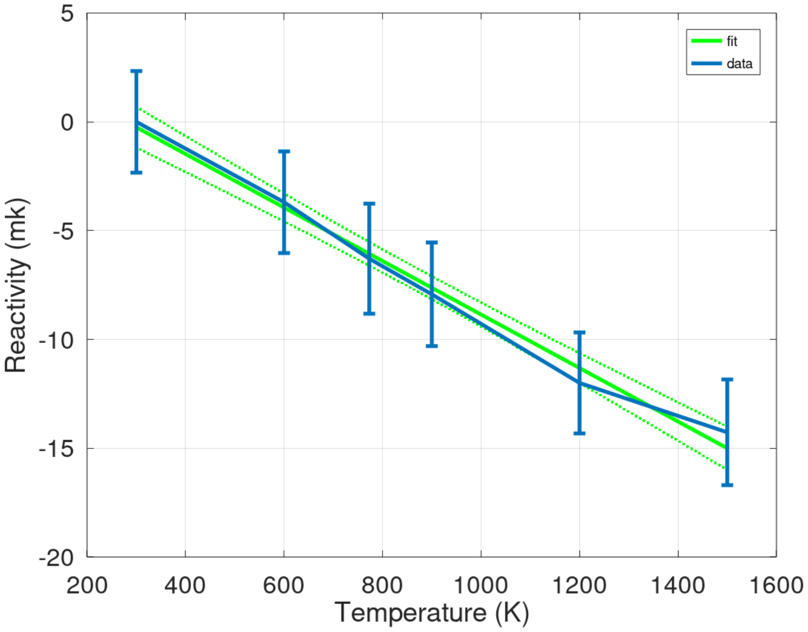

(B) MOL

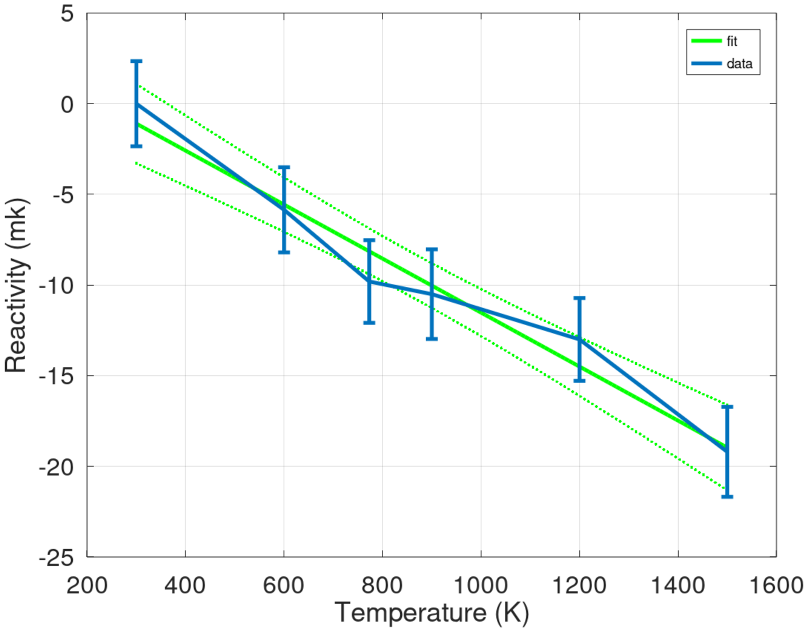

(C) EOL

FIGURE 4.8: Reactivity variation with fuel temperature.

TABLE 4.9: Fuel Temperature reactivity and FTC at BOL.

Temperature (K)	Reactivity $\pm 2\sigma$ (mk)	FTC $\pm 2\sigma$ (pcm/K)
300	0	-
600	-4.7 ± 2.3	-1.6 ± 0.8
900	-8.2 ± 2.3	-1.4 ± 0.4
1200	-11.4 ± 2.4	-1.3 ± 0.3
1500	-13.9 ± 2.3	-1.2 ± 0.2

TABLE 4.10: Fuel temperature reactivity and FTC at MOL.

Temperature (K)	Reactivity $\pm 2\sigma$ (mk)	FTC $\pm 2\sigma$ (pcm/K)
300	0	-
600	-3.7 ± 2.3	-1.2 ± 0.8
900	-7.9 ± 2.4	-1.3 ± 0.4
1200	-11.9 ± 2.3	-1.3 ± 0.3
1500	-14.2 ± 2.4	-1.2 ± 0.2

TABLE 4.11: Fuel temperature reactivity and FTC at EOL.

Temperature (K)	Reactivity $\pm 2\sigma$ (mk)	FTC $\pm 2\sigma$ (pcm/K)
300	0	-
600	-5.8 ± 2.4	-1.9 ± 0.8
900	-10.5 ± 2.5	-1.8 ± 0.4
1200	-13.0 ± 2.3	-1.5 ± 0.3
1500	-19.2 ± 2.5	-1.6 ± 0.2

An analytical calculation is done for obtaining the FTC values at BOL to compare the obtained values with the analytical results(See Appendix-B). The values for the FTC obtained using analytical calculation do not match closely to the values of the FTC obtained from Serpent within the positive uncertainty bound and also the trend for the values of FTC with temperature is similar. The small mismatch in the values can be attributed to the fact is that the analytical calculation involves the use of resonance integrals obtained from experiments done for cylindrical fuel rods, while the CNB design uses heterogeneous TRISO fuel particles.

4.6.2 Moderator and Reflector Temperature Coefficient of Reactivity

The moderator and reflector temperature coefficient of reactivity (MTC) provides additional reactivity feedback during power excursions and influences reactor stability. The temperature of the moderator affects the neutron temperature (and therefore neutron energy) much more than the temperature of fuel since the moderator is primarily responsible for neutron thermalization. In general, a negative moderator temperature coefficient of reactivity provides delayed feedback to reduce the excess reactivity during a power rise. Static criticality calculations are carried out to determine the behavior of the multiplication factor and the value of the coefficient of reactivity at graphite temperatures of 296, 400 500, 600, 700, 800, 1000, 1200, 1600, and 2000 K[6] and at nominal reactor operating temperature of 773 K.

The k_{eff} values at the various graphite temperatures are used to calculate the moderator and reflector temperature reactivity as,

$$\rho_{Gr} = \rho_{Gr}^{hot} - \rho_{Gr}^{cold} = \frac{1}{k_{\text{eff}}^{cold}} - \frac{1}{k_{\text{eff}}^{hot}}. \tag{4.8}$$

The moderator and reflector temperature coefficient of reactivity can then be calculated by dividing the value of the graphite reactivity by the difference in temperatures as given by

$$\alpha_{mT} = \frac{\rho_{Gr}}{T_{hot} - T_{cold}}. \tag{4.9}$$

The graphite temperature reactivity (with the baseline k_{eff} at 296 K) and the MTC at the BOL, MOL and EOL are given in Table-4.12, Table-4.13, and Table-4.14 respectively. A linear least-squares fit (weighted with uncertainties) is carried out for data from temperatures of 700 K to 1600 K[7] and the regression equations are obtained as

$$\rho_{BOL} = -0.2025 \times T + 91.067 \qquad [p(\chi^2 > observed) = 97.9\%] \tag{4.10}$$

$$\rho_{MOL} = -0.1991 \times T + 99.177 \qquad [p(\chi^2 > observed) = 46.8\%] \tag{4.11}$$

$$\rho_{EOL} = -0.1525 \times T + 80.196 \qquad [p(\chi^2 > observed) = 1.17\%] \tag{4.12}$$

The reactivity values at BOL, MOL, and EOL as a function of temperature and the linear fit along with uncertainty band of $\pm 2\sigma$ are shown in Figure-4.9 for temperatures between 700 and 1600 K. The moderator and reflector temperature coefficients (along

---

[6] These are the temperatures at which the neutron scattering cross-section for graphite is defined in the ENDF-B VII.I library.

[7] Using the data at remaining temperature points results in a rejection of linear fit at 1% level, implying the reactivity behaviour is linear only between 700 and 1600 K.

with the fit uncertainties) as given by above equations over the temperature range of 300 to 1500 K, are given as

$$\text{BOL} \rightarrow \alpha_{Gr} = -20.25 \pm 0.09 \; pcm/K$$

$$\text{MOL} \rightarrow \alpha_{Gr} = -19.91 \pm 0.32 \; pcm/K$$

$$\text{EOL} \rightarrow \alpha_{Gr} = -15.25 \pm 0.64 \; pcm/K$$

Table 4.12: Graphite temperature reactivity and MTC at BOL.

Temperature (K)	Reactivity $\pm 2\sigma$ (mk)	MTC $\pm 2\sigma$ (pcm/K)
296	0	-
400	-8.6 ± 1.9	-8.2 ± 1.9
500	-21.5 ± 2.0	-10.5 ± 1.0
600	-34.2 ± 2.0	-11.2 ± 0.7
700	-50.0 ± 2.0	-12.4 ± 0.5
800	-69.0 ± 2.1	-13.7 ± 0.4
1000	-110.1 ± 2.2	-15.6 ± 0.3
1200	-152.3 ± 2.2	-16.8 ± 0.2
1600	-234.2 ± 2.4	-18.0 ± 0.2
2000	-300.6 ± 2.5	-17.6 ± 0.1

Table 4.13: Graphite temperature reactivity and MTC at MOL.

Temperature (K)	Reactivity $\pm 2\sigma$ (mk)	MTC $\pm 2\sigma$ (pcm/K)
296	0	-
400	-7.5 ± 2.2	-7.2 ± 2.1
500	-18.2 ± 2.3	-8.9 ± 1.1
600	-30.3 ± 2.2	-10.0 ± 0.7
700	-42.7 ± 2.3	-10.6 ± 0.6
800	-60.2 ± 2.3	-11.9 ± 0.5
1000	-97.2 ± 2.4	-13.8 ± 0.3
1200	-138.2 ± 2.5	-15.3 ± 0.3
1600	-221.5 ± 2.7	-17.0 ± 0.2
2000	-295.9 ± 2.9	-17.4 ± 0.2

Table 4.14: Graphite temperature reactivity and MTC at EOL.

Temperature (K)	Reactivity $\pm 2\sigma$ (mk)	MTC $\pm 2\sigma$ (pcm/K)
296	0	-
400	-6.2 ± 2.5	-6.0 ± 2.4
500	-14.7 ± 2.5	-7.2 ± 1.2
600	-21.2 ± 2.4	-7.0 ± 0.8
700	-31.4 ± 2.6	-7.8 ± 0.7
800	-40.9 ± 25	-8.1 ± 0.5
1000	-66.8 ± 2.6	-9.5 ± 0.4
1200	-98.8 ± 2.7	-10.9 ± 0.3
1600	-168.3 ± 2.8	-12.9 ± 0.2
2000	-246.4 ± 3.0	-14.5 ± 0.2

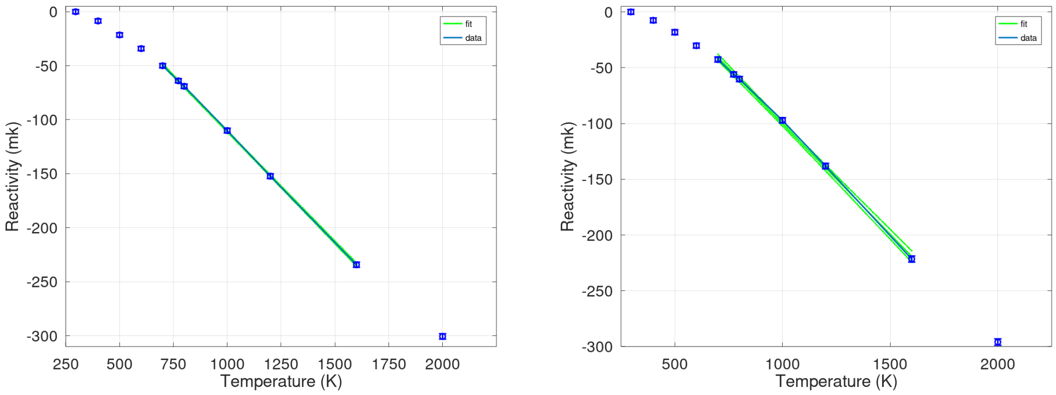

(A) BOL (B) MOL

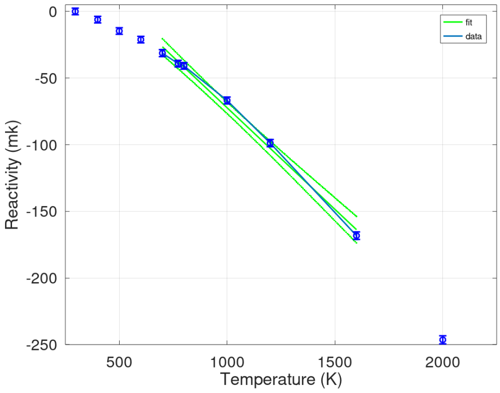

(C) EOL

FIGURE 4.9: Reactivity variation with graphite temperature.

4.7 Design of Reactivity Control System and Shutdown Margin

The design of the reactivity control system is based on the calculation of rod worths. Control (or Shutoff) rod worth is defined as the reduction in reactivity upon complete insertion of one or more rods. Control rods at different locations can have different worths depending on the neutron flux distribution. Furthermore, the worth of a given control rod may depend on the position of the other rods due to shielding action. To calculate the worth of control rods simulations are carried out to determine the value of k_{eff} with and without insertion of control rods. The control rod worth can then be calculated as

$$\text{Control Rod Worth} = \frac{1}{k_{\text{eff}}\text{CR IN}} - \frac{1}{k_{\text{eff}}\text{CR OUT}}. \tag{4.13}$$

The United States Nuclear Regulatory Commission (U.S.NRC) defines the shutdown margin (SDM) as "the instantaneous amount of reactivity by which the reactor is subcritical or would be subcritical from its present condition assuming all full-length rod cluster assemblies (shutdown and control) are fully inserted except for the single rod cluster assembly of highest reactivity worth that is assumed to be fully withdrawn." (U.S.NRC 2021). The upper subcriticality limit (USL) defined by Canadian Nuclear Safety Commission (CNSC) mentions an administrative margin of 50 mk to ensure subcriticality at all normal and credible abnormal conditions(Safety Commission 2019). This means that the rod worths should be such that the reactor has an SDM of at least 50 mk at all expected states of reactor temperatures. Hence, the control rod worth analysis is done by carrying out the Serpent simulation at two temperatures, the nominal operating temperature of 773 K, which will provide us with the hot shutdown margin and the cold point temperature of 300 K. The cold point temperature is the minimum temperature that the reactor is expected to face during its operational life (cold shutdown condition) and thus will provide the maximum reactivity rise since the fuel and moderator temperature coefficients are negative, making the cold point analysis the bounding case for calculating the shutdown margin.

4.7.1 Reactivity Control System with Seven Solid Absorber Rods

The original Core-A design consists of seven reactivity control sites. As shown in Figure-4.10, four of these sites are designated for operational control of the reactor and the remaining three sites serve the exclusive function of reactor shutdown.

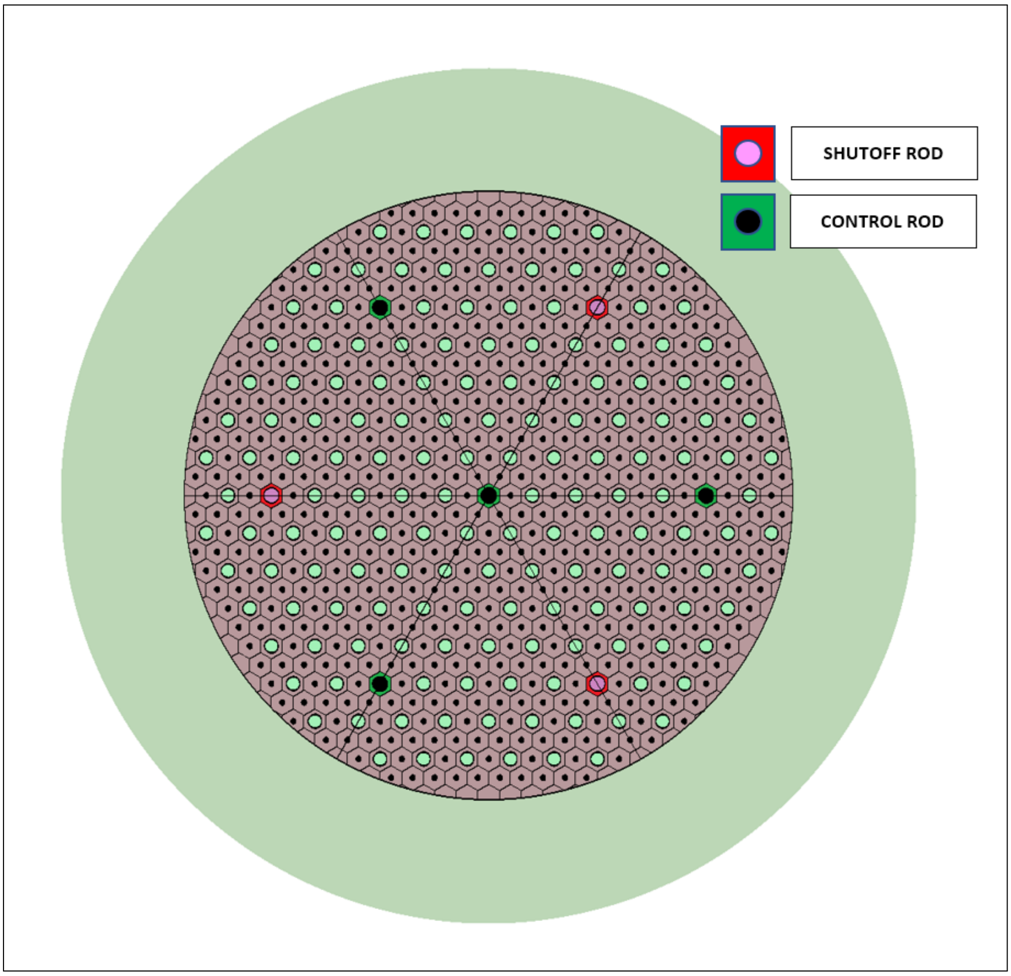

FIGURE 4.10: Rod designation for 7 rod reactivity control system

An analysis is done with seven reactivity control sites containing solid boron carbide rods 3.5 cm in radius for the Core-B design to determine if the reactivity control system worth is sufficient enough. The k_{eff} values at BOL[8] with different configurations of the rod positions at a nominal operating temperature of 773 K and cold shutdown temperature of 300 K are shown in the Table-4.15.

From the values of k_{eff}, it is clear that the reactor cannot be brought to cold shutdown with a seven-rod reactivity system even if all the rods are in completely inserted positions. Since the control rod radius is already at its mechanical maximum, we are left with only three options to improve the reactivity worth of the system:

---

[8] Rod Worth Analysis is done at BOL since the core is in the most reactive state with fresh fuel at BOL and the rod worths are expected to be the least because of the suppression of neutron flux in the core center by burnable poison.

Configuration	**$k_{eff} \pm 2\sigma$**	
	Cold Point (300 K)	**Op. Temp (773 K)**
All Rods Out	1.119 ± 0.0017	1.024 ± 0.0016
Central CR 100% In	1.109 ± 0.0019	1.017 ± 0.0017
All CRs 100% IN	1.072 ± 0.0017	0.981 ± 0.0017
All SRs 100% IN	1.082 ± 0.0019	0.989 ± 0.0018
All Rods 100% IN	1.026 ± 0.0017	0.935 ± 0.0017

Table 4.15: Variation of multiplication factor with rod configuration for 7-rod reactivity control system.

1. **Increase the absorption cross-section of the poison material:** This can be achieved either by increasing the boron enrichment or by changing the absorber material to a nuclide that has a neutron absorption cross-section higher than Boron. (e.g. hafnium, gadolinium, etc.)

2. **Change in the design of the reactivity control system:** Using control drums in the reflector since the thermal flux is higher in the peripheral region of the core at BOL.

3. **Increase the number of reactivity control rods:** This would imply that some of the heat pipe sites will need to be converted to control rod sites.

To check whether the first option of a change of absorber material will have any significant impact on the reactivity worth of the seven-rod system, a so-called black rod analysis is carried out at both the operating temperature and the cold point temperature. For the black rod analysis, the absorber material at the control rod location is changed from B_4C to black boundary condition. This means that all the neutrons that pass into the control rod location are absorbed and none escape giving an infinite absorption cross-section to the control rod sites. The results of the black rod analysis will show whether there is any advantage in increasing the boron enrichment or changing the absorber material.

The k_{eff} values at the operating temperature and cold point with at 'All Rod 100% IN position' for black control rods are obtained as

$$k_{eff} \text{ at Op. Temp (773K): } 0.919 \pm 0.0017,$$

$$k_{eff} \text{ at Cold Point(300K): } 1.008 \pm 0.0018.$$

The cold point k_{eff} shows that even with black rods in the seven-control-rod system, it is not possible to bring the reactor to cold shutdown, implying that the seven-control-rod design is doomed to fail since no amount of change in boron enrichment or better poison candidates can reduce the k_{eff} more than the black rod k_{eff}.

4.7.2 Control Drum Analysis

Control drums have been investigated to provide water submersion sub-criticality in several Nuclear Thermal Propulsion (NTP) reactor designs (Romnes et al. 2019; Lee et al. 2015). Rotating control drums are housed within the radial reflector and contain an annular sector of neutron absorber. To analyze the effectiveness of the use of control drums in achieving cold point subcriticality in the CNB, 12 control drums are modeled in the radial reflector. The radius of the control drums is 25 cm with a 120°sector of the drum containing a 2 cm thick layer of B_4C. The solid control rod system is removed and the control sites are replaced with additional heat pipes, resulting in 163 heat pipes instead of 156. As shown in Figure-4.11 the control drums can be rotated on their central axis such that the B_4C layer either faces towards or away from the reactor core to control the reactivity.

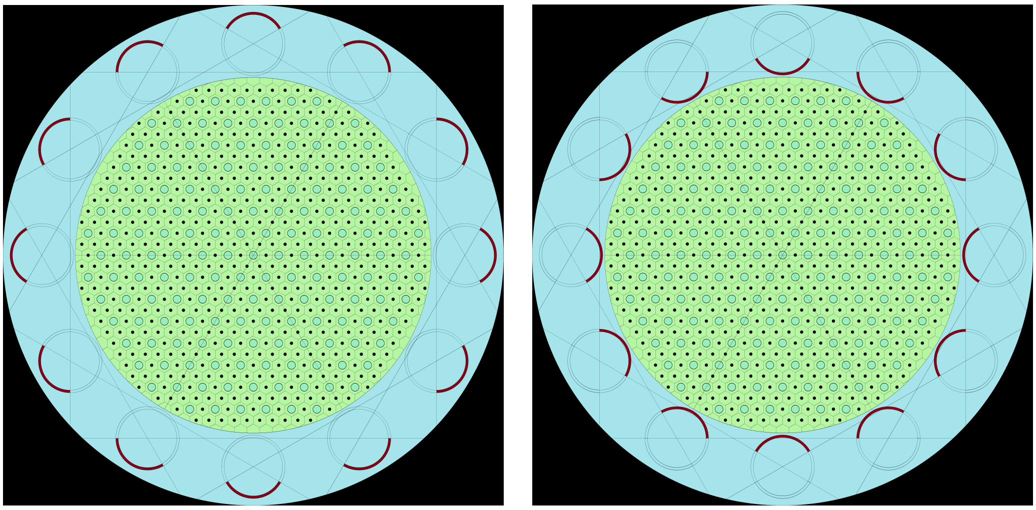

(A) CD Facing Out (B) CD Facing In

FIGURE 4.11: Control drum configuration for reactivity control.

The BOL k_{eff} with the control drum system facing towards the core and away from the core at operating and cold point temperatures are given in Table-4.16.

Configuration	Cold Point k_{eff} (300 K)	Op. Temp k_{eff} (773 K)
All Control Drums Out	1.112	1.015
All Control Drums In	1.02	0.912

TABLE 4.16: k_{eff} variation with control drum orientations.

The thermal flux mesh plot generated using the Serpent mesh utility illustrating the effect of control drum rotation on the neutronics of the systems is shown in Figure-4.12.

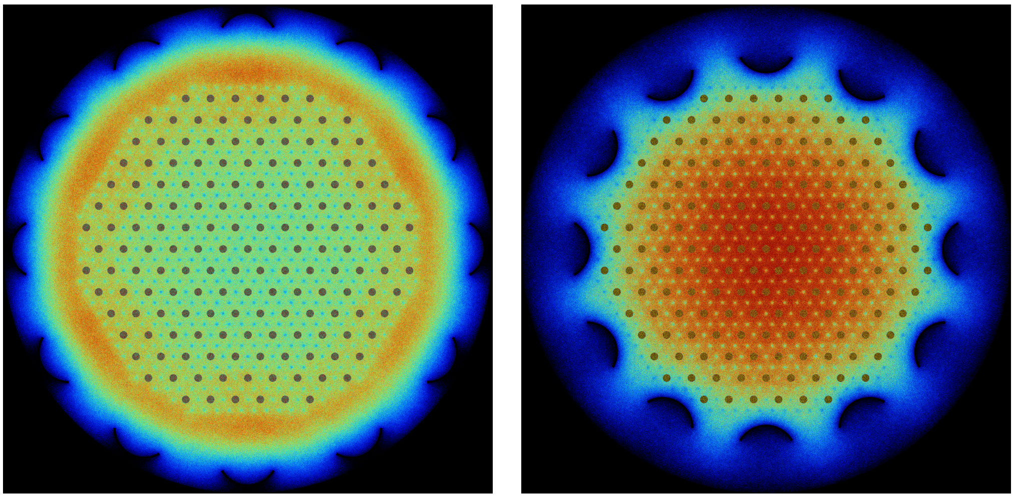

(A) CD Facing Out

(B) CD Facing In

FIGURE 4.12: Variation in thermal neutron flux with orientation of control drum system.

From the values of k_{eff} in Table-4.16, it is clear that the control drum system has almost the same worth as the 7 Rod reactivity control system and is no better at bringing the reactor to cold shutdown. Further, Figure-4.12 shows that at BOL, the control drum system pushes the thermal flux into the core, which is contrary to the action of the burnable poison. Moreover, the control drum system is a significant design change without bringing any advantage to the cold point subcriticality issue. Hence although it is a promising alternative design of the reactivity control system, it is decided for the current study to increase the number of the reactivity control rods instead of optimizing the control drum design.

4.7.3 Reactivity Control Design with 13 Solid Absorber Rods

An analysis is carried out by increasing the number of solid B_4C absorber rods from seven to 13. The radius of the control rod is kept the same at 3.5 cm. For the sole purpose of better identification of the absorber rod positions, the rods are divided into three categories, Control Rods (CR), Shutoff Rods (SR), and the Guaranteed Shutdown Rods (GSS). The rod configuration is shown in Figure-4.13.

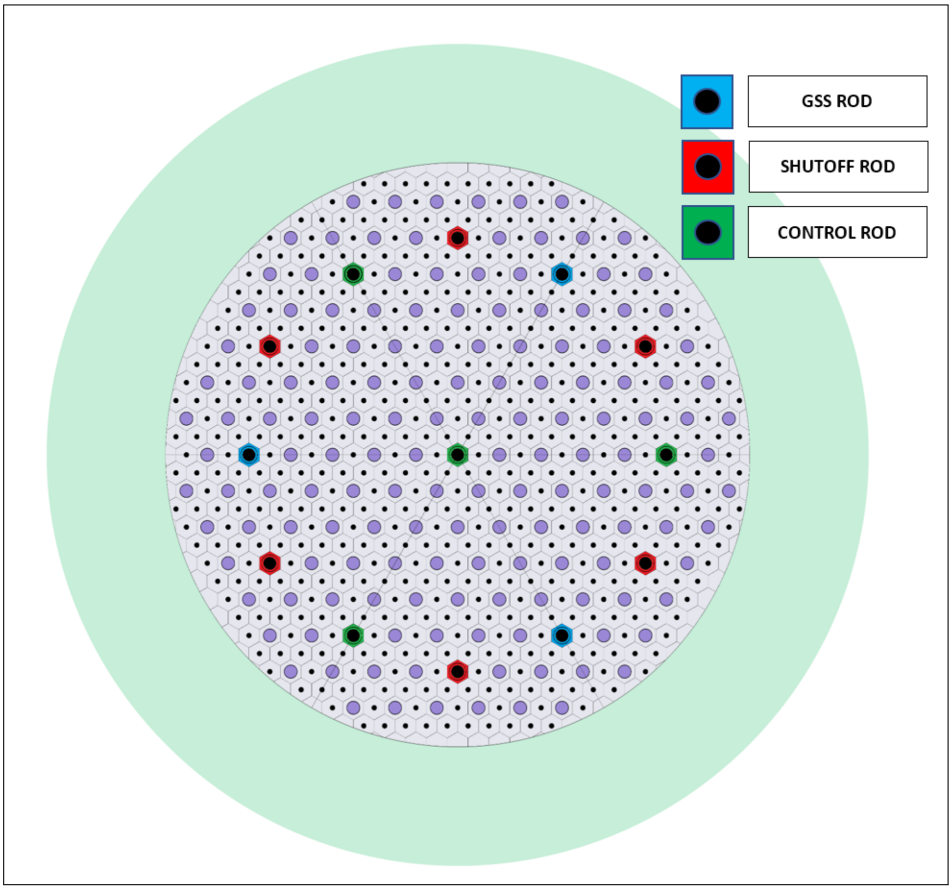

FIGURE 4.13: Rod designation for 13-rod reactivity control system.

The k_{eff} values at BOL with different configurations of the rod positions at a nominal operating temperature of 773K and cold shutdown temperature of 300K are shown in Table-4.17. The results for k_{eff} and rod worths[9] for various configuration of the rods is shown below:

---

[9] The 2σ uncertainity in k_{eff} is of the order of ± 0.002 and that in the rod worth is of the order of ± 2 mk

Configuration	**No. of Rods In**	**Cold Point k_{eff}**	**Op. Temp k_{eff}**	**Cold Worth (mk)**	**Hot Worth (mk)**
All OUT	0	1.118	1.023	-	-
Cen. CR IN	1	1.108	1.017	7.5	5.7
Peri. CRs IN	3	1.084	0.987	28.1	35.4
All CRs IN	4	1.072	0.981	37.8	42.4
GSS IN	3	1.083	0.988	28.5	34.3
SRs IN	6	1.035	0.935	71.3	92.0
GSS+SRs IN	9	1.002	0.903	103.0	130.5
All but Cen. CR IN	12	0.964	0.861	142.8	184.6
All IN	13	0.940	0.846	169.4	205.1

TABLE 4.17: k_{eff} variation with CR/SR/GSS configuration.

From the k_{eff} results in Table-4.17, it can be seen that sufficient cold point subcriticality seems to be obtained when all 13 rods are completely inserted in the core. The reactivity worth of the control rods is 42.4 mk at 773 K which is comfortably more than the reactivity swing value of 29.5 ± 2.28 mk and is sufficient to maintain the reactor critical over its entire lifetime of 20 years when operated at a power of 2.4 MW_{th} at a nominal temperature of 773 K.

4.7.4 Calculation of Shutdown Margin

To quantify the sufficiency of the cold point subcriticality with the 13-rod reactivity control system, it is necessary to calculate the shutdown margin of the reactor. As per the definition of SDM discussed previously, it is necessary to calculate the subcriticality of the core assuming that all the reactivity control rods (shutdown and control) are fully inserted except for the single rod of highest reactivity worth that is assumed to be fully withdrawn.

Table-4.17 shows that the central control rod is not the rod with the highest reactivity worth. Since the simulation is a one-sixth core simulation it is not possible to move each rod individually to assess its worth and find the rod with the highest worth among the remaining 12 rods. However, these 12 rods not only have the same design but are symmetrically located in the core-periphery approximately at the same radial distance. Thus they are expected to encounter a similar neutron flux, implying that all these rods will have almost the same reactivity worth at BOL. This assumption can be used to carry out a linear regression for rod worth vs. the number of rods as shown in Figure-4.14.

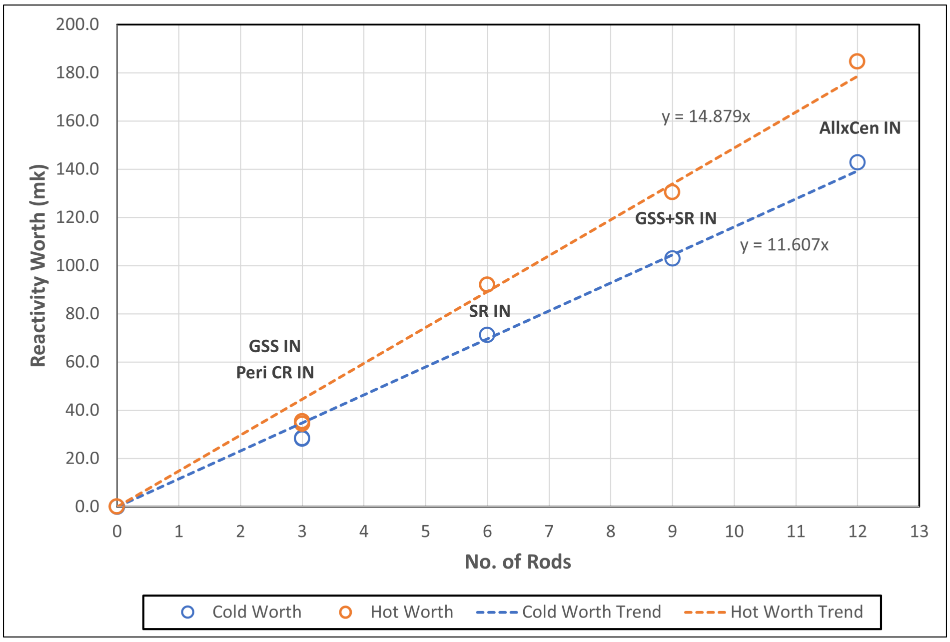

Figure 4.14: Linear fit for reactivity worth versus the number of rods to obtain individual rod worth.

Forcing the linear fit to pass through the point (0,0)[10], yields the following equations at operating temperature and cold point,

$$[\text{Rod Worth}]_{OP} = 14.879 \times n \qquad [\text{Operating Temperature}] \qquad (4.14)$$

$$[\text{Rod Worth}]_{CP} = 11.607 \times n \qquad [\text{Cold Point}] \qquad (4.15)$$

Substituting $n = 1$ in Equations-4.14 and 4.15, we obtain the worth of an individual rod as 14.88 mk. The subcriticality of the reactor with all rods fully in can be calculated from the values of k_{eff} (All IN) in Table-4.17 as,

$$\rho^{OP}_{scm} = 1 - \frac{1}{k_{\text{eff}}} = 1 - \frac{1}{0.846} = -182.0\,mk \qquad [\text{Operating Temperature}]$$

$$\rho^{CP}_{scm} = 1 - \frac{1}{k_{\text{eff}}} = 1 - \frac{1}{0.94} = -63.8\,mk \qquad [\text{Cold Point}]$$

---

[10] This is a physically consistent assumption since 0 rods would have 0 worth.

Assuming one rod failed condition, the SDM is calculated as,

$$[\text{SDM}]_{OP} = |\rho_{scm}^{OP}| - [\text{Rod Worth}]_{OP} = 167.1\, mk \qquad [\text{Operating Temperature}]$$

$$[\text{SDM}]_{CP} = |\rho_{scm}^{CP}| - [\text{Rod Worth}]_{CP} = 52.2\, mk \qquad [\text{Cold Point}]$$

Thus the 13-rod reactivity control system provides sufficient reactivity worth obtaining a SDM > 50 mk at the most reactive state of the CNB (Cold Shutdown at BOL).

4.8 Lattice Cell Multi-physics Coupling

Neutronic-Thermal hydraulic coupling is carried out for a single 3-D lattice cell of the CNB Core-B design. The single-cell geometry is modeled in Serpent with periodic radial boundary condition and black axial boundary condition such that the neutrons that go out of the radial boundary are sent back through the opposite face while the neutrons exiting the axial boundary are lost as leakage. The geometry plot obtained from Serpent is shown in Figure-4.15.

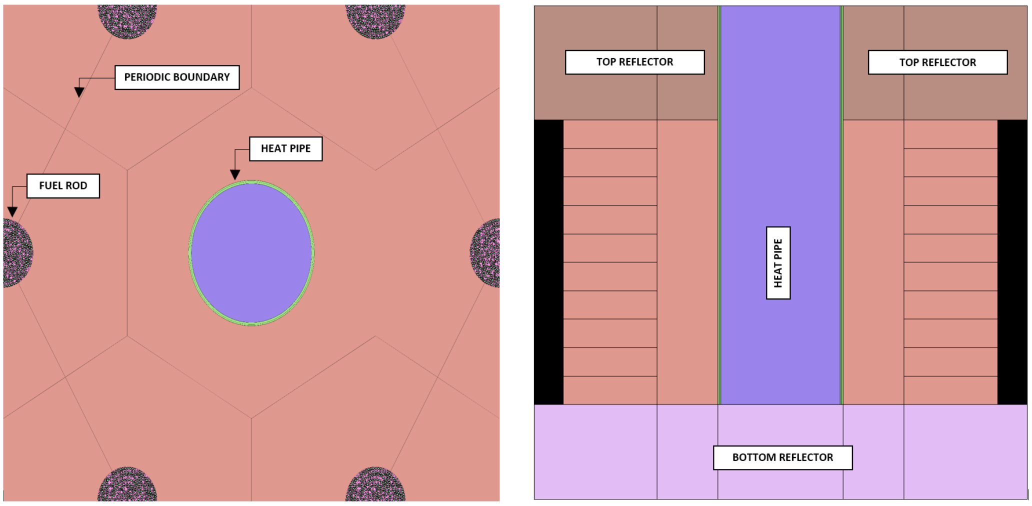

(A) Top View (B) Front View

Figure 4.15: Single lattice cell geometry in Serpent.

An analysis is first carried out with a nominal operating temperature of 773 K for all the materials in the model and volumetric heat deposition is obtained for the fuel locations. Since the fuel rods are symmetrically distributed around the center, the volumetric powers for all fuel rods are the same and vary only axially. For carrying out the thermal-hydraulic analysis an exact geometry model is constructed in the Ansys®, Academic Research Mechanical, Release 2020 R1. The Ansys geometry of the 3D lattice cell is shown in Figure-4.16.

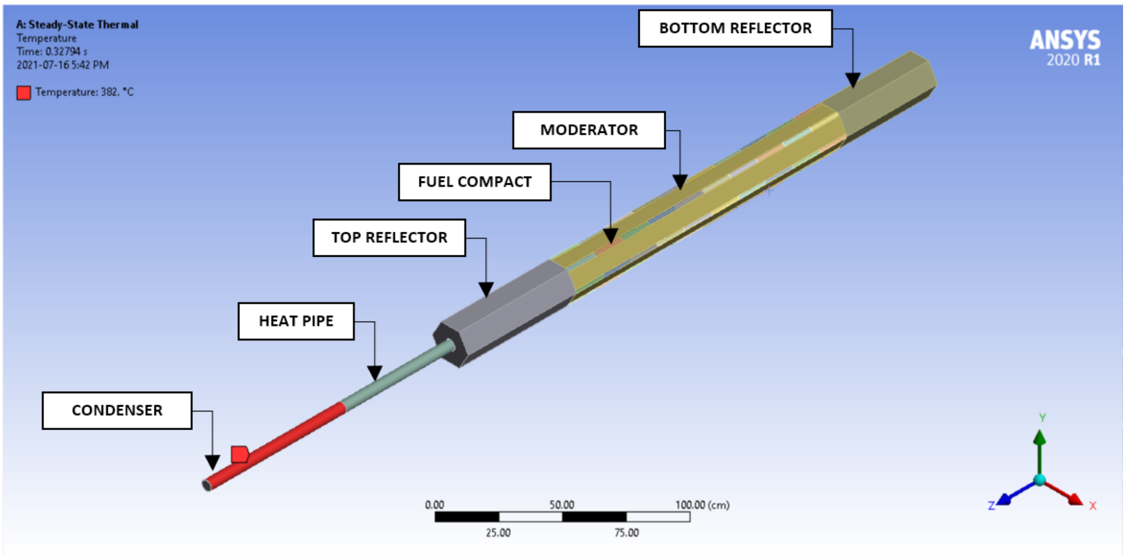

Figure 4.16: Single lattice cell 3D geometry in Ansys.

A python wrapper code is written to transfer the volumetric heat deposition as Ansys inputs in the form of Ansys readable .xml files. The assumptions and boundary conditions applied to the model are:

1. The condenser wall acts as the heat sink and is assumed to be at 382 °C. This value was arrived at such that the vapor core is maintained at 500 °C.
2. The radial and axial boundaries of the model are assumed to be adiabatic (no heat loss to the ambient).
3. The vapor core is modeled such that it has infinite thermal conductivity. This assumption is realistic since heat pipe vapor core transfers heat while maintaining an almost uniform temperature along its heated and cooled sections (Jouhara et al. 2017). This assumption also makes it possible to solve the model for temperatures using only steady-state thermal equations.

Steady-state conduction simulation is carried out to obtain the temperatures of all the materials in the model[11]. The temperature distribution obtained is shown in Figure-4.16.

---

[11] The moderator being solid and the coolant being dominantly vapor and not a strong absorber of neutrons the density variation effects on the neutronic calculations are precluded.

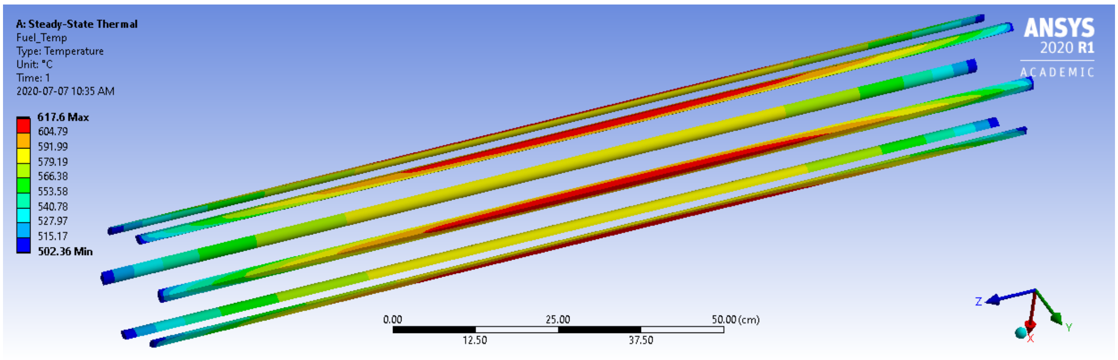

(A) Fuel temperature.

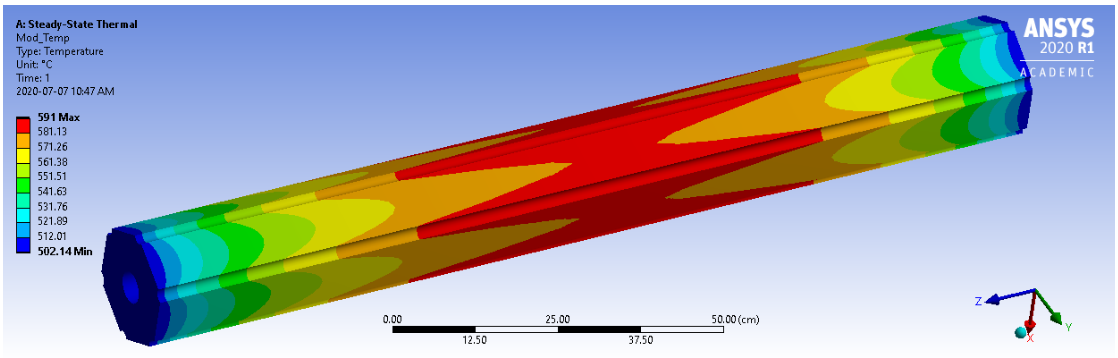

(B) Moderator temperature.

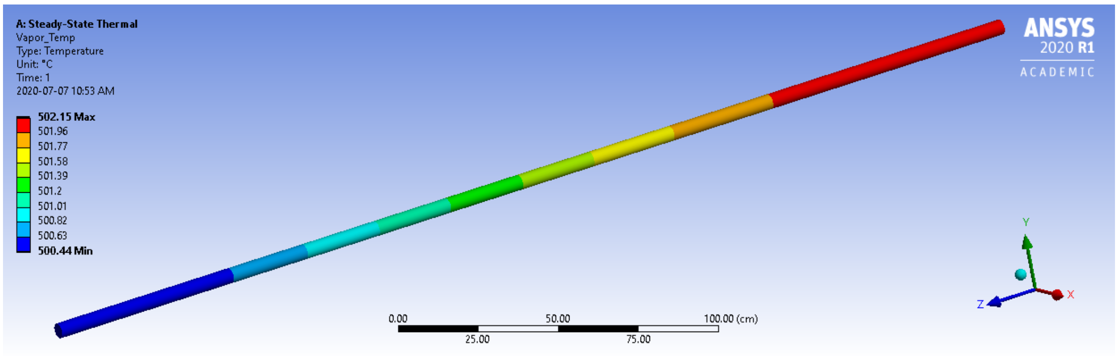

(C) Heat pipe temperature.

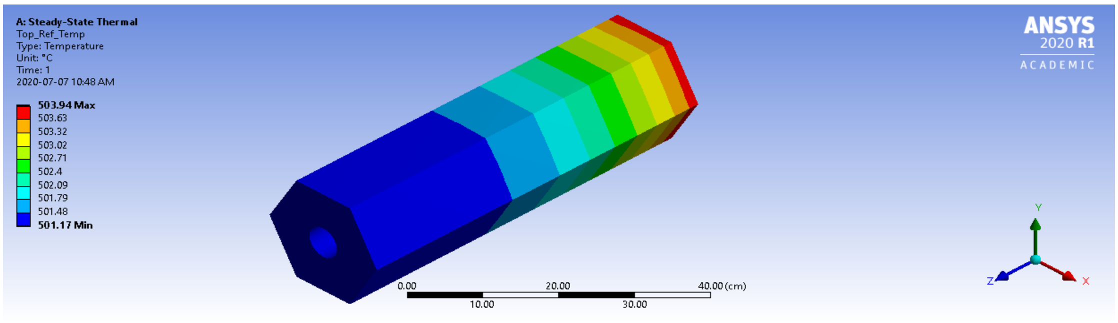

(D) Top reflector temperature.

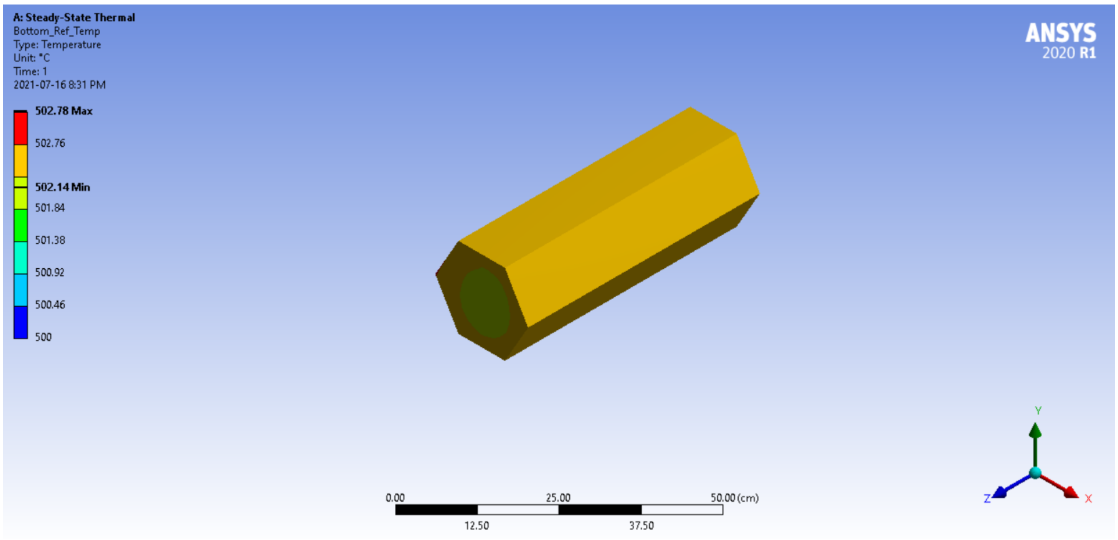

(E) Bottom Reflector Temperature

FIGURE 4.16: Temperature distribution output from Ansys.

The temperature profiles show that the temperature variation is insignificant for the top and bottom reflectors and the pipe vapor core. Hence the temperature profiles for fuel and moderator are the only ones that are imported into Serpent using the python wrapper code while the other materials are kept at a constant temperature of 773 K. Since the fuel rods in Ansys Geometry do not consist of heterogeneous fuel TRISO particles, all the layers of the fuel TRISO particles and the fuel matrix graphite are provided with the same fuel temperature as obtained from Ansys. The python wrapper code reads the material temperatures and converts them in the form of Serpent readable interface files. It also carries out coordinate axis transformation to correctly map the X, Y, and Z coordinates imported from Ansys output to their correct position in the Serpent geometry. These interface files can then be included in the main input to bring in temperatures and densities for each material in several discrete points in the geometry.

To check whether the temperatures were correctly imported at the desired points in the geometry Serpent provides for a sampling of the temperatures such that they can be mapped on a mesh with a resolution of the user's choice. The temperatures obtained from Ansys as mapped on a 500×500 mesh in the radial and the axial direction of the Serpent geometry's center-line are shown in Figure-4.17. From the figure, the temperatures seem to be correctly imported into Serpent.

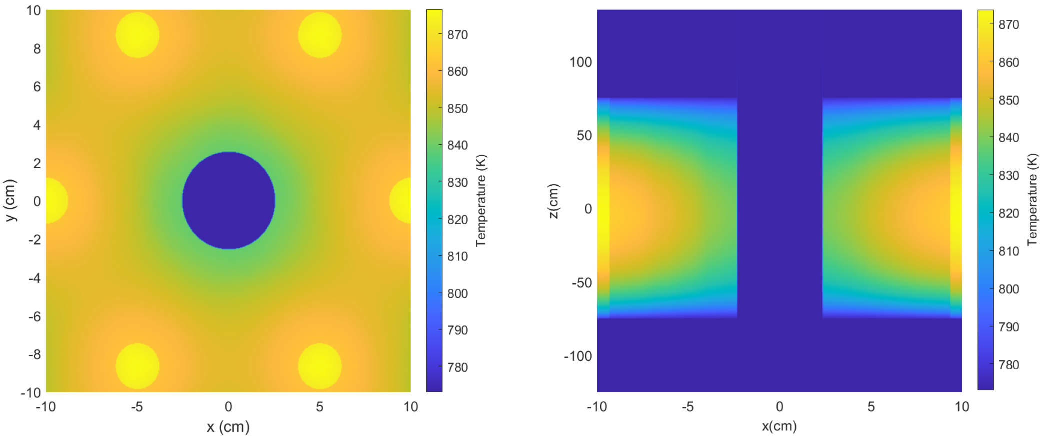

(A) Radial Centerline (B) Axial Centerline

FIGURE 4.17: Temperatures output from Ansys mapped onto Serpent geometry.

The Serpent simulation is run again, this time with the updated temperatures as obtained from the Ansys analysis. However, given that the volume-averaged fuel temperature obtained from Ansys is 579.49°C (≈80°C more than the nominal), and considering the value of the fuel temperature coefficient of reactivity at BOL, the effect on neutronic results due to the temperature change is within the uncertainty bounds of ±2 mk of the stochastic Serpent calculation. This implies that the temperature distribution should have no observable effect on the fission heat deposition. Figure-4.18 shows the comparison of the fission heat deposition at 773 K and with the implementation of the temperature distribution. As expected the fission heat deposition with the implementation of the temperature distribution is close to the uncertainty bounds of the original heat deposition distribution and further coupling iterations are not necessary. However, the systematic effect of the suppression of power at the high-temperature regions (center of the fuel rod) and increase of power at the low-temperature regions (top and bottom of the fuel rod) is seen.

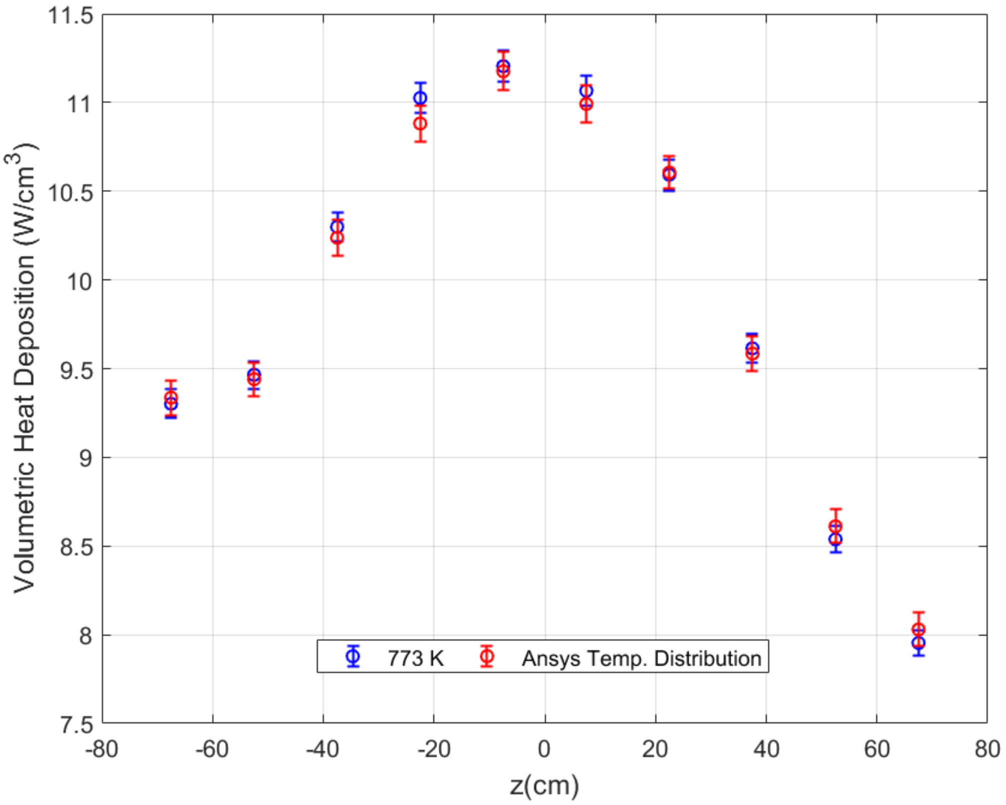

Figure 4.18: Volumetric heat deposition in the fuel rod.

Chapter 5

Conclusions and Future Work

5.1 Discussion of Results

The static criticality analysis carried out for the nuclear battery reactor demonstrates clear feasibility for the proposed reactor design from the viewpoint of reactor physics. The optimum lattice pitch for the CNB design is found to be 10 cm based on the fuel economy and the space constraints. The increase in lattice pitch from 7 to 10 cm along with an increase in fuel rod radius to 1.2 cm made it possible to increase the reactor life to 20 full power operational years (FPOYs) without refueling. With a fuel enrichment of 15 wt% ^{235}U in the inner zone and 13 wt-%^{235}U in the outer zone, along with the use of 19.35 kg natural Er_2O_3 (in the form of 150μm radius spheres in the inner region of the core), a value of reactivity swing of 29.5 ± 2.3 mk is obtained over 20 FPOYs which is well within the capability of the reactor control system.

The significantly high absorption of neutrons by potassium led to an equivalently high value of void reactivity in the extreme case of simultaneous and instantaneous voiding of all heat pipes. This prompted a significant design change in the alkali metal coolant material. The use of an equivalent amount of sodium in the heat pipes reduced the void reactivity values by a factor of three at Beginning-of-Life(BOL) and led to its selection for the latest design of CNB.

Thermal neutron flux and fission power distributions of the design were analyzed to determine the axial and radial flux peaking factors and power peaking factors at BOL, Middle-of-Life (MOL), and End-of-Life(EOL) of the reactor. A traveling burn wave is observed to form which starts at the core-periphery and travels to the center of the reactor as the poison in the inner zone depletes and releases the excess reactivity. The radial thermal flux is peaked at the core-periphery at BOL, becomes and stays almost flat over most of the reactor operational life, and then peaks at the center towards the EOL.

The fuel and moderator temperature coefficients of reactivity are negative over all the possible temperature ranges and throughout the life of the reactor and will act to provide neutronic stability during the entire operational life. The reactivity behavior as a function of fuel temperature is linear over the entire range of temperatures analyzed, and thus a single value for the coefficient was obtained from a weighted least square linear fit to the full temperature range at BOL, MOL, and EOL of the reactor. The fuel temperature coefficient of reactivity becomes increasingly negative as the reactor operates ensuring continuously increased stability of the reactor over its life. The moderator and reflector temperature coefficient was found to have a temperature dependence, but it is fairly linear in the temperature range from 700 K to 1600 K. The moderator and reflector temperature coefficient seem to become less and less negative as the reactor operates for 20 years but remains significantly negative between -6 to -20 pcm/K.

Given that the graphite temperature coefficient of the reactor is very negative, bringing the reactor to a cold state would result in significant excess reactivity being released into the system. To counter this and ensure cold point subcriticality it was necessary to modify the reactivity control system to consist of 13 solid B_4C rods instead of the seven originally used. Four of these 13 rods are designated as control rods and have sufficient worth to cover the operational reactivity swing over the life of the reactor. Out of the remaining nine rods, six are designated as Shutdown Rods and have enough worth to bring the reactor to safe hot shutdown. The shutdown margin (SDM) analysis (in one rod failed condition) showed that to bring the reactor to cold shutdown and maintain an SDM of more than 50 mk, the remaining three rods, designated as the Guaranteed Shutdown Rods are needed to be inserted in the core.

The lattice cell multi-physics analysis shows a fundamental way of interfacing Serpent and Ansys. The results for lattice cell calculation must be taken with a grain of salt given that they do not fully represent the CNB geometry. The geometry modeled was a simple lattice cell containing one heat pipe and six one-third fuel rods surrounding it. The effect of heat pipe and control rod locations as well as the core zoning was not modeled. However, the analysis does lay some groundwork for the future full-core coupling of the CNB Serpent model with any thermal-hydraulic simulation software and shows that the temperatures can be imported from an external source into Serpent with high fidelity. One of the most important conclusions of the current multi-physics study is that the variation in the fuel rod axial temperature distribution obtained has no observable impact on the fission heat deposition values in the given uncertainty bounds. Since the axial variation of fuel rod temperatures is expected to be similar for the whole-core model too, we can therefore conclude that there is no z-dependence needed for interfacing. This will simplify the creation of interface files significantly in future works and eliminate unnecessary complications.

5.2 Areas of Future Work

There is substantial scope for future work concerning the reactor physics analysis of the CNB reactor design identified below,

1. First and foremost, independent verification of the results obtained in this study is necessary, preferably with deterministic solvers as opposed to another stochastic solver and also with a sub-critical experiment, if possible.
2. The sensitivity of the results obtained to the use of cross-section libraries other than ENDF-B VII used here needs to be determined.
3. Analysis of the optimization of axial and radial reflector thicknesses and shielding calculations need to be carried out.
4. The burnable poison used is natural erbium oxide in the form of spherical particles which are randomly distributed in the fuel rods in the inner zone of the reactor core. It is acknowledged that it may not be practically possible to uniformly and randomly distribute the poison particles in a fuel compact. This makes it necessary to analyze the sensitivity of the reactor physics results to the distribution of the poison particles and the impact of the spatial bias in the poison particle distribution on the reactor criticality and burnup behavior.
5. Consequently it is also prudent to analyze a different configuration of burnable poison in the form of lumped burnable poison in which the major portion of poison is placed in rods between the fuel compacts. It is equally effective in reducing the reactivity swing and has a lower fuel penalty (Penner and Donnelly 1989). It will also provide more flexibility in design and commissioning since the fuel and poison are explicitly separated.
6. With the fuel and graphite temperature coefficients established the next natural step in the reactor physics analysis will be performing time-dependent calculations. Although Serpent does offer the capability of performing transient calculations, it

would be better to make a simpler, faster, and representative model to perform time-dependent calculations, preferably in a deterministic neutron transport solving code. If necessary, multi-group cross data can be calculated from the current Serpent model to be used in the deterministic solver.

7. To perform transient calculations in Serpent, it will be necessary to create a multiphysics interface to couple the whole core model to a thermal-hydraulic solver. The point average interface although useful in smaller geometries may not be the most effective way of interfacing for the larger geometry of the whole core based on the requirement of computational resources. A better, faster, and more intuitive interface is the hexagonal-mesh-based interface offered in Serpent. As concluded earlier, the interfacing can be z-independent leading to simpler and more compact interface files.

8. Although the control drums as reactivity control devices were found to have insufficient worth for the current design, there is significant scope in the optimization of the control drum design viz. use of absorber materials other than B_4C, increase in the poison layer thickness, use of beryllium in the non-absorbing part of the drum, etc. to increase the worth of the control drum system and make it a viable alternative to the solid absorber rod system.

Bibliography

Brown, F. B. (2006). On the use of Shannon entropy of the fission distribution for assessing convergence of Monte Carlo criticality calculations. In: *ANS topical meeting on reactor physics (PHYSOR 2006). Canadian Nuclear Society, Canada.*

Carter, L. and Cashwell, E. (1975). *Particle Transport Simulation with the Monte Carlo Method.* Technical Information Center, Office of Public Affairs USERDA, Oak Ridge,TN, 2–7.

Cetnar, J. (2006). General solution of Bateman equations for nuclear transmutations. *Annals of Nuclear Energy* 33(7), 640–645.

Cole (2015). *Serpent User Forum.* URL: https://ttuki.vtt.fi/serpent/viewtopic.php?f=3&t=2267 (visited on 06/18/2021).

Dam, H. van (2000). Long-term control of excess reactivity by burnable particles. *Annals of Nuclear Energy* 27(8), 733–743.

De Biévre, P., Gallet, M., Holden, N. E., and Barnes, I. L. (1984). Isotopic abundances and atomic weights of the elements. *Journal of physical and chemical reference data* 13(3), 809–891.

Duderstat, J. J. and Hamilton, L. J. (1976). *Nuclear Reactor Analysis.* John Wiley and Sons Inc.

Dunedin (2021). *Dunedin Energy Systems Ltd. website.* URL: https://www.dunedinenergy.ca/about (visited on 06/15/2021).

Eaton, J. W., Bateman, D., Hauberg, S., and Wehbring, R. (2020). *GNU Octave version 5.2.0 manual: a high-level interactive language for nume rical computations.*

Isotalo, A. E. and Aarnio, P. (2011). Higher order methods for burnup calculations with Bateman solutions. *Annals of Nuclear Energy* 38(9), 1987–1995.

Jouhara, H., Chauhan, A., Nannou, T., Almahmoud, S., Delpech, B., and Wrobel, L. (2017). Heat pipe based systems - Advances and applications. *Energy* 128, 729–754. ISSN: 0360-5442.

Kalos, M., F.R., N., and J., C. (1968). *Computating Methods in Reactor Physics.* Gordon and Breach Science Publisher Inc, N.Y., 365–431.

Kozier, K. S. and Rosinger, H. (1988). *The Nuclear Battery: a solid-state, passively cooled reactor for the generation of electricity and/or high-grade steam heat.* Whiteshell Nuclear Research Establishment.

Lamarsh, J. R. (1977). *Introduction to Nuclear Engineering.* Addison-Wesley Publishing Company, 42–73.

Lee, H. C., Han, T. Y., Lim, H. S., and Noh, J. M. (2015). An accident-tolerant control drum system for a small space reactor. *Annals of Nuclear Energy* 79, 143–151. ISSN: 0306-4549.

Leppänen, J. (2009). Two practical methods for unionized energy grid construction in continuous-energy Monte Carlo neutron transport calculation. *Annals of Nuclear Energy* 36(7), 878–885.

Leppänen, J. (2010). Performance of Woodcock delta-tracking in lattice physics applications using the Serpent Monte Carlo reactor physics burnup calculation code. *Annals of Nuclear Energy* 37(5), 715–722. ISSN: 0306-4549.

Leppänen, J. and Isotalo, A. (2012). Burnup calculation methodology in the Serpent 2 Monte Carlo code.

Leppänen, J. and Pusa, M. (2009). Burnup calculation capability in the PSG2/Serpent Monte Carlo reactor physics code. *Proc. M&C*, 3–7.

Leppänen, J., Pusa, M., Viitanen, T., Valtavirta, V., and Kaltiaisenaho, T. (2014). The Serpent Monte Carlo code: Status, development and applications in 2013. English. *Annals of Nuclear Energy* 82, 142–150. ISSN: 0306-4549.

Lewis, R., Bettes, P., and Hinton, E. (1984). *Numerical methods in coupled systems.* Wiley,Michigan.

MATLAB version 9.10.0.1684407 (R2021a) Update 3 (2021). The Mathworks, Inc. Natick, Massachusetts.

Penner, G. and Donnelly, J. (1987). *Evaluation of 500kW(e) Nuclear Battery Core Design Options for Uranium Carbide Fuel, SAB-TN-125.* Tech. rep. AECL.

Penner, G. and Donnelly, J. (1989). *Technical Note on Evaluation of Burnable Poison Options for the 2400-kW(t) Nuclear Battery, SAB-TN-155.* Tech. rep. AECL.

Pusa, M. and Leppänen, J. (2012). An efficient implementation of the Chebyshev rational approximation method (CRAM) for solving the burnup equations.

Rintala, V., Suikkanen, H., Leppänen, J., and Kyrki-Rajamäki, R. (Mar. 2015). Modeling of realistic pebble bed reactor geometries using the Serpent Monte Carlo code. *Annals of Nuclear Energy* 77, 223–230.

Romnes, C. J., Chavez, D. E., Martinez, B. J., Osterhaus, N. M., Ford, W. R., and Lenard, R. (2019). Low Enriched Uranium Nuclear Thermal Rocket Design Inspired by the Space Nuclear Thermal Propulsion Project. In: *Nuclear and Emerging Technologies for Space, American Nuclear Society Topical Meeting*.

Safety Commission, C. N. (Jan. 2019). *REGDOC-2.4.3, Nuclear Criticality Safety*. URL: http://www.nuclearsafety.gc.ca/eng/acts-and-regulations/regulatory-documents/published/html/regdoc2-4-3/index.cfm (visited on 07/11/2021).

Scriven, M. G. (2014). Sensitivity of lattice physics modelling of the canadian PT-SCWR to changes in lateral coolant density gradients in a channel. *MASc. Thesis*.

Subki, H. (2020). Advances in small modular reactor technology developments.

Suikkanen, H., Rintala, V., and Kyrki-Rajamäki, R. (2010). An approach for detailed reactor physics modelling of randomly packed pebble beds. In: *Proceedings of the 5th International Conference on High Temperature Reactor Technology, HTR*, 18–20.

Taylor, J. (1997). *Introduction to error analysis, the study of uncertainties in physical measurements*.

Tran, H. N., Kato, Y., and Muto, Y. (2008). Optimization of burnable poison loading for HTGR cores with OTTO refueling. *Nuclear science and engineering* 158(3), 264–271.

Tuominen, R., Valtavirta, V., and Leppänen, J. (2019). New energy deposition treatment in the Serpent 2 Monte Carlo transport code. *Annals of Nuclear Energy* 129, 224–232.

U.S.NRC (2021). *Unites States Nuclear Regulatory Commission Website*. URL: https://www.nrc.gov/reading-rm/basic-ref/glossary/shutdown-margin.html (visited on 07/11/2021).

Viitanen, T. et al. (2009). Implementing a Doppler-preprocessor of cross section libraries in reactor physics code Serpent. MA thesis.

Viitanen, T., Leppänen, J., and Forget, B. (2015). *Target motion sampling temperature treatment technique with track-length estimators in OpenMC. Preliminary results.* Tech. rep.

Woodcock, E., Murphy, T., Hemmings, P., and Longworth, S. (1965). Techniques used in the GEM code for Monte Carlo neutronics calculations in reactors and other systems of complex geometry. In: *Proc. Conf. Applications of Computing Methods to Reactor Problems*. Vol. 557. 2.

Zerkin, V. (2021). *Evaluated Nuclear Data File (ENDF) Database*. URL: https://www-nds.iaea.org/exfor/endf.htm (visited on 07/08/2021).

Zohuri, B. (2020). *Nuclear micro reactors*. Springer.

Appendix A

Uncertainty Evaluation and Error Propagation

A.1 Statistical Uncertainties in Serpent Results

Serpent being a Monte-Carlo solver inherently involves statistical uncertainty associated with its results. Serpent provides the uncertainty on the best estimate results of each output parameter in terms of the relative statistical error. The standard error of the mean (σ) can be calculated from the relative uncertainty value using,

$$\sigma = \text{Best Estimate Value (Mean Value)} \times \text{Relative Statistical Error} \tag{A.1}$$

In the current thesis, the statistical errors in all the results are presented in terms of $\pm 2\sigma$ such that the confidence interval is 95%. Error propagation is carried out when dependent variables are calculated from the results obtained from Serpent(eg. to calculate the reactivity from k_{eff}, temperature coefficients etc.).

A.2 Error Propagation

Error propagation is necessary when parameters are calculated by carrying out algebraic operations like sums, differences, products and divisions on results obtained from Serpent that have a statistical uncertainty associated with them. The error progression is carried out according to the methodology given in 'Introduction to error analysis'(Taylor 1997)

A.2.1 Sums and Differences

The provisional rule of uncertainty propagation on carrying out sums or differences state that if several quantities of value $x, ..., w$ are measured with uncertainty $\delta x, ...\delta w$ and measured values are used to compute

$$q = x + \cdots + z - (u + \cdots + w) \tag{A.2}$$

then the uncertainty in the computed value of q is the sum of all the original uncertainties,

$$\delta q \approx \delta x + \cdots + \delta z + \delta u + \cdots + \delta w \tag{A.3}$$

The rule can be summarised by saying that when two quantities are added or subtracted the uncertainties always add. However, if the original uncertainties are independent and random, which is the case in the current study, a more realistic estimate is given by adding the uncertainties in quadrature i.e.,

$$\delta q \approx \sqrt{(\delta x)^2 + \cdots + (\delta z)^2 + (\delta u)^2 + \cdots + (\delta w)^2} \tag{A.4}$$

A.2.2 Products and Quotients

The provisional rule of uncertainty propagation in carrying out the products or quotients states that if several quantities of value $x, ..., w$ are measured with uncertainty $\delta x, ...\delta w$ and measured values are used to compute,

$$q = \frac{x \times \cdots \times z}{u \times \cdots \times w} \tag{A.5}$$

then the fractional uncertainty in the computed value of q is the sum of all fractional uncertainties,

$$\frac{\delta q}{|q|} \approx \frac{\delta x}{|x|} + \cdots + \frac{\delta z}{|z|} + \frac{\delta u}{|u|} + \cdots + \frac{\delta w}{|w|} \tag{A.6}$$

Similar to the previous case, if the original uncertainties are independent and random then the fractional uncertainty in q is the sum of the quadrature of the original fractional uncertainty,

$$\frac{\delta q}{|q|} \approx \sqrt{\left(\frac{\delta x}{|x|}\right)^2 + \cdots + \left(\frac{\delta z}{|z|}\right)^2 + \left(\frac{\delta u}{|u|}\right)^2 + \cdots + \left(\frac{\delta w}{|w|}\right)^2} \tag{A.7}$$

A.3 Uncertainty in Reactivity Calculation

The reactivity computation (eg. to calculate the reactivity swing), is done from the values of k_{eff} obtained from Serpent output as,

$$\text{Reactivity Swing}(\rho_s) = \rho_{max} - \rho_{min} \tag{A.8}$$

where,

$$\rho_{max} = \frac{k_{\text{eff}}^{max} - 1}{k_{\text{eff}}^{max}}$$
$$\rho_{min} = \frac{k_{\text{eff}}^{min} - 1}{k_{\text{eff}}^{min}}$$

Hence, the reactivity swing can also be written as,

$$\rho_s = \frac{k_{\text{eff}}^{max} - k_{\text{eff}}^{min}}{k_{\text{eff}}^{min} \times k_{\text{eff}}^{max}} \tag{A.9}$$

From the laws of uncertainty propagation described above, we can write the uncertainty in the calculation of ρ_s as,

$$\frac{\delta\rho_s}{\rho_s} \approx \sqrt{\left[\frac{\delta(k_{\text{eff}}^{max} - k_{\text{eff}}^{min})}{k_{\text{eff}}^{max} - k_{\text{eff}}^{min}}\right]^2 + \left[\frac{\delta(k_{\text{eff}}^{max} \times k_{\text{eff}}^{min})}{k_{\text{eff}}^{max} \times k_{\text{eff}}^{min}}\right]^2} \tag{A.10}$$

where,

$$\delta(k_{\text{eff}}^{max} - k_{\text{eff}}^{min}) \approx \sqrt{(\delta k_{\text{eff}}^{max})^2 + (\delta k_{\text{eff}}^{min})^2} \tag{A.11}$$

$$\frac{\delta(k_{\text{eff}}^{max} \times k_{\text{eff}}^{min})}{k_{\text{eff}}^{max} \times k_{\text{eff}}^{min}} \approx \sqrt{\left(\frac{\delta k_{\text{eff}}^{max}}{k_{\text{eff}}^{max}}\right)^2 + \left(\frac{\delta k_{\text{eff}}^{min}}{k_{\text{eff}}^{min}}\right)^2} \tag{A.12}$$

Substituting A.11 and A.12 in A.10, we get

$$\frac{\delta\rho_s}{\rho_s} \approx \sqrt{\frac{(\delta k_{\text{eff}}^{max})^2 + (\delta k_{\text{eff}}^{min})^2}{(k_{\text{eff}}^{max} - k_{\text{eff}}^{min})^2} + \left(\frac{\delta k_{\text{eff}}^{max}}{k_{\text{eff}}^{max}}\right)^2 + \left(\frac{\delta k_{\text{eff}}^{min}}{k_{\text{eff}}^{min}}\right)^2} \tag{A.13}$$

Sample uncertainty calculation

For calculating uncertainty in reactivity from $k_{\text{eff}}^{max} = 1.0235$ with a relative statistical error of 0.00078 and $k_{\text{eff}}^{min} = 0.9935$ with a relative statistical error of 0.00085 as given by Serpent output,

$$
\begin{aligned}
\frac{\delta k_{\text{eff}}^{max}}{k_{\text{eff}}^{max}} &= 0.00078 \\
\delta k_{\text{eff}}^{max} &= 0.00078 \times 1.0235 = 0.0008 \\
\frac{\delta k_{\text{eff}}^{min}}{k_{\text{eff}}^{min}} &= 0.00085 \\
\delta k_{\text{eff}}^{max} &= 0.00085 \times 0.9935 = 0.00084 \\
\rho_s &= \frac{1.0235 - .9935}{1.0235 \times 0.9935} = 29.5\ mk \\
\frac{\delta \rho_s}{\rho_s} &\approx \sqrt{\frac{(0.0008)^2 + (0.00084)^2}{(1.0235 - 0.9935)^2} + (0.00078)^2 + (0.00085)^2} \\
\delta \rho_s &\approx 29.5 \times 0.0387 \approx 1.14\ mk \qquad \text{(A.14)}
\end{aligned}
$$

Thus the $\pm 2\sigma$ uncertainty in calculation of $\delta\rho_s$ is $\pm 2.28\ mk$.

A.4 Uncertainty in Temperature Coefficient of Reactivity

The temperature coefficient of reactivity is calculated as,

$$\alpha_T = \frac{\rho_{hot} - \rho_{cold}}{T_{hot} - T_{cold}} \tag{A.15}$$

Since the temperatures don't have any uncertainties associated with them, the uncertainty in the temperature coefficient of reactivity can then be given by,

$$\delta\alpha_T \approx \frac{\sqrt{(\delta\rho_{hot})^2 + (\delta\rho_{cold})^2}}{T_{hot} - T_{cold}} \tag{A.16}$$

The uncertainty in reactivities is calculated using the procedure described in Section-A.3.

Appendix B

Analytical Calculation of Fuel Temperature Coefficient of Reactivity

As explained in Chapter-4, Fuel Temperature Coefficient of Reactivity (FTC) is an almost instantaneous feedback to the increase in reactor power. Hence it is also called as the *prompt temperature coefficient* and denoted as α_{prompt}. This coefficient is negative for almost all reactors because of a phenomenon called as nuclear doppler effect as described in section-1.2.5. To calculate the α_{prompt} of the reactor the multiplication factor is written as(Lamarsh 1977),

$$k_{\text{eff}} = \text{k}_{\infty} P = \eta_T f p \epsilon P \tag{B.1}$$

where,

η_T (Thermal fission factor):	No. of fission neutrons produced per absorption in fuel
f(Thermal utilisation factor):	Probability that a neutron that gets absorbed does so in the fuel.
p (Resonance escape probability):	Probability of slowing down from fast to thermal energies without getting absorbed in the resonance.
ϵ (Fast fission factor):	Ratio of total number of fission neutrons to the number of fast fission neutrons.
P(Total non-leakage probability):	Probability that neutron of any energy will not leak out of the system

The resonance escape probability can be singled out by taking logarithms on both sides of equation-B.1,

$$\ln k_{\text{eff}} = \ln \eta_T f \epsilon P + \ln p \tag{B.2}$$

Differentiating with temperature and keeping all parameters constant except p we get,

$$\frac{d}{dT}(\ln k_{\text{eff}}) = \frac{1}{k_{\text{eff}}}\frac{dk_{\text{eff}}}{dT} = \frac{d}{dT}(\ln p)$$

or

$$\alpha_{prompt} = \frac{d}{dT}(\ln p) \tag{B.3}$$

The resonance escape probability is given by the equation (Lamarsh 1977)

$$p = \exp\left[-\frac{N_F V_F I}{\xi_M \Sigma_{sM} V_M}\right] \tag{B.4}$$

where I is the resonance integral, V_F and V_M are the volumes of the unit cells of fuel and moderator, N_F is the atomic density of fuel, Σ_{sM} is the macroscopic cross-section of the moderator andξ_M is the average increase in lethargy per collision in the moderator. The prompt coefficient is calculated assuming only fuel temperature changes and no change happens in the moderator temperature. Thus V_M, Σ_{sM} and ξ_M remain constant and the product of $N_F V_F$, which is the total number of atoms in fuel also remains constant. Thus the total temperature dependence of p is only a function of change in I with temperature. Thus equation-B.3 can be written as,

$$\alpha_{prompt} = -\frac{N_F V_F}{\xi_M \Sigma_{sM} V_M}\frac{dI}{dT} \tag{B.5}$$

The temperature dependence of I for ^{238}U has been experimentally determined for cylindrical fuel rods and is given by(Duderstat and Hamilton 1976),

$$I^{238} = I^{238}(300\ K)[1 + \beta(\sqrt{T} - \sqrt{300\ K})] \tag{B.6}$$

The parameter β is a property of fuel material and for ^{238}U is given by,

$$\beta = 61 \times 10^{-4} + 0.94 \times 10^{-2} \times \frac{S}{M} \tag{B.7}$$

where S is the surface area of the fuel rod and M is the mass of the fuel rod. Substituting $S = \pi r H$ and $M = \rho \times Volume = \rho \times \pi r^2 H$, equation-B.7 simplifies to,

$$\beta = 61 \times 10^{-4} + \frac{0.94 \times 10^{-2}}{r\rho} \tag{B.8}$$

where r is the radius of the fuel rod in cm and ρ is the density of the fuel rod in g/cm^3.

Differentiating equation-B.6 with respect to temperature we get,

$$\frac{dI^{238}}{dT} = \frac{I^{238}(300\ K)\beta}{2\sqrt{T}} \tag{B.9}$$

substituting this in equation-B.5, we get,

$$\alpha_{prompt} = -\frac{N_F V_F I^{238}(300\ K)}{\xi_M \Sigma_{sM} V_M} \frac{\beta}{2\sqrt{T}} \tag{B.10}$$

$$= \frac{\beta}{2\sqrt{T}} \ln\left[\frac{1}{p(300\ K)}\right] \tag{B.11}$$

where $p(300\ K)$ is the resonance escape probability at 300 K.

The resonance escape probability for the CNB at 300 K was found to be 0.8312 by running a Serpent simulation for Core-B design with all materials at 300 K. Substituting $r = 1.2\ cm$ and $\rho = 10.9\ g/cm^3$, the value of β is found as 0.0068. FTC is then calculated for the Core-B design at temperatures of 600 K, 900 K, 1200 K and 1500 K and the results are shown in Table-B.1 along with Serpent results at BOL obtained in Section-4.6.1 for comparison. The analytical values for FTC compare well with the results obtained from Serpent and are close to the upper uncertainty bounds. They also follow similar trend with temperatures. The mismatch can be attributed to the fact that this analysis is valid for cylindrical fuel rods and might not be directly applicable to fuel in the form of spherical TRISO particles. The FTC values at MOL and EOL cannot be

TABLE B.1: Analytical calculation of FTC at BOL.

Temperature (K)	Analytical FTC (pcm/K)	Serpent FTC $\pm 2\sigma$ (pcm/K)
600	-2.6	-1.6 ± 0.8
900	-2.1	-1.4 ± 0.4
1200	-1.8	-1.3 ± 0.3
1500	-1.6	-1.2 ± 0.2

directly compared with this analytical calculation since the buildup of fission products causes the FTC to no longer remain a function of the temperature dependence of ^{238}U resonance integrals only.